University of Oxford

A thesis submitted for the degree of Doctor of Philosophy

Development of peripheral nerve specific biomarker assays: from in vitro neuropathy models to clinical validation

Dr Roberto Bellanti

Nuffield Department of Clinical Neurosciences

University of Oxford

Supervisors:

Assoc. Professor Simon Rinaldi	Primary Supervisor, University of Oxford
Professor Michael Lunn	Secondary Supervisor, University College London
Assoc. Professor Alexander Thompson	Secondary Supervisor, University of Oxford

Declaration

I, Roberto Bellanti, declare that the work presented in this thesis is my own. To the best of my knowledge, it contains no material previously published or written by another person, except where due reference is made in the text. This thesis is submitted in full fulfilment of the requirements for the degree of Doctor of Philosophy at the University of Oxford.

Abstract

Clinical assessment of disease progression and effective design of clinical trials in peripheral neuropathy would benefit from objective biomarkers that closely reflect disease biology. This is particularly important in the inflammatory neuropathies, where reliable biomarkers of peripheral demyelination and axonal damage are needed to identify and measure active disease and responses to treatment.

This thesis describes the development of a novel ultrasensitive immunoassay to measure periaxin, a protein exclusively expressed in the peripheral nervous system, as a biomarker of peripheral demyelination. It also details the optimisation of a previously developed assay for peripherin, an intermediate filament predominantly expressed in peripheral axons, to serve as a biomarker of axonal injury. Together with neurofilament light chain (NfL), a validated biomarker of axonal damage, periaxin and peripherin form a complementary panel that improves diagnostic accuracy, disease monitoring, and supports biomarker-driven research in peripheral neuropathies. The work spans the full translational pathway, from biomarker conception and assay development to validation in patient samples, along with the use of cell-based models of neuropathy for biomarker validation. By combining clinical and in vitro work, this research establishes a biologically grounded framework for translating research findings into improved patient care.

Impact statement

My DPhil research led to the development and optimisation of ultrasensitive assays for periaxin and peripherin - biomarkers of peripheral nerve demyelination and axonal injury - with validation in patient cohorts and in vitro models. Combined with NfL, these biomarkers enhance classification of neuropathy subtypes and assessment of disease activity, with promising results in relation to outcome prediction.

A fluid biomarker of peripheral demyelination has long been sought, but previous candidates have lacked specificity or robustness for clinical use. Periaxin is the first peripheral nerve-specific biomarker with the potential to improve diagnosis and monitoring of demyelinating neuropathies, particularly when used alongside axonal biomarkers and clinical scales. It also holds promise as a surrogate endpoint to enhance the design and efficiency of early-phase clinical trials.

This work has attracted international collaborations across Europe and North America, as well as interest from pharmaceutical partners. Locally, collaborations within the Nuffield Department of Clinical Neurosciences and University College London are advancing integration into translational neuromuscular research. Future directions include application to broader disease cohorts, longitudinal studies to define clinically meaningful thresholds, and detailed profiling of disease-specific biomarker signatures to support precision diagnosis and therapy in peripheral neuropathy.

Acknowledgments

First and foremost, I would like to thank the patients who generously donated their time to support this project, including those I never had the opportunity to meet, whose samples were analysed retrospectively. Without their willingness to contribute, none of the clinical validation work would have been possible. Their donation is far more than just data: it is a vital foundation for clinical translation and future patient benefit.

I am deeply grateful to my primary supervisor, Simon Rinaldi. It is difficult to put into words just how much I owe him. Above all, Simon gave me freedom: freedom to explore, make mistakes, learn, and grow. While allowing me complete independence, he has always remained available, supportive, and generous with his time and insight. He embodies what it means to be a clinical scientist: curious, principled, committed. I remember the first email I sent him - almost four years ago - asking if I could do some lab work with him. I was drawn to the idea of combining cell-based research with clinical biomarkers, and from that point on, he's taught me so much. These years are only the beginning; wherever I go next, I know we'll keep working together.

Thank you to Mike Lunn, my co-supervisor. Mike is one of those rare people you meet once in a lifetime: at the top of his game, yet effortlessly humble. He has given so much to the neuromuscular field - shaping it through his unparalleled clinical expertise and his vision for translational research. There's something remarkable in the way he turns clinical questions into real, purposeful projects - he somehow always finds a way to make them happen. Working with him has been a real privilege. There isn't a time I don't learn something from Mike - whether from watching him, speaking with him, or just hearing him think out loud. I'm grateful for everything he's done for me.

They say to choose your supervisors wisely - I couldn't have chosen better. What makes working with Simon and Mike so effective is how we complement each other: different in style, united in purpose. Whatever challenges lie ahead, I'm confident we'll face them together, as a team.

I would also like to thank Dave Bennett, my MRC fellowship mentor. His advice on academic development has helped a lot. The Wednesday meetings of the Oxford Neural Injury Group have been a constant source of learning and inspiration - from fundamental biology to clinical translation. Dave's depth of knowledge is formidable, and he is the reason that the group is such a dynamic space for intellectual cross-fertilisation.

Thank you to Alex Thompson, who joined the internal supervisory team and whose advice I have greatly appreciated. Our collaboration with the motor neuron disease group has already been fruitful - and there is more to come.

To Alex Davies - thank you for your broad expertise and your constant willingness to help. You've made my life easier on countless occasions, and your support throughout this project has meant a great deal to me.

I'm grateful to Mary Reilly for her help with the inherited neuropathy samples. I've greatly valued the opportunity to collaborate and look forward to working more closely with her team in the future.

To the Oxford team - Mariya, Claire, Janev, Nicolas - thank you for your companionship, for sharing the highs and lows of lab work, and for all the laughs at conferences, pubs, and beyond. Thanks also to Luana - it was great to have her in Oxford and to share part of this journey together.

Thank you to the London lab team. Michael Chou was instrumental in my early lab work, helping me navigate pipettes, Simoa, immunohistochemistry, and so much more. As a clinician with no prior lab experience, I was lucky to have his guidance. Thanks also to Melanie, Miles, and Fotinie – you're not just great colleagues but lovely people to work with.

Thanks to the other side of the 9th floor at Queen Square House – Riccardo, Ilaria, Andrea Cortese and his team. It's great fun sharing lab space with you. Our conversations on just about every imaginable topic have made even the busiest days lighter and more enjoyable.

Thank you to Stephen Keddie for his help during the early stages of biomarker development - having his previous work as a reference made a great difference. Thanks also to Ryan Keh for contributing with the GBS samples - his groundwork made several key parts of this project possible, and to Aisling Carr for always thinking of our biomarker work when seeing patients in clinic - that's helped a lot. Special thanks to Kaminie Moodley for her samples, including that single one that, quite serendipitously, led me to the realisation that plasma - not serum - was the answer for periaxin. I'm glad I got there in the end.

I would like to acknowledge the generous support of the Medical Research Council, Brain, and Grifols, my funders, without whom none of this expensive work would have been feasible.

A special thank you goes to my family. To my mother - my greatest supporter, now and always – and to Zia Gabriella, Zio Gianni, and Zio Ezio: these past years have brought hardships none of us could have foreseen. I wish I could have been there more, but as every expat learns, no distance is insurmountable.

Thank you to my father. He still walks with me every step.

To my dear friends - Daniele, Jacopo, Beppe, Federica, Martina, and Marco - thank you. They say the most meaningful friendships are the ones you form when the future still feels wide open, and twenty years later, we've stayed close through it all.

And finally - most importantly - thank you to Samantha. My girlfriend, my partner, my friend, my companion in life. Six years after we first met, she somehow still hasn't had enough of me. She's put up with my long hours and emotional ups and downs with unwavering patience and support. She's kind, clever, endlessly understanding, and unfailingly knows just what to say. A PhD can be a lonely journey, but she's been my rock throughout. I can't wait for everything that's ahead of us. *Merci mon amour.*

What a privilege it is to do something I love. There is much more to discover, more to learn, and I'm filled with optimism about the future. I am fortunate to have the support, guidance and companionship that keep me going. I look forward to the next chapter. I am not alone.

Publications during the course of the DPhil

- **Bellanti R**, Keh RYS, Keddie S, Chou MKL, Misheva M, Smyth D, Baskozos G, Moodley K, Hart MS, Davies A, Reilly MM, Rinaldi S, Lunn MP. Plasma periaxin is a biomarker of peripheral nerve demyelination. Brain. 2025. *Accepted for publication.*

- Rajabally YA, Englezou C, Cluett G, **Bellanti R**, Rinaldi S, Chin MW, Hadden R, Roman M, Hewamadduma C, Murray A, Elsaddig A, Lavin T, Cousins O, Nirmalananthan N, Freiha J, Osman C, Evans M, Carr A, Holt JKL. Diagnosis and Management of Multifocal Motor Neuropathy in the United Kingdom: A Multicentre Survey. J Peripher Nerv Syst. 2025 Jun;30(2):e70018. doi: 10.1111/jns.70018. PMID: 40210218; PMCID: PMC11985232.

- **Bellanti R**, Rinaldi S. Guillain-Barré syndrome: a comprehensive review. Eur J Neurol. 2024 Aug;31(8):e16365. doi: 10.1111/ene.16365. Epub 2024 May 30. PMID: 38813755; PMCID: PMC11235944.

- **Bellanti R**, Keddie S, Lunn MP, Rinaldi S. Ultrasensitive assay technology and fluid biomarkers for the evaluation of peripheral nerve disease. J Neurol Neurosurg Psychiatry. 2024 Jan 11;95(2):114-124. doi: 10.1136/jnnp-2023-332031. PMID: 37821222.

- **Bellanti R**, Symmonds M, Chowdhury R, Hofer M, Rinaldi S. AL amyloidosis presenting with isolated lumbosacral radiculoplexus neuropathy. Practical Neurology. 2023 Jul 17:pn-2023-003788. doi:10.1136/pn-2023-003788. Epub ahead of print. PMID: 37460212

- Keddie S, Smyth D, Keh RYS, Wieske L, Michael M, Eftimov F, **Bellanti R**, Rinaldi S, Petzold A, Lunn MP. Reply: Peripherin is a biomarker of axonal damage in Guillain-Barré syndrome: a pathophysiological annotation. Brain. 2023 Aug 30:awad276. doi:10.1093/brain/awad276. Epub ahead of print. PMID: 37647107

- Keddie S, Smyth D, Keh RYS, Chou MKL, Grant D, Surana S, Heslegrave A, Zetterberg H, Wieske L, Michael M, Eftimov F, **Bellanti R**, Rinaldi S, Hart MS, Petzold A, Lunn MP. Peripherin is a biomarker of axonal damage in peripheral nervous system disease. Brain. 2023 Jul 12:awad234. doi:10.1093/brain/awad234. Epub ahead of print. PMID: 37435933

- Fehmi J, **Bellanti R**, Misbah SA, Bhattacharjee A, Rinaldi S. Treatment of CIDP. Pract Neurol. 2023 Feb;23(1):46-53. doi: 10.1136/pn-2021-002991. Epub 2022 Sep 15. PMID: 36109154.

Table of Contents

List of figures

List of tables

Abbreviations

AIN: Autoimmune nodopathy

ALS: Amyotrophic lateral sclerosis

BSA: Bovine serum albumin

CIDP: Chronic inflammatory demyelinating polyradiculoneuropathy

CLEIA: Chemiluminescent enzyme immunoassay

CMT: Charcot-Marie-Tooth disease

CNS: Central nervous system

CR: Complement receptor

CSF: Cerebrospinal fluid

DADS: Distal acquired demyelinating sensory neuropathy

ECL: Electrochemiluminescence

ELISA: Enzyme Linked Immunosorbent Assay

GBS: Guillain-Barré syndrome

IHC: Immunohistochemistry

IPSC: Induced pluripotent stem cell

IVIg: Intravenous immunoglobulin

LLOD: Lower Limit of Detection

LLOQ: Lower Limit of Quantification

MADSAM: Multifocal acquired distal sensory and motor neuropathy

MMN: Multifocal motor neuropathy

MRD: Minimum required dilution

MRI: Magnetic Resonance Imaging

MSD: Meso Scale Discovery

NfL: Neurofilament light chain

NfM: Neurofilament medium chain

NfH: Neurofilament heavy chain

NHNN: National Hospital for Neurology and Neurosurgery

PBS: Phosphate-buffered saline

PET: Positron Emission Tomography

PNS: Peripheral nervous system

POEMS: Polyneuropathy, Organomegaly, Endocrinopathy, Monoclonal gammopathy, Skin changes

SCIg: Subcutaneous immunoglobulin

Simoa: Single Molecule Array

SPE: Serum protein electrophoresis

1. INTRODUCTION

1.1 The inflammatory neuropathies

The inflammatory neuropathies are a heterogeneous group of peripheral nerve disorders driven by abnormal immune system activity and presumed immune-mediated pathogenesis. All inflammatory neuropathies are characterised by pathological evidence of immune-mediated injury, in the form of inflammatory cell infiltration or indirect immune effector mechanisms, with variable degrees of demyelination and/or axonal damage. Chronic inflammatory demyelinating polyradiculoneuropathy (CIDP) and Guillain-Barré syndrome (GBS) are the most common inflammatory neuropathies. Others include neuropathies associated with paraproteinaemia, autoimmune nodopathies (where the damage primarily occurs at the node of Ranvier or paranodal regions), and vasculitic neuropathy. Peripheral neuropathy can also develop as a secondary manifestation of systemic autoimmune conditions (such as systemic vasculitis and connective tissue diseases), infections, and as a paraneoplastic complication of cancer.

Clinical management of the inflammatory neuropathies is hampered by the lack of valid biomarkers of peripheral nerve disease. Current methods are poorly sensitive and can lead to overtreatment-related side effects or excess disability due to undertreatment. Meanwhile, demand, consumption and cost of therapies continue to increase. Objective and responsive biomarkers are urgently needed to measure peripheral nerve disease, individually tailor therapies and improve their cost-effectiveness.

1.1.1 Chronic inflammatory demyelinating polyradiculoneuropathy

CIDP is the most common chronic immune-mediated peripheral nerve disorder. It is an acquired, treatable demyelinating neuropathy with an estimated prevalence of 0.67 to 7.7 per 100,000 individuals. Males are more commonly affected than females (gender rate ratios range from 1.4 to 4.4),[1] and onset is most frequently between 40 and 60 years of age, although younger cases including paediatric can be seen.[2]

1.1.1.1 Pathophysiology

CIDP is currently thought to be the result of a complex interplay involving a combination of cellular, humoral, and cytokine-driven mechanisms. Evidence from pathological studies on nerve biopsy specimens shows that myelin is phagocytosed by macrophages,[3–9] likely activated by CD4+ T cells releasing IL-17, IL-2, IFN-γ and other proinflammatory cytokines.[10] Activated macrophages then act as antigen presenting cells and contribute to the release of cytokines, further activating CD4+ lymphocytes[11] and ultimately disrupting the integrity of the blood-nerve barrier.[12] CD8+ cytotoxic T lymphocytes have also been identified in the endoneurium[13] and have been shown to be clonally expanded in nerve biopsies.[14] Immunoglobulin treatment of CIDP leads to greater suppression of CD8+ activity compared to CD4+, which may suggest a more prominent role of CD8+ cells in CIDP pathogenesis,[15] although the same findings have not been replicated in other studies. Humoral mechanisms may also initiate or propagate demyelination in CIDP, but no antibody targets have yet been identified. Antibodies to nodal and paranodal antigens,[16] discussed later in this chapter, are found in the autoimmune nodopathies, which are now a considered to be distinct clinical entities and no longer variants of CIDP. Finally, complement is also involved in the pathogenesis of CIDP, and contributes by modulating humoral and cytotoxic responses.

Complement factors are thought to direct macrophage-associated Schwann cell phagocytosis through opsonisation and further cytokine release. Macrophages can engage complement components either directly, through complement receptors (CRs), or indirectly via Fc receptors that recognize the Fc region of immunoglobulins bound to C3b deposited on Schwann cells (Fig. 1.1).[17–22]

Figure 1.1. Immune mechanisms in CIDP

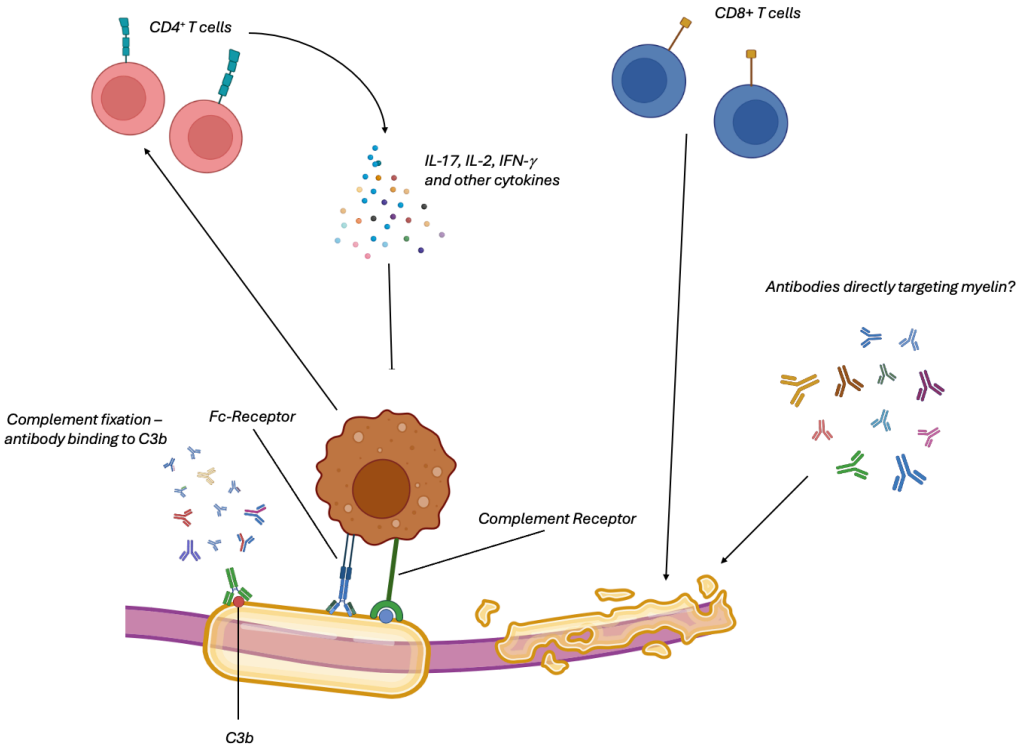

Schematic overview of immune mechanisms involved in CIDP. Macrophages, complement, antibodies, T cells, and B cells all likely contribute to nerve injury through both cellular and humoral immune pathways.

1.1.1.2 Clinical features

Typical CIDP presents with progressive or relapsing, symmetrical weakness that predominantly affects proximal more than distal muscles, in both the upper and lower limbs. Symptoms develop over a period of at least eight weeks and are accompanied by sensory involvement in two or more limbs. Deep tendon reflexes are characteristically absent. Tremor may be present, as with all demyelinating conditions, and in some cases can be prominent. In contrast, autonomic dysfunction is less usual.

Several CIDP variants have been described, each with distinct clinical characteristics that may pose diagnostic challenges. These include *multifocal* CIDP (multifocal acquired distal sensory and motor neuropathy, often referred to as MADSAM or Lewis-Sumner syndrome), *focal* CIDP, *distal* CIDP (also known as distal acquired demyelinating sensory neuropathy, or DADS), as well as *pure motor* and *pure sensory* forms. The differential diagnosis of these variants can be challenging and is discussed later in this chapter.

In some cases, CIDP may present with an acute onset (A-CIDP), characterized by rapid symptom progression within four weeks. This form can initially mimic GBS; however, A-CIDP typically progresses beyond the first month and is generally (but not always) not associated with features commonly seen in GBS, such as bulbar dysfunction (dysphagia and/or respiratory symptoms), cranial nerve involvement, or autonomic disturbance. Recognising these distinctions is crucial for accurate diagnosis and appropriate treatment.

1.1.1.3 Diagnosis of CIDP

The 2021 European Academy of Neurology/Peripheral Nerve Society (EAN/PNS) guidelines[23] recommend electrophysiology (with both motor and sensory nerve conduction studies) to support a clinical diagnosis of CIDP. If electrophysiology strongly supports demyelination, 'CIDP' is the diagnosis, whereas if the support for demyelination is weak, 'possible CIDP' should be diagnosed. In cases where clinical criteria are met but electrophysiological findings suggest only possible CIDP, additional investigations such as imaging, cerebrospinal fluid (CSF) analysis, or nerve biopsy may provide supportive evidence. Conversely, some of the CIDP mimics can also meet electrophysiological criteria for demyelination and may present with similar CSF and imaging findings, adding complexity to the diagnostic process. A positive response to immunotherapy can support a clinical diagnosis of CIDP but a lack of response does not exclude it, and improvement with treatment is not specific to CIDP alone.

1.1.1.4 CIDP mimics

A chronic, progressive neuropathy with predominantly proximal weakness is most suggestive of CIDP. The variant forms of CIDP, however, can pose diagnostic challenges, and are often misdiagnosed as other conditions with overlapping clinical features but distinct pathophysiological mechanisms.

Paraproteinaemic neuropathies

A paraprotein (also known as an M-protein or monoclonal gammopathy) is a monoclonal immunoglobulin secreted by a population of clonally expanded B cells. Normal

immunoglobulins are composed of a heavy chain, which determines the isotype (IgM, IgG, or IgA), and a light chain (either kappa or lambda). Paraproteins may be complete (formed by both heavy and light chains) or light chains only (kappa or lambda paraproteins). Paraproteins are relatively common in older adults, detected in 3%–4% of individuals over the age of 50,[24] and are found in approximately 10% of patients with a neuropathy of unknown cause.[25] Most paraproteinaemic neuropathies are IgM-related, and an IgM paraprotein is more likely to be pathogenic, particularly when the neuropathy is "demyelinating" on electrophysiology.[26–28]

Anti-myelin-associated glycoprotein neuropathy, commonly referred to as *anti-MAG neuropathy*, is a paraproteinaemic demyelinating neuropathy (PDN) where IgM antibodies selectively target MAG in Schwann cells. IgM kappa light chain paraproteins are most common, although IgM lambda can also be found. The clinical phenotype of anti-MAG neuropathy is distinctive: patients typically present with early unsteadiness and sensory ataxia, often followed by tremor and minimal distal weakness. Sensory examination reveals a striking loss of vibration sense, often extending up to the costal margins, in contrast to relatively mild impairment of small fibre function. Electrophysiology characteristically demonstrates distal, symmetrical demyelination with disproportionately prolonged distal motor latencies. Nerve biopsy will reveal widely spaced myelin, which is pathognomonic (Fig. 1.2). In anti-MAG neuropathy, the weakness is more often distal, whereas CIDP patients have proximal weakness and less profound loss of vibration. Distinguishing CIDP from anti-MAG neuropathy is crucial, as treatment strategies differ significantly: anti-MAG neuropathy typically responds to B cell depletion with rituximab, whereas IVIg and steroids alone are rarely effective.[29] However, in cases where MAG antibody testing is negative, and the clinical phenotype is CIDP-like, the presence of an IgM paraprotein may still suggest a better response to rituximab.[30,31]

Figure 1.2. Electron microscopy of normal versus widely spaced myelin

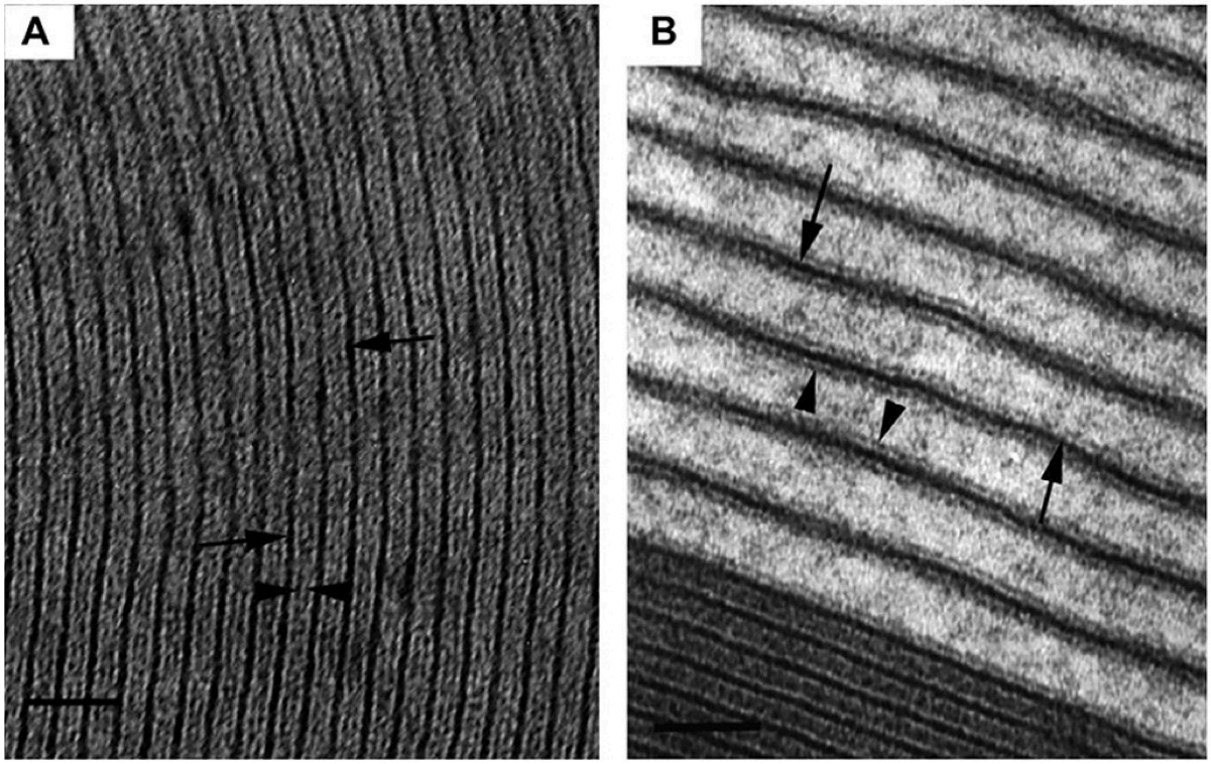

*Electron microscopy of normal myelin (**A**) versus widely spaced myelin (**B**) as observed in anti-MAG neuropathy.*[32]

- Another important differential diagnosis of CIDP is *multifocal motor neuropathy* (MMN), a less common neuropathy with a prevalence approximately one-third that of CIDP.[33] MMN is more frequently seen in men than women and is characterized by multifocal weakness that primarily affects the distal upper limbs, often with disproportionate weakness in finger extension, which can help distinguish it from other motor neuropathies. Unlike CIDP, MMN is distinguished by the absence of sensory involvement; patients may report sensory symptoms but examination should not reveal objective abnormalities, other than minor disturbance of vibration sense at the ankle.[34] As

the disease progresses, muscle wasting typically develops, particularly in the finger extensors and intrinsic hand muscles. The electrophysiological hallmark of MMN is conduction block, which helps differentiate it from other motor neuropathies, notably motor neuron disease where primary demyelination should not be present. IgM ganglioside antibodies to GM1 are detected in approximately 30-50% of cases,[35] and a paraprotein may be identified in some patients. It should be noted that, while MMN is sometimes included within the group of paraproteinaemic neuropathies (as it is here), it is not consistently classified as such as many patients have a negative serum protein electrophoresis. Although less commonly employed, magnetic resonance imaging (MRI) and ultrasound (USS) can also aid diagnosis by revealing nerve enlargement and/or contrast enhancement.[36,37] The mainstay of MMN treatment is intravenous immunoglobulin (IVIg), with subcutaneous immunoglobulin (SCIg) serving as an alternative option in some patients. Steroids often exacerbate symptoms in MMN, underscoring the importance of accurately distinguishing it from CIDP to ensure appropriate treatment.

- Polyneuropathy, organomegaly, endocrinopathy, M-protein, and skin changes (POEMS) syndrome is a paraneoplastic, multisystem disease, caused by a plasma cell neoplasm. It is a rare yet important differential diagnosis of CIDP. Like anti-MAG neuropathy and some forms of MMN, the neuropathy of POEMS syndrome is paraproteinaemic, but its pathology is associated with IgG or IgA paraproteins rather than IgM. IgG or IgA paraproteinaemic neuropathies often present as chronic, symmetrical, and predominantly sensory, and may resemble CIDP.[34] However, these presentations are generally more heterogeneous than those seen with IgM-related neuropathies. Patients with IgG or IgA MGUS (monoclonal gammopathy of undetermined significance) neuropathy often have

less weakness and relatively more sensory involvement, both clinically and electrophysiologically, compared to those with "idiopathic" CIDP.[34] Neurophysiological studies in these neuropathies are diverse, showing either demyelinating or axonal/mixed patterns in approximately equal proportions, further adding to the diagnostic complexity. Recognising such distinctive features is crucial to distinguishing POEMS syndrome and IgG/IgA-related neuropathies from CIDP and guiding appropriate management, as the treatment of POEMS syndrome primarily targets the underlying haematological cancer.

Autoimmune nodopathies

The autoimmune nodopathies (AIN) are neuropathies caused by autoantibodies targeting nodal or paranodal molecules: neurofascin 155 (NF155), neurofascin isoforms (NF140/186), contactin-1 (CNTN1), or contactin-associated protein 1 (Caspr1). Patients with AIN often have a neuropathy with more aggressive acute or subacute onset and additional symptoms including ataxia and tremor, as well as respiratory dysfunction and cranial nerve involvement – both of which are less common in CIDP. CSF protein levels tend to be significantly elevated, and patients do not respond to standard treatment with IVIg, corticosteroids, or plasma exchange (PLEX). It should be noted, however, that not all AIN patients present with such distinctive clinical features, and testing for nodal and paranodal antibodies should be pursued routinely: this is of therapeutic relevance, as robust evidence now shows that rituximab improves functional outcomes in patients with AIN, particularly if given early in the disease course.[30,38,39]

Other peripheral nerve disorders

The differential diagnosis of CIDP includes several other peripheral nerve disorders, particularly when the phenotype is atypical. In focal or multifocal presentations, entrapment neuropathies, hereditary neuropathy with liability to pressure palsies (HNPP), peripheral nerve tumours, or vasculitis should be considered. In cases of pure motor presentations, the differential may include motor neuron disease, neuromuscular junction disorders, or myopathies. Conversely, in pure sensory presentations, sensory neuronopathy is an important consideration. Charcot-Marie-Tooth (CMT) disease should be considered in patients with long-standing symptoms, particularly when these are less pronounced than clinical signs. Compared to CIDP, CMT may present with additional features such as hearing loss, scoliosis, and the development of ankle-foot deformities later in the disease course. CSF protein levels are typically normal or only mildly elevated in CMT, and standard immunotherapy is generally ineffective, further distinguishing it from CIDP.[40]

1.1.1.5 Treatment of CIDP

When warranted, treatment of CIDP should be commenced as soon as possible to minimise secondary axonal damage and associated clinical disability. First-line treatments in CIDP include corticosteroids, IVIg, or plasma exchange. IVIg is supported by the highest level of evidence,[41] there is no difference between IVIg and steroids,[42] and both are superior to placebo.[43] If tolerated, steroids may produce a longer lasting remission compared to IVIg. [44] B cell depletion with rituximab is not more effective than placebo in preventing clinical deterioration following IVIg cessation,[29] though may have a role in escalation therapy when response to IVIg is poor. Other immunosuppressants have been tried in CIDP but only cyclophosphamide has shown promise.[45] Efgartigimod (ARGX-113), a neonatal Fc receptor

(FcRn) antagonist that reduces pathogenic IgG antibodies by blocking their recycling,[46] is currently under investigation in CIDP. Steroids and plasma exchange may exacerbate symptoms and should be avoided in motor-predominant CIDP, MADSAM and MMN.

Most patients with CIDP respond to first-line immunotherapy; if clinical deterioration continues after initial treatment, diagnosis should be re-evaluated, with the caveat that IVIg can confound antibody testing and serum protein electrophoresis (which, in fact, should be done before commencing treatment) and CSF white cell count. Corticosteroids may mask neurolymphomatosis. Nerve biopsy might be needed if less invasive tests have been inconclusive and, if the most probable diagnosis remains CIDP, alternative immunosuppressive agents such as cyclophosphamide may be tried.

Ultimately, more than half of CIDP patients require assistance with walking or become bedbound at some point during their illness. At any given time, 13% of patients need mobility support or are confined to bed. Over 50% require ongoing treatment to maintain disease stability.[34,47]

1.1.2 Guillain-Barré syndrome

GBS is the leading cause of acute neuromuscular paralysis worldwide. It is a postinfectious, immune-mediated, monophasic polyradiculoneuropathy, primarily diagnosed on the basis of clinical patterns with or without the support of electrophysiology and laboratory findings. About a third of patients with GBS develop a severe, generalised neuropathy, and ultimately require mechanical ventilation due to respiratory failure. One in twenty patients die. The mainstay of treatment remains intravenous immunoglobulin or plasma exchange. Interval neurological examination and outcome measures are used to monitor disease activity and

response to treatment, whilst novel therapies are being explored and may soon contribute to clinical management.[48]

Each year, GBS affects an estimated 100,000 people worldwide.[49] Incidence varies geographically, with the lowest reported rates in Japan (0.44 per 100,000)[50] and the highest in Chile (2.12 per 100,000)[51] and Bangladesh (3.25 per 100,000),[52] likely reflecting differences in exposure to infectious organisms. Seasonal variations have been described,[53] and spikes in GBS cases have been reported following infectious outbreaks, most notably those caused by *Campylobacter jejuni*[54] and Zika virus.[55,56] GBS predominantly affects older adults, with peak incidence occurring between 50 and 70 years of age. Men are more commonly affected than women, with a male-to-female ratio of approximately 1.5:1.[49,57,58]

1.1.2.1 Pathophysiology

In GBS, disruption of axons and myelin is initiated by an immunological trigger. Most cases are postinfectious, with two-thirds of patients reporting preceding gastrointestinal or respiratory symptoms. *Campylobacter jejuni* remains the most frequently identified pathogenic trigger, causing GBS in approximately one in every 1000 cases. This occurs through molecular mimicry between the bacterium's surface lipo-oligosaccharide (LOS) and host peripheral nerve gangliosides. The resulting immune response generates cross-reactive antibodies targeting gangliosides such as GM1, GD1a, and GQ1b, ultimately leading to axoglial damage (Fig. 1.3). Other pathogens linked to GBS include Epstein-Barr virus (EBV), Cytomegalovirus (CMV), Mycoplasma pneumoniae, *Haemophilus influenzae*, influenza A virus, hepatitis E virus (HEV), and Zika virus. While the precise mechanisms underlying the relationship between most of these pathogens and nerve damage remain unclear, molecular mimicry involving *C. jejuni* and peripheral nerve glycans remains the most well-established

postinfectious mechanism in GBS. However, the process by which patients lose tolerance to self-glycans following *C. jejuni* infection has yet to be fully understood.

Some vaccines have been epidemiologically linked with a subsequent diagnosis of GBS. These include the vaccine for the 'swine flu' (A/New Jersey/76 influenza),[59] the recombinant zoster vaccine (RZV),[60] and the adenovirus-vectored SARS-CoV-2 vaccines.[61–63]

The risk of developing GBS may be increased in the six weeks following surgery,[64] with orthopaedic and gastrointestinal procedures posing the greatest risk, particularly in patients with active malignancy.[65] GBS has also been reported in stem cell transplant recipients undergoing immunosuppression with tacrolimus for graft-versus-host disease (GVHD) prophylaxis,[66] as well as in patients on immune checkpoint inhibitors.[67] Further studies are needed to clarify the exact risk associated with these treatments, as a definitive link has not been ascertained.

Figure 1.3. Molecular mimicry in GBS: cross-reactivity between *Campylobacter jejuni* LOS and nerve gangliosides

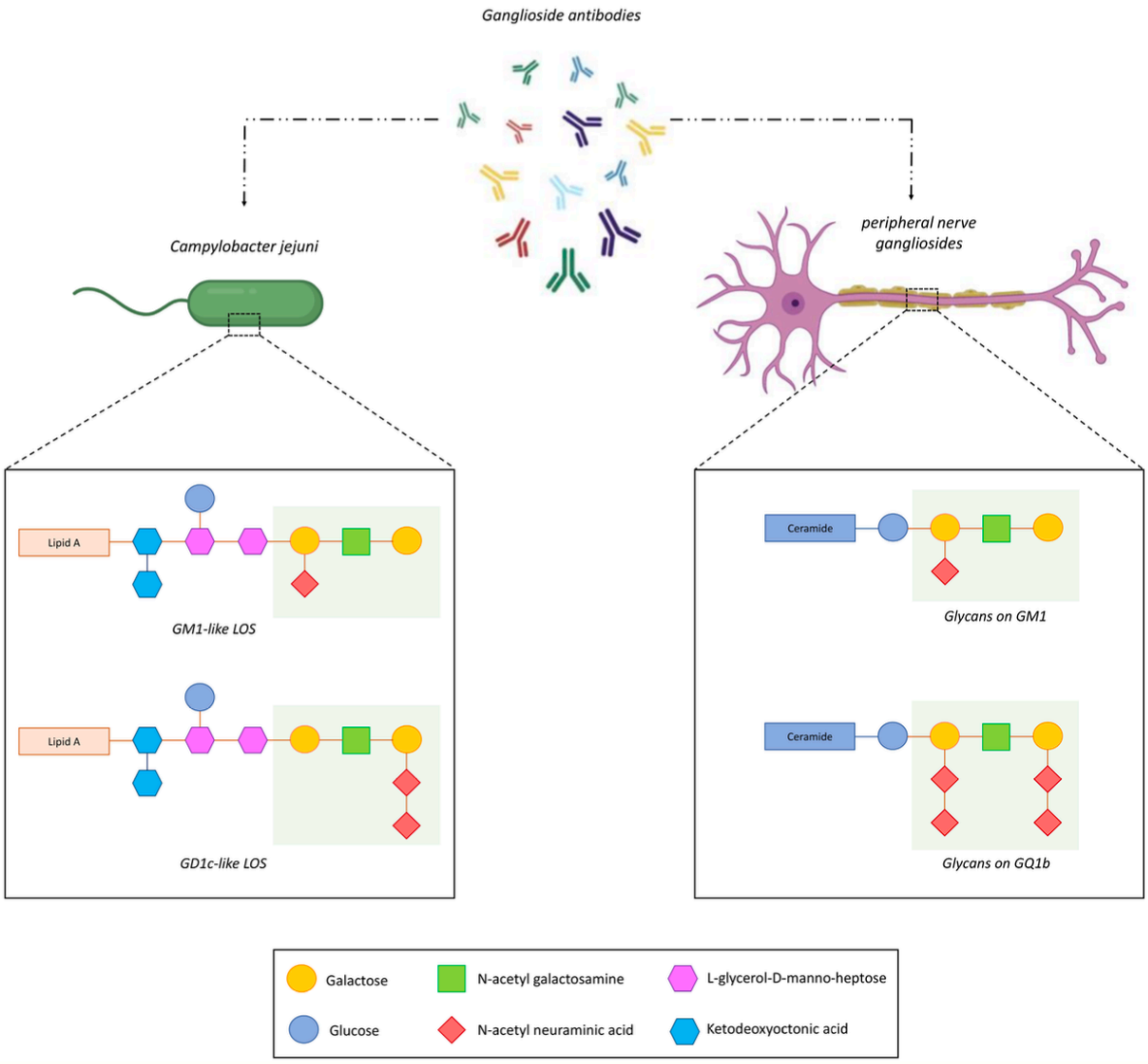

The lipo-oligosaccharide (LOS) on the outer membrane of Campylobacter jejuni induces cross-reactive antibodies which, through molecular mimicry, bind to the structurally identical glycans (areas in green) present on peripheral nerve gangliosides (GM1 and GQ1b in the example above), resulting in damage to axons and Schwann cells.[48]

Both innate and adaptive immune mechanisms are involved in the pathogenesis of GBS. While T cells, B cells, NK cells, dendritic cells, and macrophages all contribute to demyelination and axonal damage, the underlying mechanisms may vary between different electrophysiological subtypes of the disease. Traditionally, two main forms of GBS have been described: acute inflammatory demyelinating polyradiculoneuropathy (AIDP) and acute motor axonal neuropathy (AMAN). Recent research has shown that patients with AIDP have CD4+ and CD8+ T cells in their blood, CSF, and nerve tissue that are reactive to key myelin proteins, including myelin protein 0 (P0), myelin protein 2 (P2), and peripheral myelin protein 22 (PMP22)[48,68] (Fig. 1.4A). Such or similar autoreactive T cells were not found in AMAN patients. It remains to be established whether antibodies primarily targeting the Schwann cells exist, and if T cells are implicated in the activation of B cells.

Axonal damage is mediated by ganglioside antibodies[69–74] targeting axonal or glial antigens and causing damage through complement activation and MAC formation, or inducing myelin and axonal regeneration independent of complement. Membrane disruption aberrantly increases calcium influx into the axon, leading to calpain activation, and ultimately damaging the node of Ranvier, the paranode, and the motor nerve terminals (Fig. 1.4B)..[48,71,72,75,76]

The immunobiology of GBS may also be influenced by genetic factors. Polymorphisms of the tumour necrosis factor (TNF) and of the mannose-binding lectin (MBL) genes have been associated with GBS;[77,78] the latter contributes to complement activation and to the clearance of apoptotic cells by dendritic cells and macrophages. Large-scale research is still needed to clarify the genetic basis of GBS, with genome-wide association studies in well-characterized cohorts expected to provide further insights.

Figure 1.4. Pathogenesis of GBS: established and proposed immune mechanisms

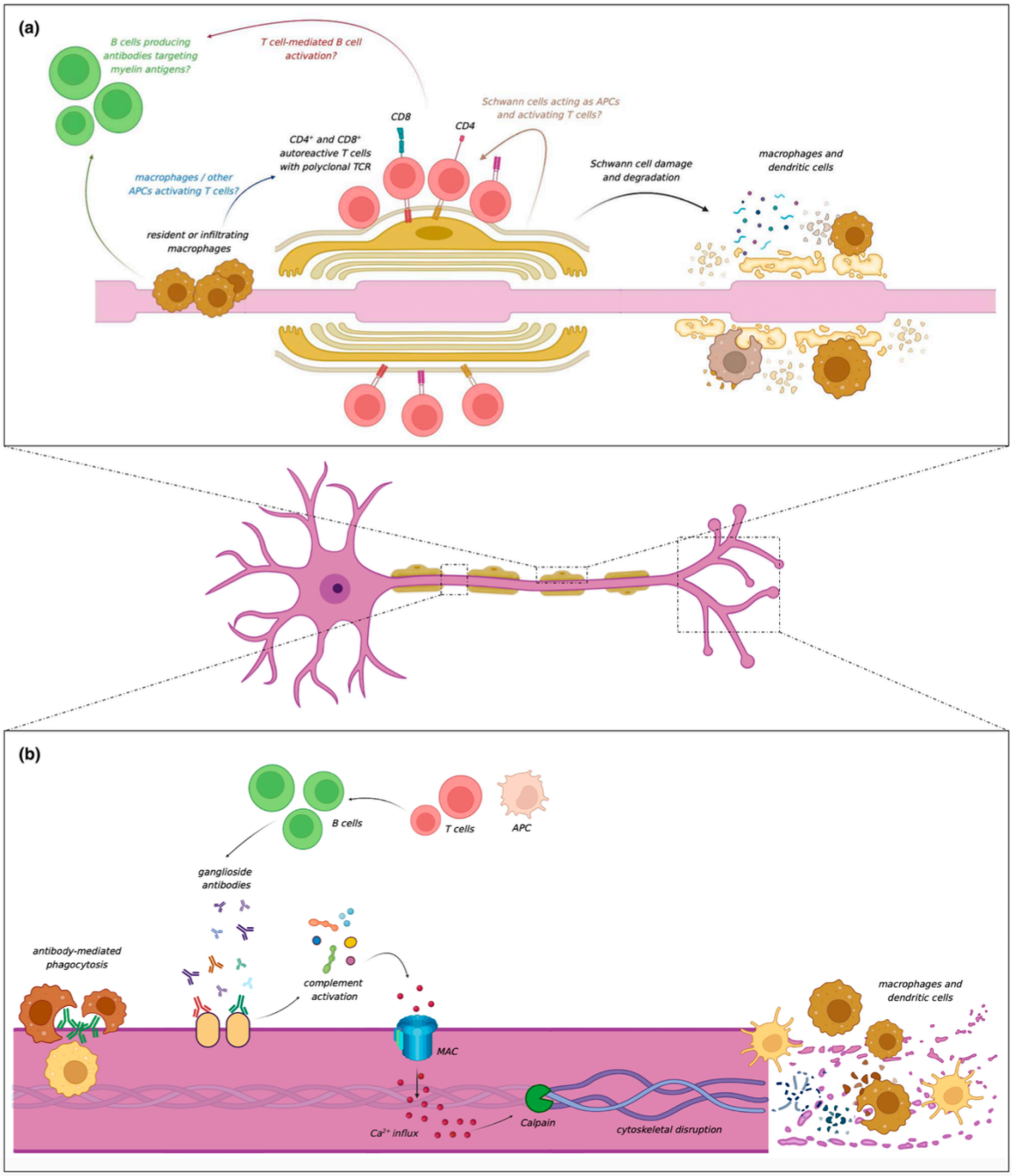

*(**A**) Autoreactive T cells targeting myelin antigens in the peripheral nervous system. Anti-myelin antibodies have not been identified yet. T cells might be activated by macrophages or other antigen-presenting cells (APCs). It has been hypothesised that the Schwann cells might act as APCs themselves. (**B**) In AMAN, ganglioside antibodies bind to their targets and induce complement activation, MAC formation, influx of calcium into the axolemma, cytoskeletal disruption, and ultimately nodal and paranodal destruction as well as damage to the motor terminals.*[48]

1.1.2.2 Clinical features and diagnosis of GBS

GBS typically presents with acute, rapidly progressive flaccid paralysis affecting the arms and legs, accompanied by absent or decreased deep tendon reflexes. Sensory disturbances may also be present, though this is variable. Most patients reach their peak disability (nadir) in the first two weeks, with symptoms rarely progressing beyond four weeks.[58,79,80]

The diagnosis of GBS is fundamentally clinical, based on clinical history and examination findings. The 2023 EAN/PNS guidelines on the diagnosis and management of GBS[81] state that progressive weakness of the upper and lower limbs developing over and not beyond 4 weeks, with absent or reduced deep tendon reflexes, are essential diagnostic criteria. While electrophysiological studies and CSF analysis can provide supportive evidence, they are not mandatory for the diagnosis. Imaging has a limited role but may occasionally be helpful (Table 1.1).

Initial hyperreflexia and sphincter dysfunction (bladder and/or bowel disturbance) are uncommon and often suggest an alternative diagnosis but do not exclude GBS. A sensory level typically points to a myelopathy, whilst encephalopathy or altered consciousness may indicate Bickerstaff brainstem encephalitis (BBE). It should be noted, however, that involvement of the thoracic roots or intercostal nerves can produce a pseudo-spinal level in GBS. This may manifest as an anterior "level" that is absent posteriorly, particularly in cases of length-dependent involvement.[48]

Some patients with GBS may experience recurrent clinical worsening following initial improvement or stabilization, a phenomenon known as treatment-related fluctuations (TRF). This can occur if the disease duration exceeds the therapeutic effect of treatment. However,

the occurrence of three or more TRFs and/or fluctuations beyond eight weeks is atypical for GBS and should prompt consideration of alternative diagnoses, such as CIDP or an autoimmune nodopathy.

CSF analysis and serology

Normal CSF protein is common during the first week of the disease and does not exclude GBS, and may be normal or only mildly elevated in the second week after onset of symptoms. Higher WCC should raise suspicion for infections (HIV, Lyme), haematological malignancy, or granulomatous inflammatory disorders such as sarcoidosis. Crucially, CSF should be sampled prior to treatment with IVIg, which typically raises both CSF protein and white cell count (WCC).

The CSF hallmark of GBS is albuminocytological dissociation, characterized by an elevated protein level with a normal WCC. Alongside an increased CSF/serum albumin quotient (Qalb), it reflects disruption of the blood-nerve barrier in the affected nerve roots, allowing proteins to diffuse into the subarachnoid space through the leaky vessels.[48] Normal CSF protein levels are common during the first week and do not exclude GBS; levels may also remain within normal range or only mildly elevated in the second week after symptom onset. A higher WCC should prompt consideration of alternative diagnoses such as infections (HIV, Lyme disease), granulomatous inflammatory conditions (sarcoidosis), or haematological malignancies.

Table 1.1 Guillain-Barré syndrome diagnostic criteria (2023 EAN/PNS guidelines)

Essential criteria

- Progressive weakness of upper and lower limbs
- Absent or decreased deep tendon reflexes
- Progression of clinical worsening not beyond 4 weeks

Clinical features supportive of GBS

- Symmetrical neuropathy
- Mild or absent sensory symptoms (compared to motor)
- Cranial nerve involvement (especially bilateral facial palsy)
- Respiratory failure
- Autonomic dysfunction
- Recent gastrointestinal or respiratory infection (<6 weeks)
- Back pain (interscapular or radicular)

Other supportive findings

- CSF albuminocytological dissociation
- Electrophysiology confirming peripheral neuropathy

The presence of ganglioside antibodies (of the IgG and/or IgM isotype) supports a diagnosis of autoimmune neuropathy, but their absence does not exclude GBS,[82] nor does it impact on clinical management or monitoring. On a prognostic level, high and persistent anti-GM1 antibody titers are associated with poor clinical recovery.[83] Anti-GQ1b antibodies have the highest specificity and should be tested in cases of suspected Miller Fisher syndrome (MFS) or GBS/MFS overlap. Nodal and paranodal antibodies should be tested in patients with poor response to treatment or recurrent TRFs, as a diagnosis of autoimmune nodopathy would impact on management and prognosis.

Electrophysiology

Traditionally, slowing of conduction velocity (CV), prolonged distal motor latencies, delayed F waves, temporal dispersion, and conduction block have been associated with the acute inflammatory demyelinating polyradiculoneuropathy (AIDP) form of GBS. Conversely, patients with substantially reduced compound muscle action potentials (CMAP) and relatively less severe conduction slowing have been classified as having the acute motor (and sensory) axonal neuropathy (AM[S]AN) form of GBS. Such distinction is no longer endorsed in the 2023 EAN/PNS guidelines, fundamentally because there is no gold standard to select among the various published criteria.[48,81]

The presence of a sural-sparing sensory pattern helps distinguish GBS from mimics,[84,85] whereas absent H-reflexes may suggest a radiculopathy[86,87] and their presence makes GBS unlikely.[88,89] It should be noted that neurophysiology may be normal in the first week, or show inexcitable nerves, indicating severe nerve damage, but a normal study several weeks after disease onset is extremely unusual.

Imaging

MRI and USS may be helpful in cases with diagnostic uncertainty. Spinal cord MRI might help discriminate between peripheral neuropathy and myelopathy, and may show nerve root contrast enhancement or enlargement in radiculopathies. However, diffuse nerve thickening is highly non-specific and can be found in a wide range of neuropathies including inflammatory, infective, infiltrative and genetic.[48]

1.1.2.3 Differential diagnosis of GBS

An acute or subacute onset with progressive symptoms over days or weeks, elevated CSF protein, and symptom improvement with immunotherapy are features that suggest an inflammatory neuropathy. GBS is most likely if the neuropathy is acute, inflammatory, and monophasic. The differential diagnosis includes other peripheral neuropathies, NMJ disorders and myopathies (discussed here) and CNS diseases (summarised in Fig. 1.5). In some cases, the diagnosis of GBS can only be confirmed or excluded with time.

Peripheral nerve

Autoimmune nodopathies can present with an acute, monophasic course similar to GBS, but they frequently exhibit additional distinguishing features. Patients with NF186 or pan-neurofascin (NF155, NF140 and NF186) antibodies often develop a severe neuropathy resembling GBS, characterised by cranial nerve involvement, respiratory compromise, and autonomic dysfunction. Clinical features that increase the likelihood of a diagnosis of autoimmune nodopathy or A-CIDP include the presence of three or more treatment-related fluctuations (TRFs), disease progression or relapse beyond eight weeks from symptom onset,

marked sensory ataxia, and the presence of nephrotic syndrome (often found in CNTN-1 autoimmune nodopathy).[90] A subacute disease onset (defined as a time to nadir exceeding two weeks) and/or prominent early reductions in motor conduction velocity may further support an alternative diagnosis to GBS. Differentiating GBS from CIDP is critical, as CIDP typically responds to corticosteroids, may require long-term or repeated immunotherapy, and can benefit from steroid-sparing agents. Autoimmune nodopathies, instead, tend to respond poorly to standard treatments, but may show clinical improvement if B-cell depleting therapy with rituximab is given early.[30,38,39]

Other peripheral nerve disorders may mimic GBS. Vasculitic neuropathies, while occasionally presenting acutely, more commonly follow a subacute course with symptom onset over several weeks and progression over months. The pattern is typically asymmetrical, multifocal, characteristic of a *mononeuritis multiplex* - in contrast to the generally symmetrical presentation of GBS and its variants (with the exception of rare monomelic forms). Pain in early GBS is most frequently located in the lower back, interscapular region, or follows a radicular distribution, and may persist for months despite immunosuppressive treatment.[91]

Certain infectious neuropathies can also mimic GBS by presenting with acute flaccid paralysis. These include neuropathies associated with Lyme disease, HIV, paralytic forms of rabies, and diphtheric polyneuropathy. Additionally, poliovirus infection targets the anterior horn cells of the spinal cord, leading to a poliomyelitis-related neuronopathy, particularly in unvaccinated individuals. This typically follows a prodromal phase marked by fever and myalgia, before the onset of motor symptoms.[92,93]

Non-polio enteroviruses more commonly present with gastrointestinal symptoms such as diarrhoea, fever, and general malaise. In approximately 20% of cases, these systemic symptoms are followed - typically one to two weeks later - by the development of a peripheral neuropathy.[94] HIV-associated neuropathy is often related to seroconversion and can closely mimic GBS; however, it is usually distinguished by a markedly elevated CSF white cell count. In patients with advanced HIV infection and profound immunosuppression (low CD4 counts), neuropathy may also result from opportunistic infections. Causative pathogens in such cases include CMV, EBV, HSV, and VZV. In rare instances, weakness may arise as a complication of antiretroviral therapy or from nutritional deficiencies, such as vitamin B1 deficiency.[93,95]

Toxic neuropathies caused by exposure to heavy metals - such as thallium, lead, arsenic, and mercury - can also mimic GBS and may present acutely or subacutely. These neuropathies can exhibit distinctive clinical patterns, including predominant upper limb weakness with wrist drop in lead poisoning, or pronounced sensory symptoms with sensory ataxia in mercury toxicity. Similarly, thiamine (vitamin B1) deficiency can produce a neuropathy that shares clinical features with GBS, such as areflexia and progressive ascending weakness. However, unlike GBS, it does not show CSF albuminocytological dissociation and lacks demyelinating features on neurophysiology.

Finally, acute intermittent porphyria (AIP) may cause a neuropathy that mimics GBS. This typically begins with symmetrical, proximal upper limb weakness, which may progress to involve the lower limbs. Less commonly, the initial presentation includes distal weakness, such as foot or wrist drop, with sensory symptoms being relatively uncommon.[96] Porphyric neuropathy can rapidly progress to tetraparesis, respiratory failure, and potentially death if not promptly treated. It is usually preceded by a prodromal phase featuring neuropsychiatric

disturbances, abdominal pain, gastrointestinal symptoms (nausea and vomiting), and autonomic dysfunction. While both AIP-related neuropathy and GBS are characterised by acute onset, rapid progression, and frequent autonomic involvement, porphyric neuropathy is typically axonal on nerve conduction studies, lacks albuminocytological dissociation in CSF, and does not respond to immunotherapy.

Figure 1.5. Differential diagnosis of GBS

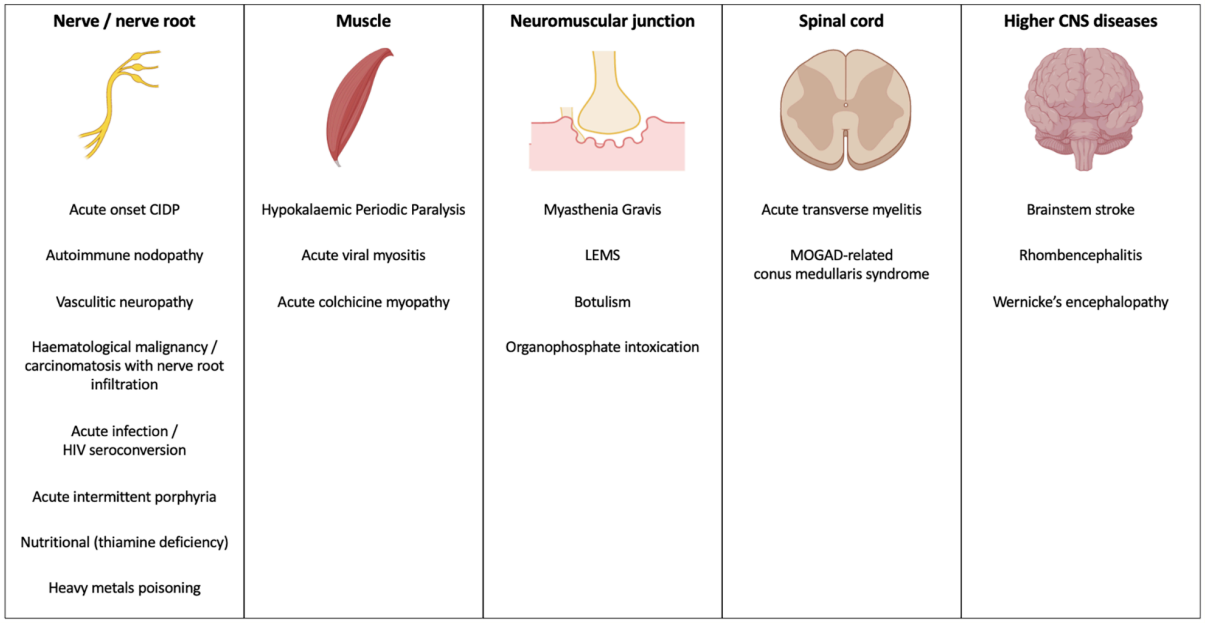

Differential diagnosis of Guillain-Barré syndrome. LEMS, Lambert–Eaton myasthenic syndrome; MOGAD, myelin oligodendrocyte glycoprotein antibody-associated disease.

Neuromuscular junction disorders

Myasthenia gravis (MG), the most prevalent disorder of the neuromuscular junction, is characterised by fatigable muscle weakness, often with diurnal fluctuations, preserved deep tendon reflexes, and a decremental response on repetitive nerve stimulation during electrophysiological testing. Bulbar-onset MG and MG associated with anti-muscle-specific kinase (anti-MuSK) antibodies can clinically resemble the pharyngeal-cervical-brachial variant of GBS, and vice versa. Lambert-Eaton myasthenic syndrome (LEMS), frequently paraneoplastic in origin, typically presents with proximal weakness that improves with exertion, reduced or absent reflexes, and an incremental response to repetitive nerve stimulation. While MG, LEMS and GBS can all present with muscle weakness, features such as fluctuating symptoms and activity-dependent changes in strength are not characteristic of GBS, where reflexes are generally absent.

Botulism, another NMJ disorder, may also mimic GBS, presenting with acute flaccid paralysis. However, botulism typically manifests with descending weakness and prominent autonomic signs such as fixed dilated pupils (mydriasis). Similarly, organophosphate poisoning leads to flaccid paralysis but is distinguished by a constellation of cholinergic features, including diarrhoea, urinary frequency, lacrimation, hyperhidrosis, hypersalivation, miosis, and bradycardia.

Myopathies

Acute muscle disorders that may mimic GBS include hypokalaemic periodic paralysis, certain forms of viral-induced acute myositis, and acute colchicine myopathy. Hypokalaemic periodic paralysis is characterised by recurrent episodes of flaccid weakness, typically

without sensory symptoms, sphincter dysfunction, or involvement of bulbar or respiratory muscles - features that help distinguish it from GBS. Viral myositides, such as those caused by influenza A, can present with rapid-onset paralysis accompanied by myalgia, fever, and rhabdomyolysis. These cases are often preceded by a prodromal phase of flu-like symptoms. In contrast to GBS, the presence of fever and rhabdomyolysis is more typical of viral myositis and less commonly observed in GBS. Acute colchicine myopathy may also mimic GBS, presenting with rapidly progressive weakness often preceded by gastrointestinal symptoms such as diarrhoea. However, key distinguishing features include the absence of cranial nerve involvement, elevated serum creatine kinase levels, and the presence of myotonic discharges on electromyography.[97]

1.1.2.4 Treatment of GBS

IVIg and PLEX are currently the only disease modifying therapies in GBS. Corticosteroids do not improve neurological outcome,[98,99] may delay recovery or cause side effects,[100,101] and are not beneficial even combination with IVIg.[102] Immunoadsorption, a procedure that selectively removes IgG from the blood by passing separated plasma through an absorption column, may be a safe and effective treatment. However, it is costly, not widely available, and not currently recommended as a first- or second-line therapy for GBS.[81]

IVIg and plasma exchange are equally efficacious but IVIg is less likely to be discontinued.[103] The choice of which therapy to offer is often guided by practical considerations and patient or clinician preference, with current guidelines not favouring one treatment over the other.[81] PLEX may be unavailable in some centres, while IVIg is generally easier to administer. Conversely, small vol PLEX may be only option in settings with poor resources. IVIg is usually well tolerated but carries a risk of thromboembolism,

particularly in patients with a history of thrombotic events.[104] PLEX is also well tolerated but can cause complications such as hypotension due to rapid fluid shifts, fluid overload, and vasovagal episodes. These may be more frequent in GBS patients, who often have labile blood pressure due to autonomic dysfunction. Allergic or anaphylactic reactions can also occur and are typically linked to the infusion of plasma or human albumin solution. Additionally, complications related to vascular access, such as line infections, sepsis, hematomas, venous thrombosis, and vascular injury, should be considered when selecting PLEX as a treatment option.[48,105]

Potential therapies and future directions

Several new therapies targeting the complement system are under investigation for GBS, though none have yet been adopted in routine clinical practice. Among these, eculizumab, a humanized monoclonal antibody that inhibits complement protein C5, has been tested in clinical trials. However, due to a lack of proven efficacy,[106] high costs, and potential adverse effects, eculizumab is not currently recommended for GBS treatment. Another complement inhibitor, ANX005, a monoclonal antibody targeting C1q, has shown promising early results. Preliminary data suggest that ANX005 may reduce neurofilament light chain (NfL) levels and reduce disability in the early stages of the disease.[107] Ongoing studies are assessing its long-term safety and efficacy. Imlifidase, an IgG-degrading enzyme derived from *Streptococcus pyogenes*, offers a novel approach by cleaving and inactivating all four subclasses of human IgG. In vitro studies have demonstrated its ability to indirectly block complement activation,[108] and in animal models of GBS with axonal injury, imlifidase reduced axonal degeneration and improved recovery.[109] While these therapies show promise, robust evidence from larger clinical trials is required before they can be integrated into standard GBS management.

1.1.2.5 Prognosis

GBS is a treatable disease and most patients ultimately recover. Around half of those affected return to their baseline function within a year,[110] and approximately 80% regain the ability to walk independently. However, GBS can lead to significant complications. Up to 10% of patients require prolonged mechanical ventilation, and severe, lasting disability occurs in more than 10% of cases. Mortality rates are estimated at 3–7% across all GBS patients,[110–112] increasing to approximately 20% in those who require ventilatory support. Death is usually due to sepsis, acute respiratory distress syndrome, pulmonary embolism, or cardiac arrest.[113] Factors associated with a worse prognosis include older age, rapidly progressing weakness (onset to hospital admission within seven days), severe weakness at presentation, ventilatory dependence, preceding diarrheal illness, and electrophysiological evidence of severe neuropathy.

1.1.3 Current outcome measures

Outcome measures in the inflammatory neuropathies are usually ordinal composite measures, and sum scores are generally used. These include the MRC sum score, the Inflammatory Rasch-built Overall Disability Scale (I-RODS, which however is not ordinal in its centile version), the Inflammatory Neuropathy Cause and Treatment (INCAT) disability scale, and the Overall Neuropathy Limitation Scale (ONLS). In GBS, disability is also measured using the GBS Disability Scale (GDS), also known as Hughes Disability Score.

MRC Sum Score

The MRC Sum Score (MRC-SS) was first developed to assess bedridden or ventilated patients with GBS and has then subsequently been used in a wide range of neurological diseases of the peripheral and central nervous system. It measures global muscle strength by assessing six muscle groups on both sides, with a scoring that ranges from 0 to 60. MRC-SS has served as an outcome measure in several clinical trials in patients with inflammatory neuropathies, and its interobserver agreement is 89%.[114,115]

I-RODS

The Inflammatory Rasch-built Overall Disability Scale (I-RODS) is a linearly weighted scale that focuses on day-to-day life functional limitations in patients with GBS and other inflammatory neuropathies (CIDP, multifocal motor neuropathy and paraproteinemic neuropathies).[116] Based on the Rasch model, which enables the conversion of ordinal data into an interval metric, I-RODS includes a wide range of item difficulties, from simple tasks such as “reading a newspaper” to “standing for hours” and “running”.

INCAT

The INCAT disability score evaluates upper and lower limb functional impairment based on the ability to perform daily life tasks.[117–119] Each category is scored from 0 to 5 and the total INCAT score ranges between 0 and 10, with higher scores indicating more severe impairment.

ONLS

The Overall Neuropathy Limitation Scale (ONLS) is often used to assess patients with GBS and was derived from the Overall Disability Sum Score (ODSS), which was the first scale designed to evaluate arm and leg functional limitations in patients with immune-mediated peripheral neuropathies, including GBS, CIDP and paraprotein-associated neuropathies.[120] Although the Arm Scale is identical in ODSS and ONLS, the latter was modified to include climbing stairs and running. The Arm Scale score ranges from 0 to 5, the Leg Scale from 0 to 7, and the total ONLS is 0-12.

GBS Disability Scale

The Guillain-Barré syndrome Disability Scale (GDS) was first introduced in a multicentre, randomised trial of prednisolone in GBS, and has been the most widely used outcome measure in the majority of GBS trials to date. Patient disability is graded on a seven-point scale ranging from 0 (no symptoms) to 6 (dead).[100]

Prediction of respiratory insufficiency in GBS

Early identification of patients at risk of severe GBS is crucial for timely intervention. The Erasmus GBS Respiratory Insufficiency Score (*EGRIS*) is a clinical tool designed to predict the likelihood of respiratory failure within the first week of hospital admission. This score is calculated based on specific clinical features identified at presentation.[121] A more recent version, the modified EGRIS (mEGRIS), extends this predictive capability to assess the risk of respiratory failure at any point during the first two months following symptom onset, rather than being limited to the first week. In practice, certain clinical features indicate a

higher risk of respiratory compromise. These include rapid disease progression within the first four weeks, bulbar palsy, and weakness of the neck and hip flexors. Such individuals should be monitored closely, with a low threshold for intensive care unit (ICU) admission if deterioration occurs.[122,123]

Prediction of functional outcome in GBS

The modified Erasmus GBS Outcome Score (*mEGOS*) is a predictive tool that estimates the likelihood of being unable to walk independently after GBS onset.[124] It incorporates three key variables: age at onset, preceding diarrhoea (which may suggest *Campylobacter jejuni* infection, severe axonal injury, and poorer prognosis), and the severity of muscle weakness, assessed both at admission and on day 7 using the Medical Research Council sum score (MRC-SS).

1.1.4 Limitations of non-fluid biomarkers

While neurological examination, electrophysiology and clinical scales remain cornerstone tools in the diagnosis and monitoring of peripheral neuropathies, several limitations hinder their utility as outcome measures, particularly in longitudinal settings. These limitations span issues of subjectivity, practicality, patient experience, accessibility, and sensitivity to disease progression.

1. **Subjectivity and inter-rater variability**

   Neurological examination findings and the interpretation of electrophysiological data are inherently subjective and prone to inter-observer variability. Even among experienced clinicians, differences in technique, interpretation, and scoring can result in

inconsistencies that limit the reproducibility of assessments. This lack of standardisation can be particularly problematic when attempting to compare disease status over time or across different clinical settings.

2. **Time consumption and resource intensity**

   Electrophysiological investigations are time-consuming, requiring considerable clinician input and infrastructure. Nerve conduction studies (NCS) and electromyography (EMG) often demand lengthy appointments, particularly when multiple nerves and limbs are assessed for comprehensive evaluation. This practical burden can limit their feasibility in routine clinical practice or in studies requiring serial assessments.

3. **Patient discomfort and poor tolerability**

   Electrophysiological tests are frequently poorly tolerated by patients due to the discomfort associated with electrical stimulation and needle EMG. This is especially relevant in patients with sensory hypersensitivity or severe weakness, where repeated testing may be contraindicated or refused. Poor tolerability can compromise data quality and hinder longitudinal follow-up.

4. **Requirement for specialist expertise and equipment**

   These assessments require trained personnel and specialised equipment, which may not be readily available in all clinical settings, particularly in resource-limited environments. This restricts their generalisability and makes them less suitable for widespread implementation, especially in multicentre studies or routine outpatient monitoring.

5. **Limited sensitivity and semi-quantitative nature**

Although useful for identifying specific patterns of nerve involvement (e.g. demyelinating vs axonal), both clinical examination and electrophysiology offer limited sensitivity to subtle or evolving pathological changes. Their semi-quantitative nature often fails to capture small but clinically meaningful variations in disease activity. For example, significant functional deterioration may occur without corresponding changes in nerve conduction parameters, particularly in chronic or patchy disease processes.

6. **Suboptimal for longitudinal monitoring**

   Given the combination of the above factors, these methods are poorly suited for tracking disease progression or treatment response over time. Variability in assessments, lack of granularity, and practical constraints limit their effectiveness in providing reliable, repeatable longitudinal data. This presents a major challenge in both clinical trials and real-world practice, where accurate monitoring of disease dynamics is critical.

Taken together, these limitations highlight the need for complementary biomarkers that are objective, sensitive, minimally invasive, and feasible for repeated measurement - characteristics increasingly sought in fluid biomarkers for peripheral neuropathies.

1.2 Fluid biomarkers in peripheral nerve disease

The development of ultrasensitive technologies for biomarker detection has led to increasing interest in fluid biomarkers - measured in blood or CSF - for peripheral nerve disorders. Both established and emerging biomarkers are being explored, including neuronal biomarkers of axonal degeneration and glial biomarkers indicative of peripheral demyelination.[82]

1.2.1 Neuronal biomarkers of axonal degeneration

Biomarkers of peripheral axonal degeneration hold significant promise for clinical application, with potential uses ranging from detecting nerve pathology to monitoring disease activity and therapeutic response. They may facilitate early identification and quantification of axonal injury, particularly in GBS, where elevated levels have been shown to correlate with poorer functional outcomes.[125] In CIDP, the degree of axonal damage is a key determinant of clinical disability and, consequently, an important predictor of long-term prognosis.

Neurofilaments

Neurofilaments are intermediate filaments located within the neuronal cytoplasm. Alongside microtubules and actin filaments, they constitute a major structural component of the axonal cytoskeleton in both the central and peripheral nervous systems. They are classified into light (NfL), medium (NfM), and heavy (NfH) chains based on their molecular weight and degree of phosphorylation, with each subtype contributing uniquely to the organization and function of the cytoskeletal framework.

NfL is an important but generic biomarker of axonal damage in the central and peripheral nervous systems.[126,127] In CIDP, plasma NfL is marginally higher before treatment with IVIg compared to healthy controls and in patients with active versus stable disease. Although NfL may decrease in some after treatment, it does not increase again with relapse after treatment withdrawal.[128–130] In GBS, serum NfL levels correlate with disease severity and axonal neurophysiology, and high baseline levels in early disease are associated with worse functional outcomes.[131,132] As such, NfL could contribute to improved clinical measures and

prognostic models in CIDP and GBS. However, due to the ubiquitous expression of NfL throughout the nervous system, it is not specific to any one disease,[133] and high levels of NfL can be found in over 80 peripheral and CNS conditions, as well as some non-neurological disorders.[133] The difference between plasma NfL in active or untreated disease compared to controls is marginal and often not definitive in indicating disease activity or progression in individual patients.

NfH, the larger and more heavily phosphorylated isoform, has been extensively investigated in amyotrophic lateral sclerosis (ALS),[134] where elevated levels in plasma, serum, and CSF have been linked to faster disease progression. In contrast, NfH appears to have limited utility as a biomarker in Charcot-Marie-Tooth disease (CMT), with studies reporting no significant differences in plasma concentrations between patients and healthy controls, and minimal change over time[21] - likely reflecting the slow and chronic nature of axonal degeneration, which is insufficient to exceed excretion or decay kinetics. In diabetic neuropathy, plasma NfH levels are only mildly increased compared to controls.[136] From an analytical perspective, NfH is also less robust than NfL. Its larger molecular size (200–220 kDa) increases susceptibility to hook effects, whereby excessively high analyte concentrations can result in artifactually low measurements and variability in plasma quantification[137,138] - limitations not typically observed with NfL.[139]

Neuron-specific enolase (NSE)

Neuron-specific enolase (NSE) is an intracellular enzyme expressed in neurons and neuroendocrine tumours, traditionally used as a prognostic biomarker in hypoxic-ischaemic brain injury. Elevated NSE levels have been observed in individuals with diabetes (both type 1 and type 2) and peripheral neuropathy, compared to diabetic patients without neuropathy.[26]

NSE has demonstrated a diagnostic sensitivity of 66.3% and a specificity of 72.5% for diabetic peripheral neuropathy.[26–28] However, longitudinal data on NSE levels over time are lacking. Further research is required to determine its clinical relevance and potential role in the monitoring of peripheral nerve disease.

Total Tau (t-tau)

Total tau (t-tau) is an established biomarker of axonal injury in the CNS.[33,34] It is expressed in both central and peripheral axons, with the highest concentrations found in the cerebral cortex,[35] where it plays a fundamental role in stabilising microtubules and supporting axonal transport.[36] Pathological aggregation of T-tau is characteristic of neurodegenerative diseases such as Alzheimer's disease (AD) and progressive supranuclear palsy (PSP).[37,38] Elevated serum levels have also been reported in AD, traumatic brain injury (TBI),[39] and hypoxic brain injury following cardiac arrest.[40] An observational, single-centre, retrospective study evaluating axonal injury biomarkers in inflammatory neuropathies[3] reported higher CSF T-tau levels in patients with CIDP compared to healthy controls. In the same study, plasma T-tau concentrations were elevated in patients with GBS, CIDP, paraproteinaemic demyelinating neuropathies (PDN), and MMN, compared to disease-free and healthy controls. While these findings suggest that plasma T-tau may have diagnostic value in acute and chronic inflammatory neuropathies, its prognostic or monitoring utility remains uncertain, as no data are currently available correlating T-tau with clinical outcome measures such as I-RODS. Moreover, the source of increased CSF T-tau in CIDP remains unclear - whether of central or peripheral origin - leaving its specificity for peripheral nerve pathology yet to be established.

1.2.2 Glial biomarkers for peripheral demyelinating disorders

Demyelination is the predominant pathological correlate in most cases of GBS, occurring in approximately 60–80% of patients in North America and Europe. In CIDP, macrophage-mediated myelin damage is thought to play a central role in pathogenesis, and demyelination is an important contributor to disability. Dysmyelination - the absence or abnormal development of peripheral myelin - is the pathological hallmark of certain genetic neuropathies. A fluid biomarker capable of detecting peripheral demyelination would be valuable for clinical management and disease classification. However, no such biomarker has yet been validated for clinical use. Several candidates have been investigated, including two glial proteins, TMPRSS5 and GFAP, as well as the myelin sphingolipid sphingomyelin.

Transmembrane Protease Serine 5 (TMPRSS5)

TMPRSS5 has been investigated as a potential Schwann cell biomarker in a study that profiled plasma from CMT1A patients and healthy controls.[41] Plasma levels of TMPRSS5 were significantly elevated in CMT1A compared to controls; however, no correlation was observed with clinical severity scores, nerve conduction velocities, or patient age. Importantly, TMPRSS5 levels were not significantly increased in other forms of CMT, including CMT2A, CMT2E, CMT1B, or CMT1X. Despite these limitations, TMPRSS5 represents the first Schwann cell-specific plasma protein shown to be elevated in patients with CMT1A.

Glial Fibrillary Acidic Protein (GFAP)

GFAP, an intermediate filament protein expressed in both the CNS and PNS, has been reported to be significantly elevated in the serum of patients with chronic axonal neuropathies—including vasculitic, toxic-alcoholic, diabetic, and idiopathic forms—when compared to individuals with CIDP, MMN, and healthy controls. Increased GFAP levels correlated with reduced sensory nerve action potential amplitudes and greater disease severity.[42] In the same study, GFAP was also modestly elevated in MMN compared to controls, although no significant difference was observed between CIDP and MMN. Longitudinal data on GFAP dynamics over time are lacking. Based on current evidence, GFAP appears to have limited utility for detecting or quantifying demyelination, and its performance relative to neuronal markers such as neurofilaments in assessing axonal degeneration remains unclear.

Sphingomyelin

In a prospective multicentre cohort study,[43] serum and CSF levels of sphingomyelin were assessed in patients with CIDP, axonal and demyelinating subtypes of GBS, non-demyelinating central nervous system disorders, and healthy controls. A fluorescence-based assay was employed, involving lipid extraction followed by a series of enzymatic reactions: sphingomyelin was first hydrolysed into phosphorylcholine and ceramide, then phosphorylcholine was converted to choline, which was subsequently oxidised to generate hydrogen peroxide and betaine. In the final step, horseradish peroxidase catalysed the reaction between hydrogen peroxide and dihydroxyphenoxazine, producing resorufin—a highly fluorescent compound used for quantification. Sphingomyelin concentrations were significantly elevated in the CSF of patients with CIDP and demyelinating GBS compared to

controls, while serum levels did not differ across diagnostic groups. However, the lack of peripheral nerve specificity, along with the absence of elevated serum levels in patients with active disease, limits the clinical utility of sphingomyelin as a biomarker for peripheral nerve demyelination.

Biomarkers of inflammation

Sialylated IgG-Fc - the Fc region of IgG antibodies bearing terminal sialic acid residues on their glycans - has been proposed as a biomarker of disease activity in CIDP. A study showed that both the absolute levels of sialylated IgG-Fc and the ratio of sialylated to agalactosylated IgG-Fc are reduced in the serum of patients with CIDP compared to healthy controls, correlating with clinical severity and increasing following IVIg treatment.[143] Elevated tumour necrosis factor alpha (TNF-α) levels have also been reported in a subset of CIDP patients with active disease, potentially correlating with the extent of electrophysiological conduction slowing.[144] Similarly, serum levels of endothelial leucocyte adhesion molecule 1 (ELAM-1 or selectin E) have been found to be higher in patients with CIDP and acute GBS compared to those with ALS, stroke, or healthy controls.[145] While sialylated IgG-Fc, TNF-α, and ELAM-1 may reflect inflammatory activity to some extent, they are non-specific markers of inflammation and are unlikely to have clinical utility in peripheral nerve disorders. Furthermore, these findings are based on small study cohorts and have yet to be independently validated.

1.2 Ultrasensitive assays for the measurement of fluid biomarkers

For many years, enzyme-linked immunosorbent assay (ELISA) has served as the practical gold standard for quantifying fluid biomarkers. However, this technique has notable

limitations, including the relatively large sample volumes required (typically 50-100 µl per test) and the need for millions of analyte molecules to produce a detectable signal, which restricts its sensitivity. Detection limits rarely fall below the nanogram per millilitre (ng/ml) range, rendering it unsuitable for identifying proteins present at lower concentrations in blood or CSF.

Recent advances have led to the development of ultrasensitive and multiplexed technologies capable of detecting disease biomarkers and other low-abundance molecules. While these methods are based on the same core principle as sandwich ELISA - the formation of immune complexes between antibodies and their target analytes - they incorporate novel approaches to antigen capture and presentation, signal amplification, imaging, and data analysis. The result is enhanced sensitivity by several orders of magnitude, which allows the detection of previously unmeasurable biomarkers using smaller sample volumes. Additionally, many of these platforms enable multiplexing, facilitating the simultaneous quantification of multiple analytes.

Single molecule array (Simoa) technology, chemiluminescence, electrochemiluminescence (ECL), proximity extension assays (PEA), and microfluidic immunoassays are the only ultrasensitive technologies that have thus far been applied in the study of peripheral neuropathies.

1.2.3 Single molecule array technology (Simoa)

The advent of single molecule array (Simoa) technology has marked a paradigm shift in biomarker discovery, allowing for routine detection of analytes that were previously beyond the reach of conventional methods. Its ultra-high sensitivity can be likened to detecting and

quantifying a single spoonful of sugar dissolved in an Olympic-sized swimming pool.[82] Compared to conventional ELISA, Simoa requires only minute amounts of analyte - down to 50 femtograms - to detect ultra-low concentrations of proteins and nucleic acids. This results in a dramatic increase in sensitivity and allows for detection limits in the attomolar range (10^{-16} M), vastly surpassing the capabilities of traditional methods.

Simoa is based on the capture and enzyme-labeled antibody detection of target analytes using paramagnetic beads, which are distributed into arrays of microwells for digital or analogue quantification. Paramagnetic beads are functionalised with capture antibodies that selectively bind the analyte of interest, which is then detected using biotinylated detection antibodies to form a classic immuno-sandwich complex. This complex - comprising the bead, capture antibody, analyte, and detection antibody - is subsequently labelled with an enzyme conjugate, streptavidin-β-galactosidase (SBG), as shown in Fig. 1.6. The labelled beads are resuspended in a fluorogenic substrate, resorufin β-D-galactopyranoside (RGP), and loaded onto a disc containing over 200,000 microwells, each designed to accommodate a single bead. A vacuum draws the beads into individual wells, and an oil layer is applied to remove excess beads and seal the wells. Fluorescent signal is generated when the enzyme catalyses the substrate, and a single analyte molecule can produce a detectable signal. This signal is captured via high-resolution imaging. At low analyte concentrations, the system operates in a digital mode, counting individual fluorescent wells in a binary ‘on–off’ manner. At higher concentrations, multiple immunocomplexes may form per bead, resulting in increased fluorescence intensity and enabling quantification in analogue mode. This dual-mode capability allows Simoa to achieve wider dynamic ranges and significantly greater sensitivity than conventional immunoassays.

1.2.4 Chemiluminescence and electrochemiluminescence (ECL)

Luminescence refers to the emission of light resulting from a chemical (chemiluminescence) or electrochemical (electrochemiluminescence, ECL) reaction. Both chemiluminescent enzyme immunoassays and ECL-based platforms have been used to measure biomarkers in disorders of the central and peripheral nervous systems.

Figure 1.6. Single Molecule Array (Simoa) technology

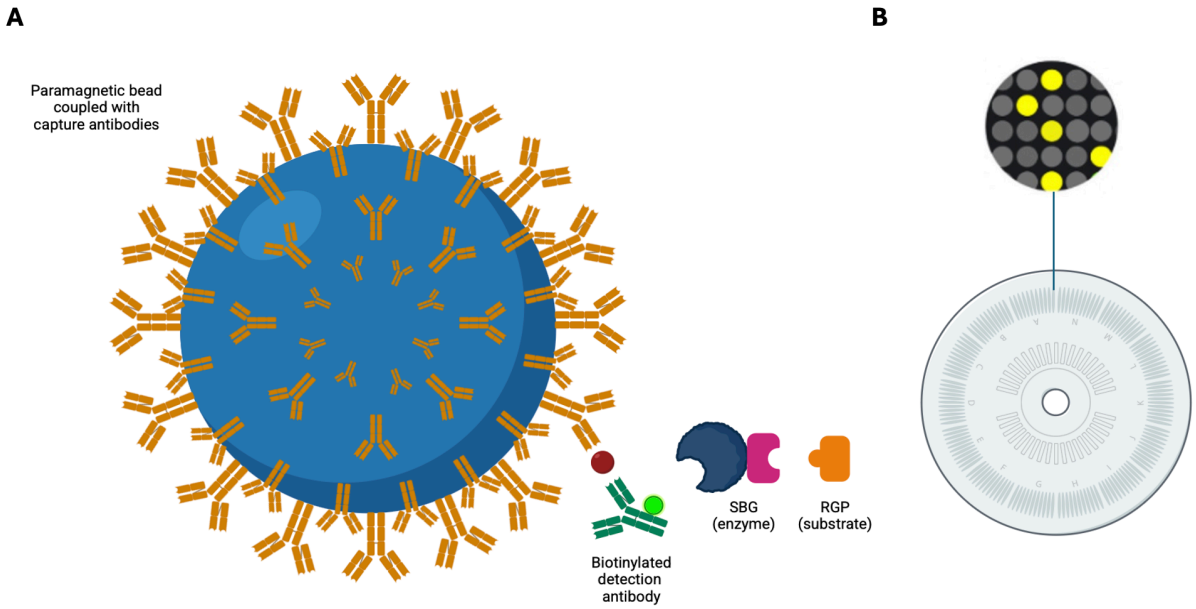

(A) *In Simoa assays, paramagnetic beads coated with capture antibodies specifically bind the target analyte. A biotinylated detection antibody then forms a sandwich complex, which is subsequently labeled with an enzyme (streptavidin-β-galactosidase, SGB) and incubated with a fluorescent substrate (resorufin-β-D-galactopyranoside, RGP) for signal development and analyte quantification.* ***(B)*** *The formed immune complexes are loaded onto a microwell array disc, where wells containing single bead-analyte complexes emit a fluorescent signal, enabling digital detection and quantification.*[82]

ECL is combined with multi-array technology for the simultaneous detection of multiple proteins within a single sample. This approach offers several advantages over traditional ELISA, including reduced background noise, signal amplification, enhanced sensitivity, and a broader dynamic range. Many ECL platforms support multiplexing, allowing for the quantification of up to 10 analytes from a single sample. Most assays are performed using multi-spot microplates, where electrodes are integrated at the base of each well. Each spot is coated with a distinct capture antibody. Following incubation with the sample, detection antibodies are introduced. A ruthenium-based SULFO-TAG is then applied, along with tripropylamine, to catalyse a light-emitting reaction upon application of an electrical current to the electrodes (Fig. 1.7). The intensity of the emitted light is proportional to the concentration of the target analyte. The SULFO-TAG can be directly conjugated to the detection antibody, to a secondary antibody, or coupled to streptavidin for use with biotinylated detection antibodies (Fig. 1.8).

Two widely used ECL-based platforms include Elecsys (Roche) and MSD (Meso Scale Discovery). Elecsys is primarily used in clinical diagnostics and operates as a single-analyte system on fully automated platforms such as the cobas analyzers. In contrast, MSD is designed for research applications and supports multiplex detection, allowing up to 10 analytes to be measured simultaneously within a single well. Both platforms use ECL detection based on ruthenium chemistry, but differ in throughput, clinical applicability, and degree of multiplexing.

A comparative study of conventional ELISA, ECL and Simoa technologies for the measurement of NfL in serum and CSF demonstrated that both Simoa and ECL are substantially more sensitive than ELISA. The reported limits of detection were 0.62 pg/ml for

Simoa, 15.6 pg/ml for ECL, and 78.0 pg/ml for ELISA[146] although the latest Simoa NfL assay kits now offer detection limits as low as 0.085 pg/ml.

Chemiluminescent enzyme immunoassay (CLEIA) technology is similar to ECL in that both rely on light emission generated by a chemical reaction for analyte detection. However, a key distinction is that ECL requires an electrode surface to initiate the luminescent reaction, whereas CLEIA does not. Chemiluminescent assays can also support multiplexing, and many platforms offer automation, which helps reduce intra- and inter-assay variability and improves precision. CLEIA is employed by several commercial platforms including Lumipulse (Fujirebio), now widely used in clinical and research settings for high-throughput and sensitive protein quantification. CLEIA has been applied to measure total tau levels in the CSF of patients with both acute and chronic inflammatory neuropathies,[147] with a previously reported detection limit of 141 pg/ml.[148]

Figure 1.7. Electrochemiluminescence

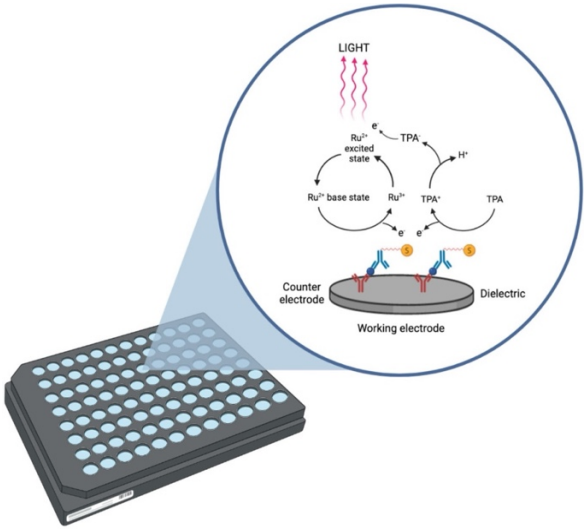

When an electrical potential is applied, the ruthenium (Ru) SULFO-TAG and tripropylamine (TPA), both electrochemically active, react and emit light. The ruthenium label is oxidised at the electrode surface and, simultaneously, TPA is oxidised to a radical cation that loses a proton. The resulting TPA radical reacts with oxidised ruthenium, which shifts to an excited state and decays, emitting a photon (620 nm).[82]

Figure 1.8. Immune sandwich configurations in ECL assays

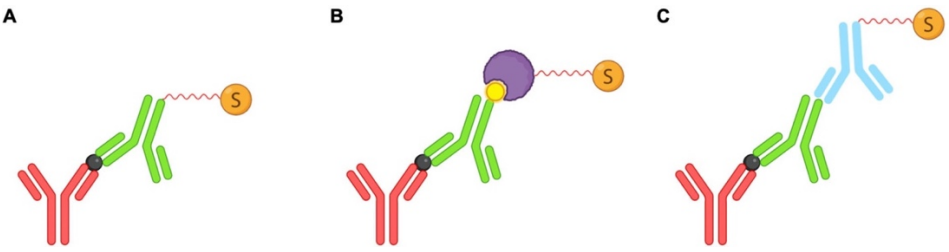

*Schematic representation of the three possible electrochemiluminescence immune sandwich configurations. In all combinations, the capture antibody (red) selectively binds to the analyte (black), which is then detected by the detection antibody (green). (**A**) Direct tagging of the detection antibody (green); (**B**) SULFO-TAG coupled with streptavidin (violet) binding to biotinylated detector antibody (green); (**C**) tagged secondary antibody (light blue) binding to detector (green).*[82]

1.2.5 Proximity Extension Assays (PEA)

Proximity Extension Assay (PEA) technology is based on the principle of immuno–polymerase chain reaction (immuno-PCR), combining the specificity of antibody-based detection with the amplification power of PCR. The assay begins with the binding of capture and detection antibodies to the target analyte, forming an immunocomplex. The detection antibody is conjugated to an oligonucleotide sequence, which pairs with a complementary oligonucleotide primer. This allows for DNA polymerase–dependent extension and subsequent PCR amplification. As a result, the signal generated by the immunocomplex is greatly amplified, achieving assay sensitivities up to 1,000 times higher than traditional ELISA.

However, early forms of immuno-PCR were limited by high background signals and long turnaround times due to multiple incubation and wash steps. These limitations have been addressed by the development of a more advanced PEA platform based on proximity-dependent DNA ligation. In this system, matched pairs of capture and detection antibodies bind to adjacent epitopes on the target protein.[149–151] Each antibody is conjugated to a unique single-stranded DNA (ssDNA) sequence specific to the analyte. Upon binding, the complementary ssDNA strands hybridize and serve as a primer for DNA polymerase–mediated extension during PCR. The resulting signal intensity is directly proportional to the protein concentration (Fig. 1.9). The use of complementary DNA sequences enhances specificity, reduces background signal, and eliminates the need for wash steps typically required in traditional immunoassays, thereby shortening turnaround times. This technology forms the basis of the Olink platform, a widely used commercial system for high-throughput protein biomarker profiling in research settings.

Proximity Extension Assay (PEA) typically reports results as Normalised Protein expression (NPX) values on a log2 scale, enabling the interpretation of relative differences in protein levels between samples or groups. Changes in NPX values can be translated into fold changes; for example, a difference of 1 NPX unit corresponds to a twofold change in protein concentration. While this relative quantification is useful for comparing protein expression patterns across conditions, it has important limitations. NPX values are not absolute concentrations, making it difficult to compare results across different platforms or studies. Additionally, reliance on fold changes may overemphasise biologically insignificant differences if baseline expression levels are low. Without absolute quantification, interpreting the clinical significance of changes - particularly for low-abundance proteins - can be challenging. Therefore, while fold changes derived from PEA offer valuable insights, they should be interpreted cautiously and ideally supported by orthogonal validation methods.

Figure 1.9. Proximity extension assay technology

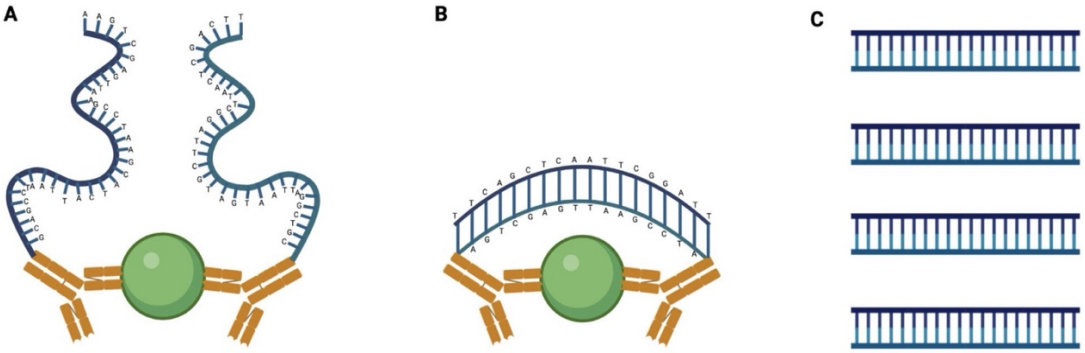

*(**A**) A pair of antibodies labelled with DNA oligonucleotides bind their target analyte. (**B**) Brought into proximity, oligonucleotides hybridise and are extended by a DNA polymerase. (**C**) This newly formed DNA barcode is then amplified by PCR ready for readout by quantitative PCR.*[82]

1.2.6 Microfluidic immunoassays

Microfluidic technology, implemented on platforms such as the enzyme-linked ligand assay (ELLA), uses cartridge-based assays to measure analytes and, like traditional and digital ELISA, relies on antigen capture followed by enzyme-labelled antibody detection. However, instead of combining multiple assays in a single reaction chamber as in conventional multiplex systems, each sample is divided into parallel microfluidic channels - each coated with a distinct capture antibody (Fig. 1.10). This design is more accurately described as "multi-analyte" rather than multiplex. By separating assays into individual channels, this parallel-plexing approach enhances sensitivity - reportedly achieving limits of detection as low as 2.7 pg/ml[152] - and minimises the risk of cross-reactivity between antibody pairs.

In a study comparing Simoa, Ella, Lumipulse (CLEIA), and Elecsys (ECL) for the measurement of NfL in patients with ALS, the results were consistent and reproducible across platforms, supporting the reliability and robustness of these methods for biomarker quantification.[153]

Figure 1.10. Microfluidic immunoassay technology

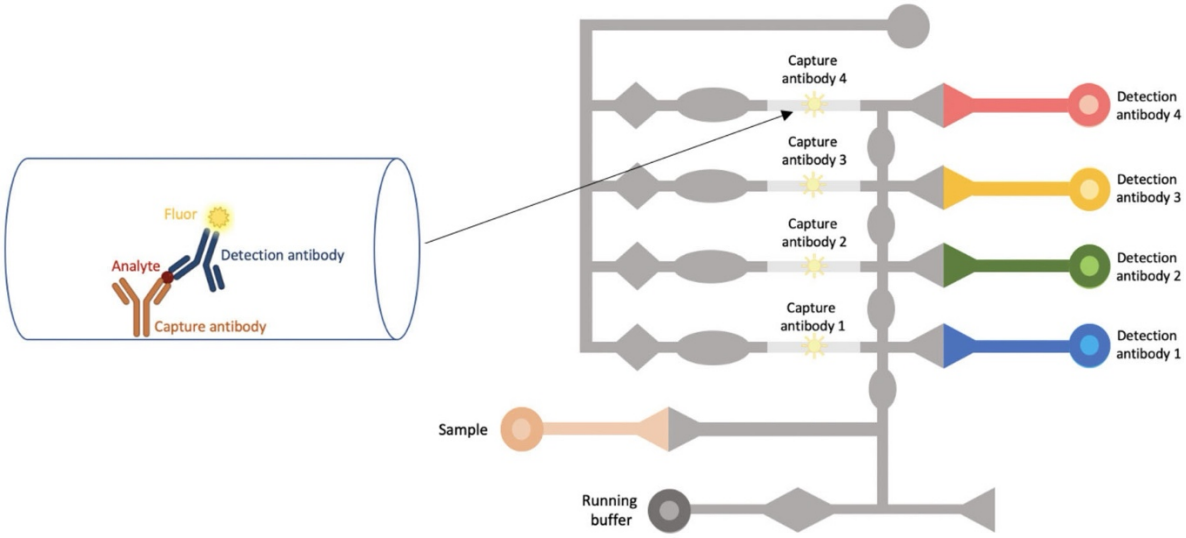

Schematic representation of a microfluidic immunoassay. Each sample is divided into four parallel, isolated microfluidic channels, with each channel containing a single-plex immunoassay designed to detect a specific analyte.

1.3 Aims, objectives and hypotheses

1.3.1 Rationale for the study

Assessing disease progression and informing clinical trials in peripheral neuropathy would benefit from objective and responsive fluid biomarkers closely linked to disease biology. This is particularly important in CIDP and GBS, where reliable biomarkers of peripheral demyelination and axonal damage would help identify, and potentially measure, active disease and responses to treatment.

The primary aim of this study was to develop an ultrasensitive assay to measure periaxin, a protein exclusively expressed by myelinating Schwann cells, and to evaluate its potential as a biomarker of peripheral nerve demyelination. A secondary aim was to optimise a previously developed assay for peripherin, an intermediate filament protein predominantly expressed in the peripheral nervous system. Periaxin and peripherin were investigated as candidate biomarkers of peripheral nerve disease, alongside NfL, with periaxin indicating demyelination and peripherin and NfL both reflecting axonal injury.

The full process of assay development – from initial conception through to analytical validation - is described in Chapter 3. Chapter 4 discusses the use of in vitro models of neuropathy for assay validation. Chapters 5 and 6 evaluate the clinical utility of periaxin, peripherin and NfL in peripheral neuropathy.

1.3.2 Study hypotheses

1. Peripheral myelin and axon specific proteins are released in the systemic circulation upon peripheral nerve damage. Their levels can be accurately measured in plasma and/or serum using ultrasensitive immunoassays.
2. The ratio of periaxin to peripherin - and vice versa - distinguishes primary demyelinating from axonal neuropathies and correlates with the severity of peripheral nerve damage.
3. Periaxin and peripherin are not released in the absence of peripheral nerve disease or with isolated central nervous system pathology.
4. Periaxin and peripherin distinguish active from quiescent demyelination or axonal loss, respectively.
5. Levels of periaxin and peripherin correlate with neurological outcomes in patients with inflammatory neuropathies.

1.3.3 Study aims

1. Develop an ultrasensitive assay for the measurement of periaxin in blood (plasma and/or serum) and cell culture supernatants.
2. Optimise the previously developed Simoa-based peripherin assay.
3. Develop biomarkers to distinguish PNS from CNS pathology, and disease from healthy conditions.
4. Develop biomarkers capable of discriminating primary demyelinating from axonal peripheral nerve injury.
5. Develop biomarkers which can differentiate active from quiescent disease in CIDP.
6. Develop biomarkers that correlate with neurological outcome at one year, as measured by validated clinical scales.

2. METHODS

This chapter outlines the key methodologies employed in this study. Humanised myelinating peripheral nerve cocultures were used to model antibody-mediated demyelination and axonal degeneration in vitro. Biomarker levels in culture supernatants were then correlated with the directly observed type and extent of morphological injury. To support clinical relevance, the assays were subsequently validated using blood samples from patients with inflammatory and inherited neuropathies. Accordingly, this chapter details the generation and maintenance of myelinating cocultures, methods for inducing axoglial injury, immunohistochemistry protocols, the Simoa NfL assay, participant recruitment, and ethical approvals. The technical development and optimisation of the periaxin and peripherin biomarker assays are covered separately in Chapter 3.

2.1 Generation and maintenance of myelinating cocultures

Myelinating coculture systems were generated using human induced pluripotent stem cell (IPSC) derived sensory neurons and rodent Schwann cells. IPSC from healthy control subjects were obtained through the IMI/EU sponsored StemBANCC consortium via the Human Biomaterials Resource Centre, University of Birmingham, UK.

2.1.1 Induced pluripotent stem cell maintenance and differentiation

IPSCs were thawed and plated onto Matrigel®-coated plasticware in mTeSR1 medium, which was refreshed daily. Cells were passaged at approximately 80% confluence using TrypLE Express (ThermoFisher) onto fresh Matrigel®-coated plates. A Rho-associated,

coiled-coil containing protein kinase (ROCK) inhibitor (ScienCell) was added to the medium at a final concentration of 10 μM for 24 hours following each passage to enhance cell survival. Prior to initiating differentiation, IPSCs were seeded onto Matrigel®-coated 6-well plates. After 24 hours, the medium was switched from mTeSR1 to mouse embryonic fibroblast (MEF)-conditioned medium (ScienCell) supplemented with 10 ng/mL human recombinant FGF2. Cells were expanded in this medium until reaching ~50% confluence, at which point differentiation was initiated.[154]

Differentiation proceeded via a stepwise transition from knockout serum replacement medium to N2 medium over an 11-day period. On day 11, immature neurons were dissociated using TrypLE (Gibco) and replated onto Matrigel®-coated coverslips in 100% N2 medium supplemented with human recombinant NGF, GDNF, BDNF, and NT3. Medium changes were performed twice weekly thereafter. This differentiation protocol yielded a highly pure neuronal population within 2–3 weeks following completion of the small molecule inhibitor stage.

2.1.2 Schwann cell harvesting and culture

All procedures involving animals were conducted in accordance with UK Home Office legislation (Animals [Scientific Procedures] Act 1986). Schwann cells were isolated from the sciatic nerve and brachial plexus of postnatal day 3 or 4 rats. Rat-derived Schwann cells were used due to the availability of well-established culture protocols and their proven capacity for multiple in vitro expansions, enabling the generation of cryopreserved cell stocks. Nerve tissues were enzymatically dissociated by incubation in collagenase (3 mg/mL; Sigma) and dispase II protease (2.5 mg/mL; Sigma) for 1 hour at 37°C. Following digestion, the tissue was gently triturated using a P1000 pipette tip and plated onto poly-D-lysine (PDL) and laminin-coated plastic in Schwann cell expansion

medium [DMEM/F12 (ThermoFisher) supplemented with 10% foetal bovine serum (ThermoFisher), 200 ng/mL NRG1-β1 EGF domain (R&D Systems), 10 ng/mL recombinant murine NGF (Peprotech), and 4 μg/mL forskolin (Sigma)]. To minimise fibroblast contamination, cultures were serially treated with 5–10 μM cytosine β-D-arabinofuranoside (araC). After approximately four passages - each time doubling the culture surface area - cells were cryopreserved using a Mr Frosty freezing container (ThermoFisher) and stored in liquid nitrogen.

2.1.3 Generation of myelinating cocultures

To initiate cocultures, frozen Schwann cells were rapidly thawed in a 37°C water bath, then washed by centrifugation in phosphate-buffered saline (PBS) and resuspended in a defined Schwann cell basal medium. This medium consisted of DMEM/F12 (ThermoFisher) supplemented with 5 μg/ml insulin (Sigma), 100 μg/ml transferrin (Millipore), 25 ng/ml recombinant human NGF (Peprotech), 25 ng/ml selenium (Sigma), 25 ng/ml thyroxine (Sigma), 30 ng/ml progesterone (Sigma), 25 ng/ml triiodothyronine (Sigma), and 8 μg/ml putrescine (Sigma). Prior to Schwann cell addition, the medium on IPSC-derived neuronal cultures was switched from N2 medium to the Schwann cell basal formulation. Between 25,000 and 50,000 Schwann cells suspended in 100 μl were gently added to each well of a 96-well plate containing the neurons, carefully avoiding contact between the pipette tip and the well bottom. Plates were immediately returned to the incubator to facilitate Schwann cell attachment. Two days after plating, the culture medium was refreshed. A second medium change followed at day 4 post-Schwann cell addition. One week after initiating coculture, myelination was triggered by replacing the medium with a myelination-inducing formulation consisting of N2 medium supplemented with 1:300 phenol-free Matrigel® (Scientific Laboratory Supplies), 5% charcoal-stripped fetal bovine serum (ThermoFisher), 25 ng/ml recombinant human NGF (Peprotech), and 50 μg/ml ascorbic acid (Sigma). From this point onward, the medium was changed once per week to support ongoing myelination.

2.2 Methods for inducing axoglial damage in vitro

Demyelination was induced by applying serum with previously validated IgG reactivity against myelin to the cultures[155] at a 1:50 dilution. To model axonal injury, a monoclonal anti-GD2 antibody (14G2A) was used at a concentration of 10 µg/ml in neurobasal medium supplemented with N2 (Cat. No. 17502-048), B27 (Cat. No. 12587-010), Glutamax (Cat. No. 35050-038), and an antibiotic-antimycotic mixture containing penicillin, streptomycin, and amphotericin (Cat. No. 15240-062), all from Gibco, Life Technologies. This complete neurobasal medium also contained recombinant human β-NGF (rhNGF) at 25 ng/ml (Cat. No. 450-01, Peprotech). One hour following incubation with either antibody or serum, 20% normal human serum (NHS 20%) was added to induce complement-mediated demyelination and/or axonal injury. Culture supernatants were then collected at defined time points from three wells per condition - demyelination, axonal injury, and control (complete neurobasal medium with β-NGF) - as detailed later.

2.3 Immunohistochemistry

2.3.1 Immunohistochemistry of fixed cell-cultures

For immunocytochemistry, coverslips were transferred to PBS, fixed with 4% paraformaldehyde for 30 minutes, and washed three times in PBS. Cells were then permeabilized with ice-cold methanol for 20 minutes, followed by three additional PBS washes. Blocking was performed using PBS containing 5% normal goat serum (NGS), after which cells were washed and incubated overnight at 4°C with primary antibodies. For axonal staining, either chicken anti-neurofilament heavy chain (NFH) antibody (Abcam, ab204893; 1:10,000) or mouse anti-peripherin monoclonal antibody (Santa Cruz, sc-377093; 1:1,000) was used. For myelin detection, rat anti-myelin basic protein (MBP) antibody (Abcam,

ab40390; 1:500), mouse anti-periaxin monoclonal antibody (Santa Cruz, sc-515672), or rabbit anti-periaxin polyclonal antibody (Biorbyt, orb413079) were applied. Following primary antibody incubation, cells were washed in PBS and incubated for 1 hour at room temperature on an orbital shaker (500 rpm, protected from light) with the appropriate secondary antibodies: goat anti-chicken Biotin (1:500, Life Technologies BA9010), goat anti-rat Alexa Fluor 546 (1:1,000, Life Technologies A11081), goat anti-mouse Alexa Fluor 647 (Thermo Fisher A-21236), or goat anti-rabbit Alexa Fluor 488 (Thermo Fisher A-11008). After further PBS washes, Streptavidin-Pacific Blue (1:500, Life Technologies S11222) was applied. Coverslips were then mounted onto Superfrost Plus microscope slides (Thermo Scientific) using Vectashield mounting medium (Vector Laboratories). Demyelination and axonal degeneration were confirmed through confocal microscopy, and systematic random sampling was used to ensure objective coverage across the coverslip. Myelin fragmentation was quantified using thresholded MBP signal in ImageJ, calculated as: (myelin fragment area) / (total myelin area – non-specific particle area) x 100. Confocal imaging was performed using a Zeiss LSM700 confocal microscope or an Olympus SpinSR10 spinning disk confocal microscope.

2.3.2 Immunohistochemistry of nervous tissue

Frozen human tissue samples were obtained from the cerebral cortex, cerebellum, optic nerve, and spinal cord. Rodent spinal cord tissue was dissected from postnatal day 56 (P56) Sprague Dawley rats, sectioned into 1 cm segments, and snap-frozen in liquid nitrogen. All samples were stored at −80°C until further use. Thoracic spinal cord segments were further subdivided into 0.2 mm transverse slices, cryosectioned at 10 μm thickness, and mounted onto Polysine slides (631-0107, Avantor). For peripheral nerve tissue, pre-prepared slides containing monkey peripheral nerve cross-sections (504210, NOVA Lite) and formalin-fixed, paraffin-embedded (FFPE) human peripheral nerve

sections were used. FFPE sections underwent dewaxing in xylene to remove paraffin and unmask epitopes, followed by graded washes in xylene and ethanol. Rehydration was completed using decreasing concentrations of ethanol in water, ending with a final rinse in distilled water. Immunostaining was performed at room temperature. All tissue sections were blocked with 5% bovine serum albumin (BSA) for 1 hour. Primary antibodies—mouse monoclonal anti-periaxin (sc-515672, Santa Cruz) at 1:250 and chicken polyclonal anti-β-tubulin III (302306, Synaptic Systems) at 1:1000—were diluted in 1% BSA and applied for 1 hour. Sections were then washed three times in phosphate-buffered saline (PBS), each for 10 minutes. Secondary antibodies—goat anti-mouse Alexa Fluor 647 (A-21236, Thermo Fisher) and goat anti-chicken Alexa Fluor 555 (A-21437)—were applied at 1:1000 dilution in 1% BSA-PBS for 1 hour, followed by PBS washes. Nuclei were counterstained with PureBlu Hoechst 33342 (135-1304, Bio-Rad), diluted to 1 mg/mL in distilled water, incubated for 10 minutes, and washed. Imaging was conducted using a NanoZoomer S60 Digital Scanner (model C13210-01).

2.4 Simoa NfL assay

NfL concentrations were quantified using the Quanterix NF-light® v2 Advantage Kit (Cat. No. 104073) on the Simoa HD-X Analyzer, according to the manufacturer's instructions for the two-step digital immunoassay format. Calibrators and controls were stored at −80°C, while all other reagents were kept upright at 2–8°C. Prior to the assay, all reagents were brought to room temperature. Serum and plasma samples were loaded onto the plate undiluted, with a 1:4 onboard dilution performed automatically by the instrument. Each 96-well plate included eight calibrators in triplicate, two controls in duplicate, and 34 test samples in duplicate. Calibrators were added at 130 µl per triplicate set, and samples and controls were added at 80 µl per well. The calibrator range extended from 0 to 450 pg/ml, corresponding to a measurable concentration range of up to 1,800 pg/ml for serum and

plasma. The assay was performed using a two-step protocol. In the first step, paramagnetic beads coated with anti-NfL capture antibodies were incubated with each sample and a biotinylated detector antibody. During this incubation, NfL present in the sample formed a sandwich complex with the capture and detector antibodies. After a wash step to remove unbound material, the second step involved incubation with streptavidin-conjugated β-galactosidase, followed by a final wash and addition of the fluorescent substrate. Signal detection was performed on the HD-X Analyzer using digital counting of individual enzyme-labelled beads in reaction wells, enabling high-sensitivity single-molecule quantification. A standard curve was generated (Figure 2.2) using the calibrators, and sample concentrations were interpolated using a four-parameter logistic (4PL) model. All measurements were performed in duplicate. Only values with intra-assay coefficients of variation below 15% were considered acceptable for downstream analysis.

Figure 2.2. NfL Simoa standard curve

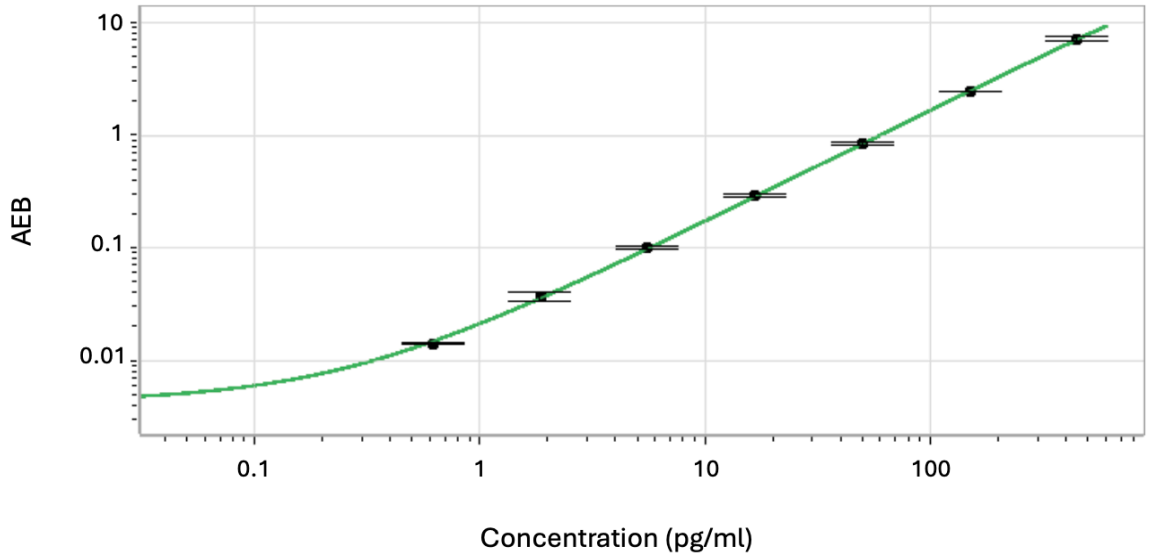

Simoa NfL standard curve. Lower limit of detection: 0.34 pg/ml. AEB: Average Enzyme per Bead.

2.5 Participants and clinical samples

2.5.1 Sample sources

Samples were obtained from multiple clinical centres.

- CIDP samples were collected from the Manchester Centre for Clinical Neurosciences at Salford Royal Hospital, the John Radcliffe Hospital in Oxford, the National Hospital for Neurology and Neurosurgery (NHNN) in London, and the Department of Neurology at the University of KwaZulu-Natal in Durban, South Africa.
- GBS samples were obtained from Salford Royal Hospital, with CSF samples also collected in Durban.
- Samples from patients with MMN, anti-MAG neuropathy and POEMS syndrome were sourced from NHNN and the John Radcliffe Hospital.
- Charcot-Marie-Tooth (CMT) and transthyretin (TTR) amyloid neuropathy samples were obtained from NHNN.
- Amyotrophic lateral sclerosis samples were obtained through a collaboration with the Oxford Motor Neuron Disease Centre.
- Healthy control samples were collected at the John Radcliffe Hospital and NHNN.

Further details are provided in Chapter 5 and Chapter 6.

2.5.2 Sample collection and processing

As samples were obtained from multiple biobanks, full standardisation of collection and processing procedures was not possible. However, all samples were plasma, serum or CSF,

centrifuged within five hours of collection, and stored at −80°C. None had undergone more than one previous freeze–thaw cycle.

2.6 Funding and ethical approval

This study was supported by a Medical Research Council (MRC) clinical research training fellowship (MR/Y001826/1) and a Guarantors of Brain pre-doctoral fellowship. All samples were collected and analysed under the ethically approved Biomarker Investigation & Study of Pathology in Neuropathy (Bio-SPiN) protocol (REC reference: 14/SC/0280) and the Queen Square Research Ethics Committee approval (REC reference: 16/LO/1852; study ID: 190929). Written informed consent was obtained from all prospectively recruited participants, including consent for data storage in compliance with the Data Protection Act. The study was conducted in accordance with Good Clinical Practice (GCP) guidelines and the principles outlined in the World Medical Association Declaration of Helsinki.

3. ASSAY DEVELOPMENT

3.1 Introduction

3.1.1 Periaxin

The first step in developing a biomarker assay is the selection of a relevant and system-specific target. For the measurement of peripheral nerve injury, it is ideal to choose an analyte whose presence in biological fluids would reflect peripheral pathology without confounding from central nervous system involvement. For peripheral demyelination, only three are Schwann cell proteins are truly PNS-specific: periaxin, myelin protein zero (P0), and early growth response protein 2 (Egr2). Periaxin is a cytoplasmic protein expressed exclusively by myelinating Schwann cells.[156–158] Its expression begins early in development, as Schwann cells first ensheathe axons in a 1:1 relationship. Initially localized to the adaxonal surface (apposing the axon) during the formation of myelin, periaxin later shifts to the abaxonal compartment (apposing the basal lamina) as myelination matures. In adult peripheral nerves, its expression remains confined to the abaxonal surface of myelinating Schwann cells. In developing and regenerating nerves, periaxin immunoreactivity is detected prior to the expression of other major myelin proteins such as MAG, myelin basic protein (MBP), and P0, consistent with its early and likely fundamental role in Schwann cell differentiation and myelin formation. Mutations in the periaxin gene (PRX) cause CMT4F, a severe autosomal recessive form of Charcot-Marie-Tooth disease[159] characterised by early-onset demyelination, providing further evidence for its critical developmental role in peripheral nerve biology. Compared to P0, an integral membrane protein tightly embedded within compact myelin, and Egr2, a nuclear transcription factor, periaxin's cytoplasmic

distribution and ultimate localisation to the abaxonal surface - adjacent to the extracellular environment - make it more accessible to release into the surrounding tissue and circulation, facilitating its detection during early Schwann cell injury and demyelination. For this reason, and because of its strict PNS specificity, periaxin was selected as the most suitable candidate for assay development, offering a biologically relevant and specific marker of Schwann cell injury and peripheral nerve demyelination. This chapter details the development and analytical validation of a novel immunoassay to measure periaxin.

3.1.2 Peripheral nerve specificity of periaxin: immunohistochemical evidence

Immunohistochemistry of human nervous tissue across the neuroaxis demonstrates that periaxin is strongly and selectively expressed in the PNS, with minimal background signal or complete absence in CNS structures such as the cerebral cortex, cerebellum, optic nerve, and spinal cord (Fig. 3.1A). The absence of co-localisation with β-tubulin, an axonal marker, confirms that periaxin is not expressed by axons but rather by myelinating Schwann cells. Notably, periaxin is absent in the optic nerve, where myelination is provided by oligodendrocytes instead of Schwann cells. High-resolution sections of peripheral nerve fascicles (Fig. 3.1B) reveal that periaxin is a prominent structural component of Schwann cells, outlining individual axons (stained with β-tubulin, yellow), consistent with its role in the formation and maintenance of peripheral myelin.

Figure 3.1. IHC localisation of periaxin in human nervous system tissues

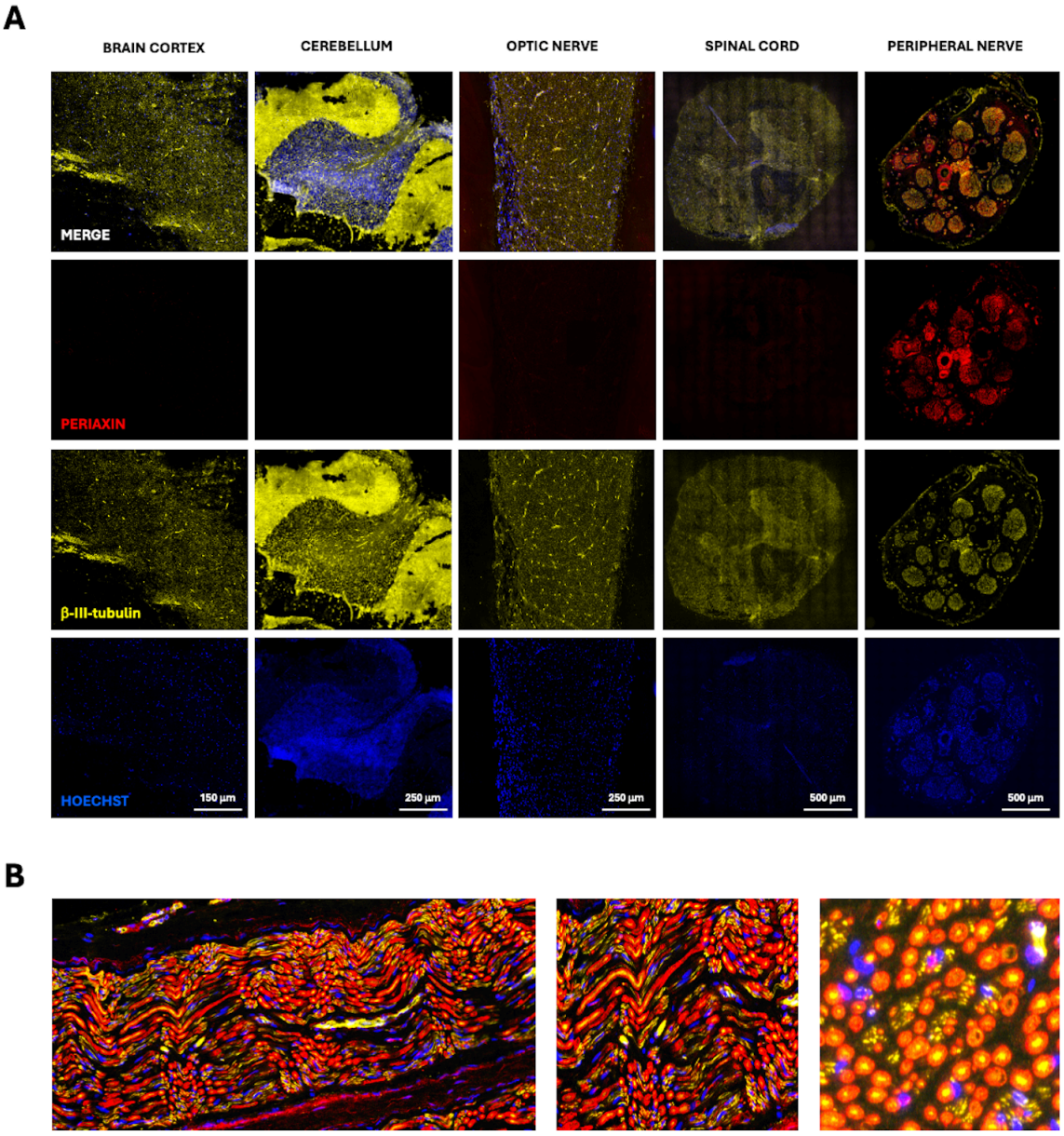

*(**A**) Immunohistochemistry of human brain cortex, cerebellum, optic nerve, spinal cord, and peripheral nerve cross-sections. Periaxin (in red) is absent in the central nervous system but is strongly expressed in peripheral nerve tissue. In contrast, β-tubulin (yellow), an axonal marker, is robustly expressed in both central and peripheral tissues. **(B)** Longitudinal section of peripheral nerve tissue (left) showing that periaxin is located within the Schwann cells, surrounding each axon, with greater detail visible in the zoomed-in section (middle). The right panel presents a magnified view of the peripheral nerve transverse cross-section shown in (**A**). Scale bars as indicated.*

These findings are conserved across species. In rat tissue, periaxin is not detected within the spinal cord itself (Fig. 3.2C), but is present in the preganglionic segments of sensory fibres as they enter the cord dorsally (white arrows, Fig. 3.2C) and in ventral motor roots as they exit the cord (yellow arrows, Fig. 3.2C), both of which are myelinated by Schwann cells. In contrast, peripheral nerve tissue from monkey shows strong periaxin expression (Fig. 3.2G), consistent with its selective presence in the PNS. Meanwhile, β-tubulin is broadly expressed in both central and peripheral nerves (Fig. 3.2B-F), further reinforcing the specificity of periaxin to the Schwann cell lineage. Altogether, these results demonstrate that periaxin is a reliable and specific marker of myelinating Schwann cells in the PNS, and its absence in CNS structures reflects the distinct cellular mechanisms of myelination between Schwann cells and oligodendrocytes.

Figure 3.2. Periaxin in rat and monkey

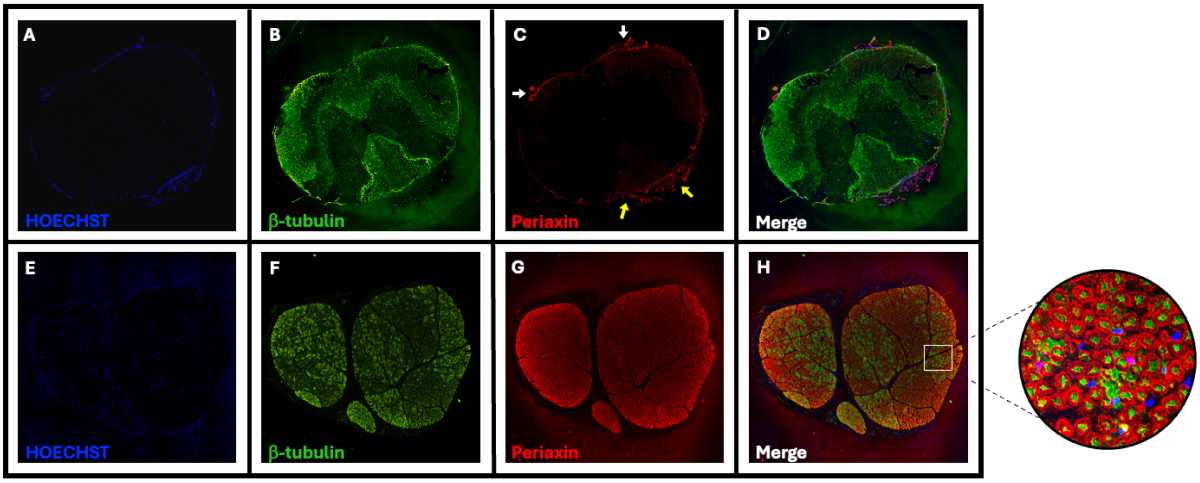

*Immunohistochemistry of frozen rat spinal cord (**A-D**) and monkey peripheral nerve (**E-H**) cross sections. Periaxin is absent inside the spinal cord (**C**) but can be detected in the preganglionic segments of the afferent sensory fibres as they enter the cord dorsally (white arrows) and in the ventral motor neurons exiting the cord (yellow arrows). In the peripheral nerve, instead, periaxin is strongly expressed (**G**). On the contrary, β-tubulin, axonal marker, is strongly expressed both centrally and peripherally (**B, F**). The zoomed-in section (round image, merge peripheral nerve staining) shows that periaxin (in red) is located within the Schwann cells, surrounding each axon (β-tubulin, green).*

3.2 Development of ultrasensitive assays for the measurement of periaxin

3.2.1 Purification of full-length recombinant periaxin

a) Transient transfection of human embryonic kidney cells

Human embryonic kidney cells (HEK293T) were transiently transfected with a full-length periaxin plasmid (OHu25883D, GenScript) to establish expression in a HEK cell-based system. Successful expression of periaxin was confirmed using a cell-based assay with a commercial mouse monoclonal antibody (clone G-5, sc-515672, Santa Cruz) alongside a range of three custom-made polyclonal antibodies, as shown in Fig. 3.3.

b) Affinity chromatography purification of periaxin

Method

HEK293T cells expressing FLAG-tagged periaxin were harvested by detachment and centrifugation. Cell pellets were thawed on ice and resuspended in a lysis buffer containing Tris-HCl (pH 7.5), 150 mM NaCl, 1 mM EDTA, 1 mM sodium orthovanadate, 10 mM NaF, protease inhibitors (1 mM benzamidine, 0.5 mM TLCK, 10 µg/ml antipain, and a protease inhibitor cocktail), and detergents (1% NP-40, 0.5% sodium deoxycholate, 0.1% SDS), supplemented with 1% Triton X-100. The lysates were incubated on ice for 20 minutes and clarified by centrifugation at 20,000 × g for 30 minutes at 4°C. The resulting supernatant was filtered through a 0.2 µm PES filter and incubated in batch mode with 0.4 ml of equilibrated 50% anti-FLAG M2 affinity gel (Sigma) for 2 hours at 4°C with gentle rotation. Beads were transferred to a mini-batch column (Generon) and washed three times with 0.5 ml of lysis

buffer. Bound protein was eluted in five fractions using 0.2 ml of elution buffer (20 mM HEPES pH 8.0, 150 mM NaCl, 0.1 mg/ml 3X FLAG peptide), with a 5-minute incubation between each elution step. Elution fractions were analyzed by SDS-PAGE using 4–20% pre-cast TGX gels (Bio-Rad), stained with Coomassie blue, and visualized alongside a Fermentas PageRuler Plus Prestained protein ladder (Cat No. SM1811). Eluted fractions (typically 1–4 or 1–5) were pooled and dialysed against a detergent-free storage buffer containing protease inhibitors. Following buffer exchange, samples were centrifuged at 20,000 × g for 10 minutes at 4°C to remove any precipitated protein. Protein concentration and purity were estimated by BCA assay and band densitometry. Purified protein was supplemented with 0.1% BSA, snap-frozen in aliquots, and stored at –80°C.

Results

Two independent rounds of periaxin purification were performed using the protocol described above. In the first round, fractions 1–5 were pooled and dialysed against storage buffer. Protein concentration was estimated at 76.7 µg/ml (~40% purity based on the top band) or 143.9 µg/ml (~75% purity when including the top three bands, likely corresponding to FLAG-tagged periaxin with varying levels of post-translational modification; Fig. 3.4B). The sample was aliquoted, snap frozen, and stored at –80°C. In the second purification, fractions 1–4 were pooled and dialysed against the same storage buffer. The resulting protein concentration was 170 µg/ml (~54% purity based on the top band) or 244 µg/ml (~78% purity including the top three bands). Both purification rounds yielded successful enrichment of FLAG-tagged periaxin using anti-FLAG M2 affinity gel, with reproducible results. The consistent three-band pattern observed in SDS-PAGE is in line with expected post-translational modifications of periaxin.

Figure 3.3. Cell-based assay for periaxin

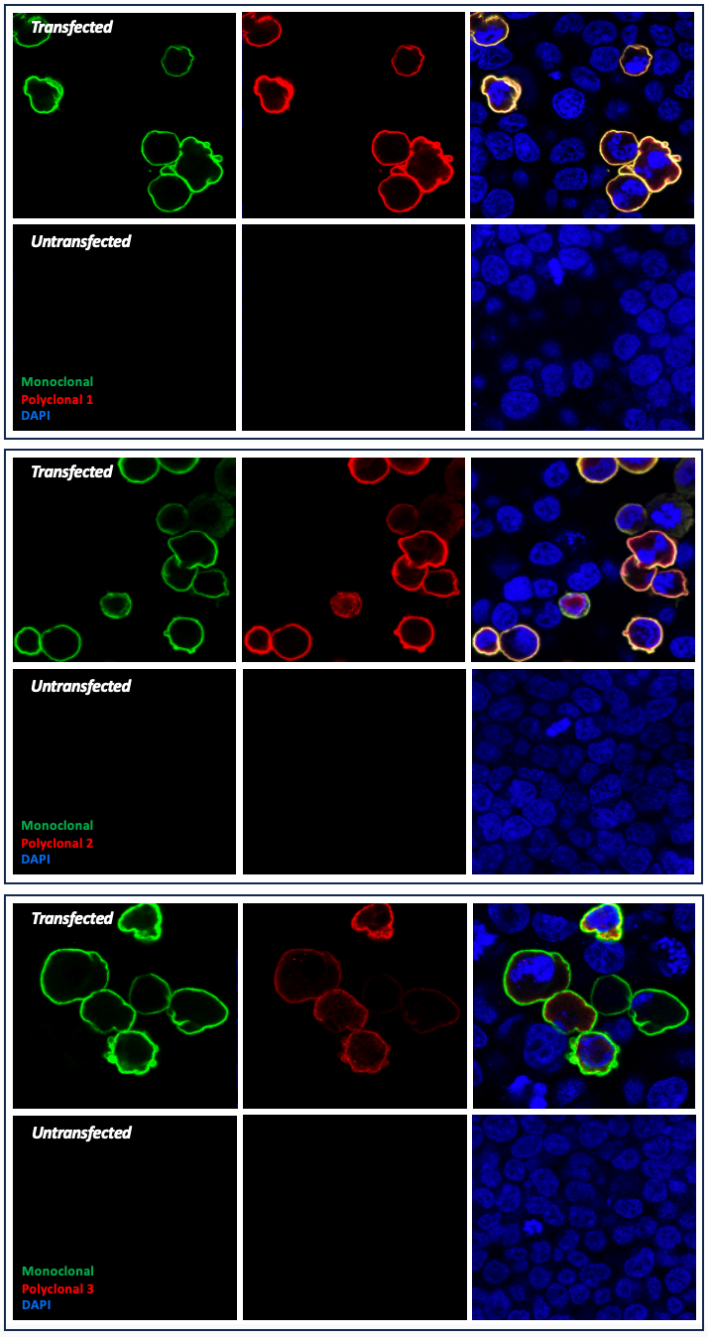

Confirmation of periaxin expression in transiently transfected HEK293T cells using a panel of antibodies. Three custom-made polyclonal antibodies and one commercial monoclonal antibody were tested in a cell-based assay to detect recombinant periaxin. All antibodies demonstrated binding to periaxin-expressing HEK cells, supporting successful expression.

Figure 3.4. Periaxin purification

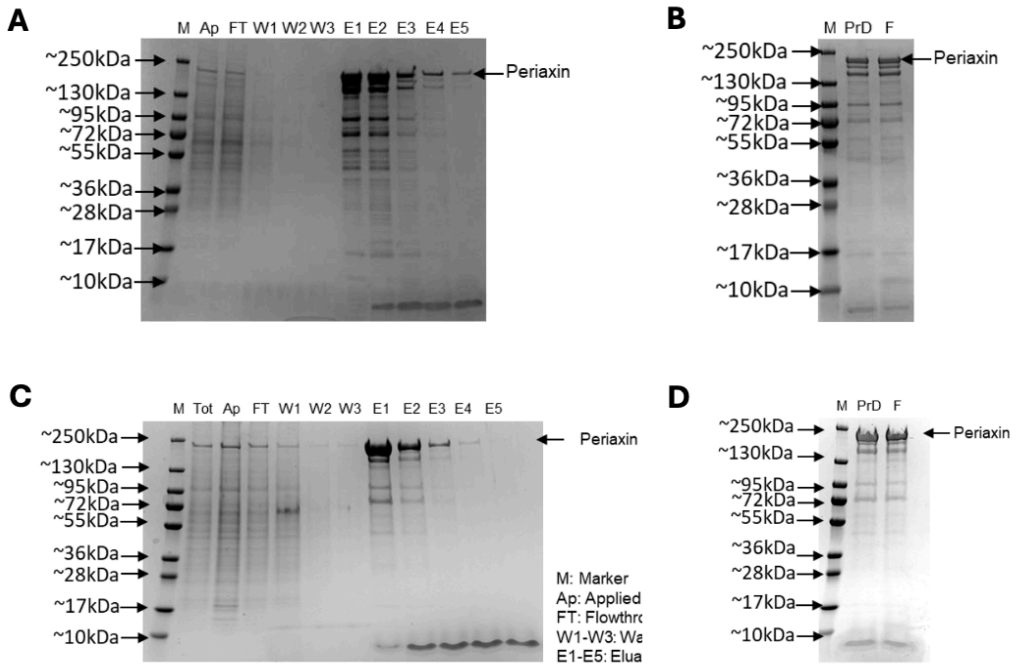

*(**A, C**) Coomassie blue stained SDS-PAGE gels of purified periaxin_FLAG fractions using anti-FLAG affinity resin. (**B, D**) Final Periaxin_FLAG purified samples. Volumes in brackets show amount of sample loaded on the SDS-PAGE gels. M, marker; Ap: applied sample (1 ml); FT: flowthrough (1ml); W1-W3: wash 1 to 3 (6.5 ml); E1-E5: eluates 1 to 5 (6.5 ml); PrD: pre-dialysis (5 ml); F: final sample post-dialysis (5 ml).*

3.2.2 Development of an ECL-based periaxin immunoassay

Method

The full-length recombinant periaxin protein, purified from transiently transfected HEK293T cells, was used to evaluate the performance of a selected antibody pair across a broad range of concentrations, with the aim of identifying the optimal signal-to-noise ratio. A mouse

monoclonal antibody (G5 clone, sc-515672, Santa Cruz) was chosen as the capture antibody, and a rabbit polyclonal antibody (orb413079, Biorbyt) as the detector. Both antibodies had been previously validated for applications including Western blotting, ELISA, immunocytochemistry, and immunohistochemistry, and were therefore selected for testing in an ECL-based assay format. ECL was initially explored to determine whether its sensitivity would be sufficient to detect periaxin in both disease and healthy biological samples. Capture and detector antibodies were tested using a checkerboard approach across various concentrations: 2–6 µg/ml for the capture antibody and 0.5–4 µg/ml for the detector antibody, with periaxin concentrations ranging from 0 to 400.000 pg/ml. The optimal concentrations for capture and detection antibodies were found to be 2 µg/ml and 4 µg/ml, respectively, as shown in Table 3.1. A SULFO-TAG labelled anti-rabbit secondary antibody (Meso Scale Discovery, MSD R32AB-5) was added at 1 µg/ml, as per manufacturer recommendations. MSD standard plates were chosen over high-bind plates based on better signal-to-noise ratio. Plates were coated with 30 µl of capture antibody at 2 µg/ml in PBS per well, sealed and incubated overnight at 4°C. Plates were then washed with PBST, and 150 µl of blocking solution [PBST + 5% MSD blocker A (R93AA-2)] were added to each well. After 1 hour of incubation (RT, 800 rpm), plates were washed, and 25 µl of calibrator (full-length recombinant periaxin) were added to each well prior to incubation [1 hour, room temperature (RT), 800 rpm]. Wells were then washed, 25 µl of detection antibody were added and incubated for 1 hour (RT, 800 rpm) prior to further washing. 25 µl of TAG-labelled secondary antibody were added and incubated for 1 hour (RT, 800 rpm). Finally, 150 µl of MSD read buffer (MSD, R92TC-3) were added and the plate was read immediately on the MSD instrument.

Results

The lower limit of detection (LLOD), defined as 2.5 times the standard deviation (SD) plus the mean average ECL signal of ten replicate results of the blank calibrator, was 30 pg/ml. The final standard curve is illustrated in Fig. 3.5. The LLOD represents the lowest concentration that can be distinguished from background noise, but not necessarily quantified reliably. The lower limit of quantification (LLOQ), in contrast, refers to the lowest concentration at which the assay can produce results with acceptable accuracy and consistency. In practice, the LLOQ is typically higher than the LLOD. Given this, it was uncertain whether the effective quantification threshold of the ECL assay would be sufficient to detect the low endogenous levels of periaxin postulated in biological samples. In light of this uncertainty, and to maximize sensitivity for detecting low-abundance proteins in complex matrices such as plasma and serum, further assay development was transitioned to the Simoa platform, which offers superior analytical sensitivity.

Table 3.1. Selection of optimal antibody concentration for the ECL-based periaxin assay

Plate	Capture antibody	Detector antibody	Secondary antibody	LLOD (pg/ml)
Standard	Mouse mono 2ug/ml	Rabbit poly 4ug/ml	Anti-rabbit-TAG 1 ug/ml	137
	Mouse mono 2ug/ml	Rabbit poly 2ug/ml	Anti-rabbit-TAG 1 ug/ml	919
	Mouse mono 2ug/ml	Rabbit poly 1ug/ml	Anti-rabbit-TAG 1 ug/ml	380
	Mouse mono 2ug/ml	Rabbit poly 0.5ug/ml	Anti-rabbit-TAG 1 ug/ml	1060
Standard	Mouse mono 6ug/ml	rabbit poly 4ug/ml	Anti-rabbit-TAG 1 ug/ml	4808
	Mouse mono 6ug/ml	rabbit poly 2ug/ml	Anti-rabbit-TAG 1 ug/ml	2651
	Mouse mono 4ug/ml	rabbit poly 4ug/ml	Anti-rabbit-TAG 1 ug/ml	1846
	Mouse mono 4ug/ml	rabbit poly 2ug/ml	Anti-rabbit-TAG 1 ug/ml	875
Standard	Rabbit poly 4 ug/ml	Mouse mono 2ug/ml	Anti-mouse-TAG 1 ug/ml	3292
	Rabbit poly 2 ug/ml	Mouse mono 2ug/ml	Anti-mouse-TAG 1 ug/ml	3995
	Rabbit poly 4 ug/ml	Rabbit poly-TAG 2ug/ml		12321
	Rabbit poly 2 ug/ml	Rabbit poly-TAG 2ug/ml		11799
Standard	mouse mono 2ug/ml	Rabbit poly 4ug/ml	Anti-rabbit-TAG 1 ug/ml	1007
	mouse mono 2ug/ml	Rabbit poly 2ug/ml	Anti-rabbit-TAG 1 ug/ml	9164
	mouse mono 2ug/ml	Rabbit poly 4ug/ml	Anti-rabbit-TAG 1 ug/ml	572
	mouse mono 2ug/ml	Rabbit poly 2ug/ml	Anti-rabbit-TAG 1 ug/ml	2377
Standard	mouse mono 2ug/ml	Rabbit poly 4ug/ml	Anti-rabbit-TAG 1 ug/ml	37.7
	mouse mono 2ug/ml	Rabbit poly 4ug/ml	Anti-rabbit-TAG 1 ug/ml	37.2
	mouse mono 2ug/ml	Rabbit poly 4ug/ml	Anti-rabbit-TAG 1 ug/ml	37
	mouse mono 2ug/ml	Rabbit poly 4ug/ml	Anti-rabbit-TAG 1 ug/ml	194
High bind	mouse mono 2ug/ml	Rabbit poly 4ug/ml	Anti-rabbit-TAG 1 ug/ml	1127
	mouse mono 2ug/ml	Rabbit poly 2ug/ml	Anti-rabbit-TAG 1 ug/ml	806

Figure 3.5. Periaxin ECL standard curve

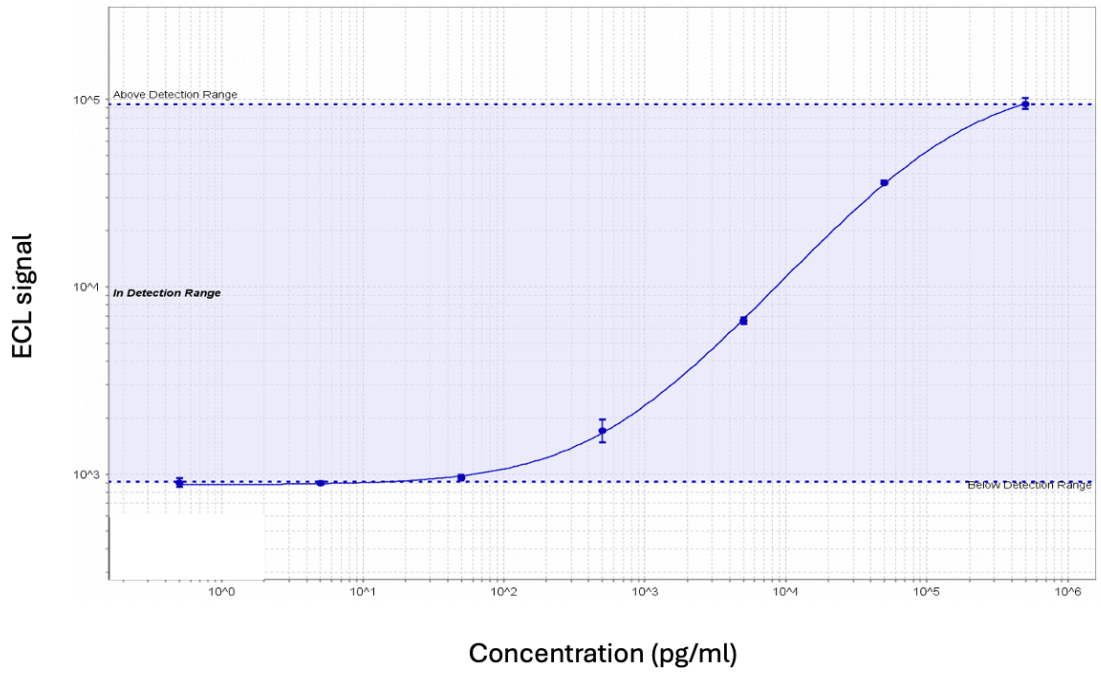

Standard curve of the ECL-based periaxin assay. The lower limit of detection, calculated as the mean plus 2.5 standard deviations of the blank signal, was 30 pg/ml.

3.2.3 Development and optimisation of a Simoa periaxin assay

3.2.3.1 Standard curve

Method

The capture antibody was buffer exchanged into the recommended bead conjugation buffer using Amicon Ultra-0.5 50 kDa centrifugal filters (Merck), as per the Simoa Homebrew Assay Development Guide (Quanterix®). Paramagnetic dyed singleplex assay beads (TECH-

0143 488, Quanterix) were washed and prepared to provide a supply of 1.4 x 10^9 beads/ml of capture antibody solution. Beads were activated using 1-ethyl-3-(3-dimethylaminopropyl) carbodiimide (EDC), and capture antibodies were then conjugated to the beads with incubation at room temperature for 30 minutes on a rollator (HulaMixer, Thermo Fisher). Conjugated beads were washed and blocked with blocking solution for 45 min at 2–8°C. Following three washes, the conjugated beads were resuspended and stored at 4°C. The detection antibodies were buffer exchanged into Quanterix® biotinylation reaction buffer using Amicon Ultra-0.5 50 kDa filters. The detector antibody was biotinylated with NHS-PEG4-biotin (A39259, Thermo Fisher Scientific) at a 40:1 challenge ratio, and incubated for 30 minutes at room temperature. Bead-conjugated capture antibody and biotinylated detector were then tested to detect recombinant periaxin protein across a range of concentrations from 0 to 100,000 pg/ml. For analyte quantification, capture and detection can be performed using a 2-step or 3-step assay protocol. In a 3-step protocol, the analyte is first captured by antibody-coated beads, followed by the addition of a biotinylated detection antibody in the second step to form an antibody-analyte sandwich. In the third step, the complex is labelled with the enzyme (SBG). A wash step is included between each incubation to remove unbound components and reduce background signal. In a 2-step protocol, the sample, capture beads, and detection antibody are incubated together, allowing the sandwich complex to form in a single step before washing and enzyme labelling.

Efficient assay performance depends on coating the beads with a high density of monomeric capture antibody. The coupling reaction exploits carboxyl groups on the bead surface, which react with primary amines on the capture antibody via EDC-mediated crosslinking. Traditionally, Quanterix® protocols recommend a two-step conjugation process where beads are first activated with EDC alone, followed by a two-hour incubation with the antibody. To

enhance coupling efficiency, a sulfo-N-hydroxysulfosuccinimide (S-NHS) can be added during bead activation. Although during bead activation EDC forms a reactive O-acylisourea intermediate with carboxyl groups on the bead surface, this intermediate is unstable in aqueous environments and rapidly hydrolyzes. The addition of Sulfo-NHS stabilizes the intermediate by converting it to a more robust sulfo-NHS ester, thereby improving the efficiency of covalent coupling to the antibody's amine groups (Fig. 3.7).

Results

A 2-step protocol was chosen over a 3-step protocol, as the former displayed higher dose-response and lower background noise. A comparison of preliminary standard curves generated using the two assay protocols – each optimised over a concentration range of 0 to 100,000 pg/ml, expected to encompass the plausible physiological and pathological levels of periaxin in serum or plasma - is shown in Fig. 3.8.

Figure 3.7. EDC/Sulfo-NHS chemistry for bead conjugation

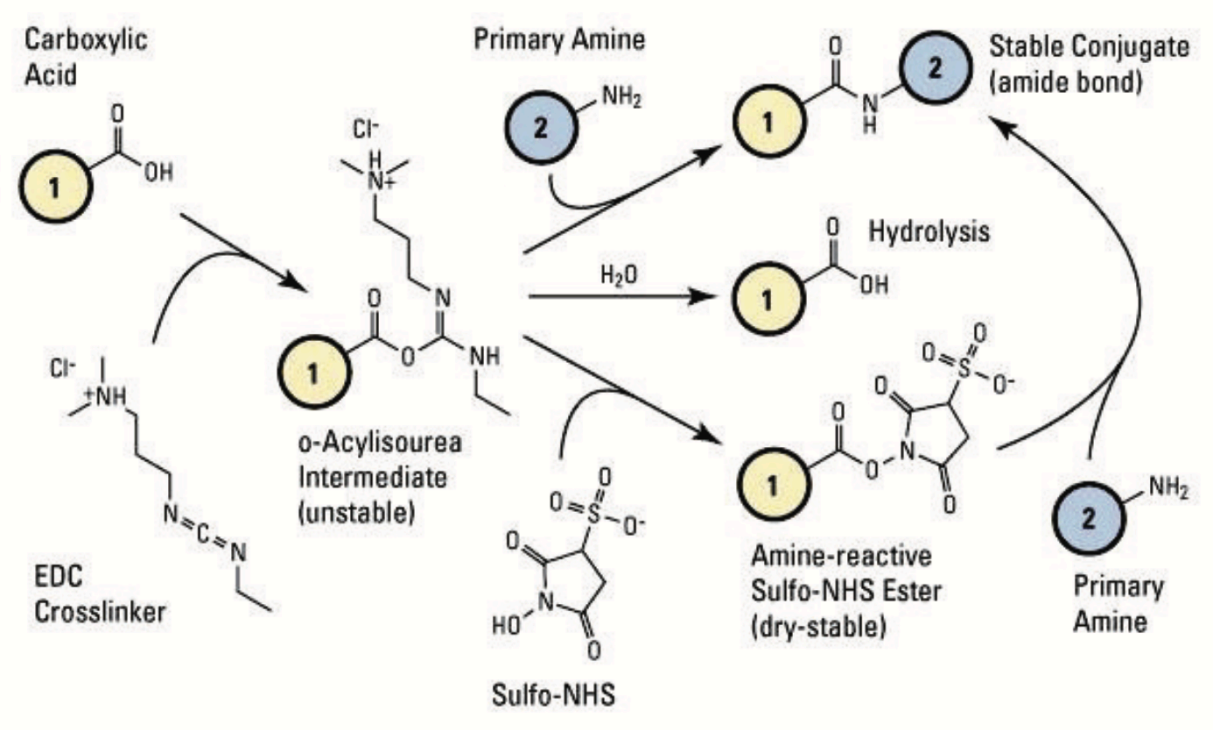

Schematic of EDC/Sulfo-NHS chemistry used for covalent coupling of capture antibodies to carboxylated beads. Sulfo-NHS stabilizes the reactive intermediate formed by EDC, enhancing the efficiency of antibody immobilization through amine-reactive sulfo-NHS ester formation. Image source: Thermo Fisher

Figure 3.8. Comparison between assay protocols: 3 steps vs 2 steps

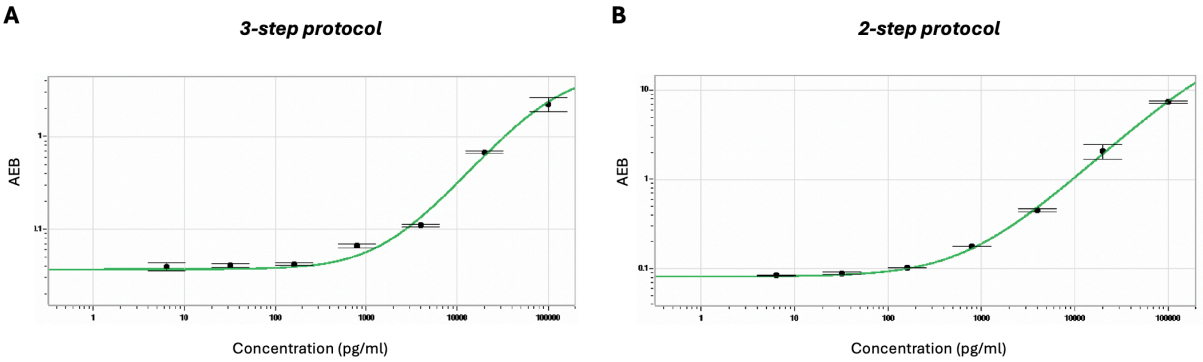

*Comparison of preliminary standard curves generated using a 3-step (**A**) and a 2-step (**B**) assay protocol, each optimized over a concentration range of 0 to 100,000 pg/ml. The 2-step protocol demonstrated superior performance, with a stronger dose-response - defined as a more pronounced increase in signal with increasing analyte concentration - and lower background signal at low concentrations, indicating improved sensitivity and signal-to-noise ratio compared to the 3-step protocol.*

Bead coating efficiency was evaluated by comparing the traditional EDC-only protocol (pH 6.5) with the modified protocol incorporating S-NHS and a lower activation pH of 5.0. With EDC alone, coating efficiency ranged from 35% to 50%, indicating suboptimal conjugation of the capture antibody to the bead surface. In contrast, the inclusion of S-NHS during activation and lowering the pH to 5.0 significantly improved coupling efficiency, consistently achieving values between 85% and 98%, as shown in Fig. 3.9. These results support the use of S-NHS-enhanced conjugation chemistry and optimised pH conditions to maximise bead loading and assay reproducibility.

Figure 3.9. Bead conjugation methods compared: EDC only vs ECC + S-NHS

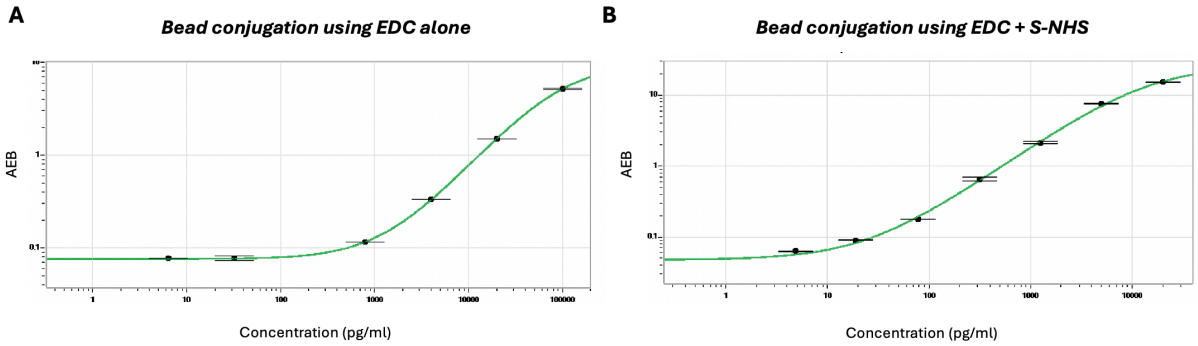

Standard curves generated using beads conjugated under two different activation conditions. (A) Beads coated using EDC alone at pH 6.5 resulted in lower assay sensitivity and reduced signal across the dynamic range. (B) Beads conjugated with EDC and Sulfo-NHS at pH 5.0 produced significantly improved signal response, reflecting higher coating efficiency (85–98%) and enhanced assay performance.

To optimise assay performance, a range of detector antibody concentrations was evaluated, including 1.0 µg/ml, 1.5 µg/ml and 2.0 µg/ml (Fig. 3.10). Concentrations of 1.0 µg/ml and 1.5 µg/ml produced the most favourable results, showing strong dose-response curves with acceptable background signal (AEB <0.05). Based on these findings, a concentration of 1.25 µg/ml was selected as a compromise between the two optimal conditions, in order to maximise signal across the dynamic range while maintaining minimal background noise.

To optimise the signal amplification step, two concentrations of SBG were evaluated: 150 pM and 300 pM. While both concentrations produced comparable signal intensities at higher analyte concentrations, the 300 pM condition resulted in noticeably higher background signal at the lower end of the curve (blank AEB > 0.1). Therefore, 150 pM was selected for the final

assay protocol, as it provided sufficient signal amplification while maintaining low background noise and overall assay specificity (Fig. 3.11).

To improve the signal-to-noise ratio, helper beads were introduced into the assay. Helper beads are non-functional magnetic beads that do not carry capture antibodies but are added alongside functional assay beads to maintain an optimal total bead number per cuvette. By improving bead resuspension and ensuring consistent bead fill during cuvette loading, helper beads help reduce variability and background signal, particularly at the lower end of the standard curve. This strategy is recommended by the manufacturer for late-stage assay optimisation and not as an initial parameter to be tuned. Four combinations of assay and helper beads were tested while keeping the total bead number constant at 500,000 per cuvette:

- 100% assay beads
- 75% assay / 25% helper (350K/150K)
- 50% assay / 50% helper (250K/250K)
- 25% assay / 75% helper (150K/450K).

As shown in Fig. 3.12, the 100% assay bead condition yielded strong signal intensity but did not significantly outperform the 75%/25% mix. The 75% assay / 25% helper configuration produced comparable signal while reducing background noise, resulting in an improved signal-to-noise ratio. In contrast, the 50%/50% and 25%/75% mixes were associated with progressively higher background signals, with the 50%/50% condition showing the highest non-specific background (blank AEB > 0.1) and poorest curve definition. Based on these findings, the 75% assay / 25% helper bead ratio (350K/150K) was selected as the optimal configuration for the assay.

Figure 3.10. Optimisation of detector antibody concentration

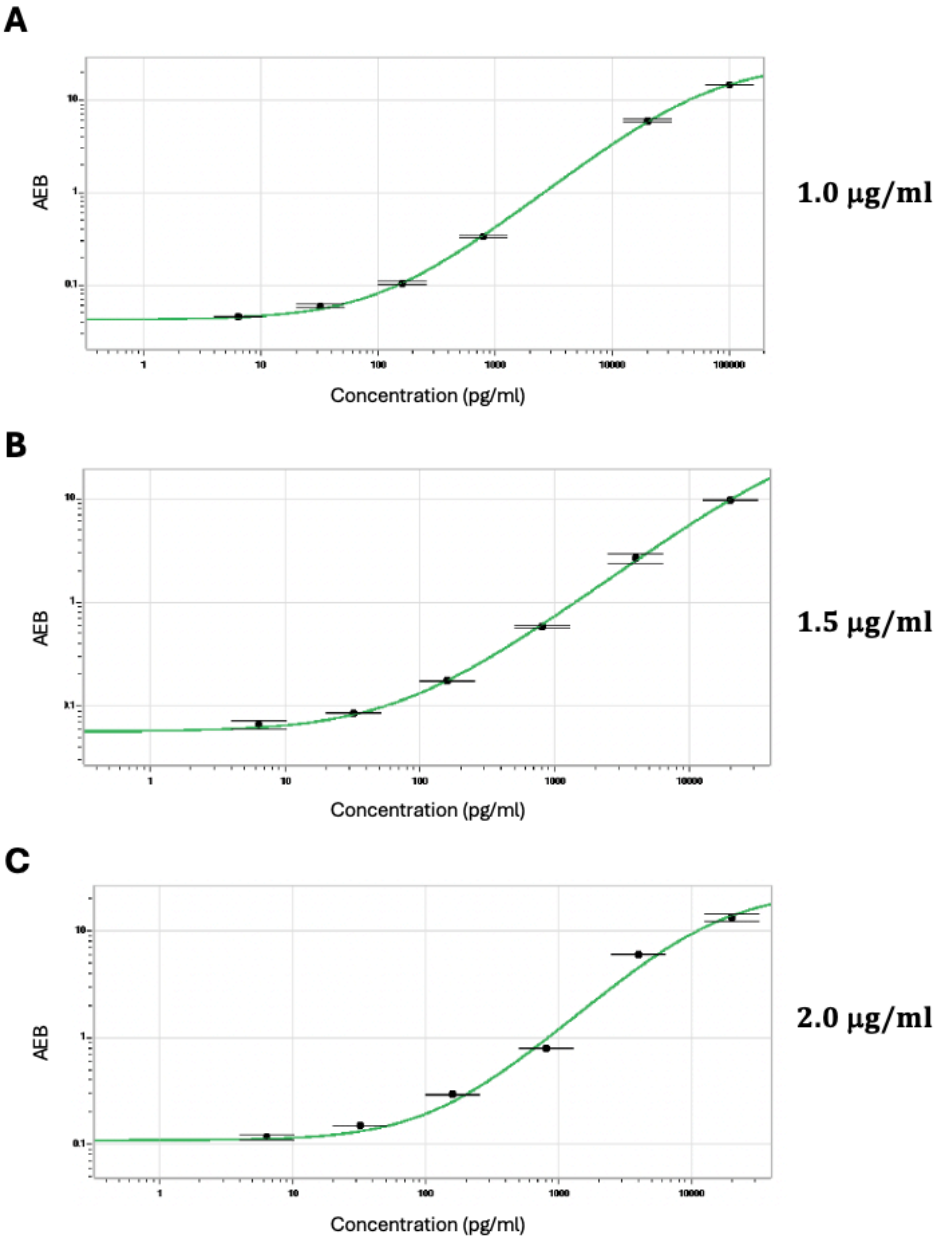

Standard curves were generated using a range of biotinylated detector antibody concentrations (1.0, 1.5, and 2.0 µg/ml). Concentrations of 1.0 and 1.5 µg/ml yielded optimal performance with strong dose-response and low background signal. A final concentration of 1.25 µg/ml was selected to balance sensitivity and background, providing consistent signal across the dynamic range.

Figure 3.11. Optimisation of SBG concentration

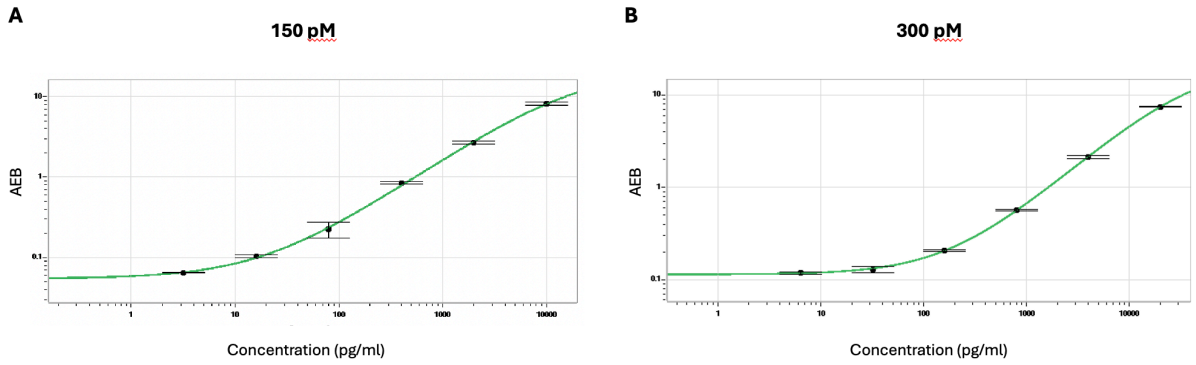

*Standard curves generated using two concentrations of streptavidin-β-galactosidase (SBG): (**A**) 150 pM and (**B**) 300 pM. While both concentrations produced adequate signal at higher analyte levels, the 300 pM condition showed increased background at lower concentrations. As a result, 150 pM was selected for the final assay to maximise specificity and minimise background noise.*

Figure 3.12. Helper beads

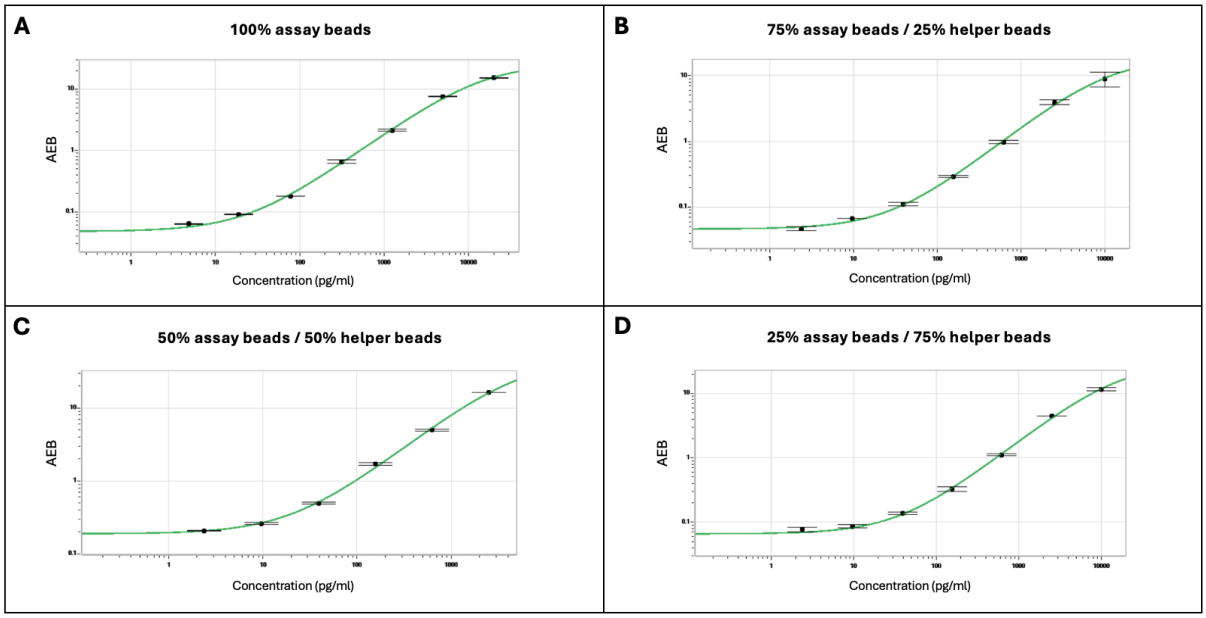

*Standard curves were generated using (**A**) 100% assay beads, (**B**) 75% assay / 25% helper beads (350K/150K), (**C**) 50% assay / 50% helper beads (250K/250K), and (**D**) 25% assay / 75% helper beads (150K/450K). The 75%/25% combination (**B**) produced the most favourable signal-to-noise ratio, maintaining strong dose-response while minimising background. Higher proportions of helper beads were associated with increased background signal and reduced assay performance.*

Finally, to further minimise background noise and maximise overall assay sensitivity, detector antibody labelling was optimised. Three different biotinylation reagents were compared: NHS-PEG4-Biotin (the manufacturer-recommended reagent), NHS-LC-Biotin, and NHS-LC-LC-Biotin (Fig. 3.13). All three reagents were used to label the same detector antibody under identical conditions, and their performance was assessed by comparing standard curves generated using each biotinylated antibody. While all reagents supported analyte detection, NHS-LC-LC-Biotin consistently produced the lowest background signal,

particularly at low analyte concentrations, without compromising overall signal intensity. This suggests that the increased spacer length provided by the LC-LC linker may enhance accessibility of the biotin moiety for enzyme binding, thereby improving signal-to-noise ratio. Based on these results, NHS-LC-LC-Biotin was selected for further assay development.

Fig. 3.14 illustrates the standard curve for the final optimised periaxin assay, incorporating all key parameters established during assay development. The assay was configured as a 2-step protocol using beads conjugated with EDC and S-NHS at pH 5.0, a biotinylated detector antibody labelled with NHS-LC-LC-Biotin, and SBG at 150 pM. The detector antibody was used at a final concentration of 1.25 µg/ml, and a 75% assay / 25% helper bead ratio (350K/150K) was included to enhance signal-to-noise performance. This configuration yielded a robust dose-response curve with low background and an analytical sensitivity of 0.2 pg/ml (LLOD), as determined in buffer. This optimised assay was subsequently applied to the analysis of serum and plasma, to enable quantification of endogenous periaxin and evaluate potential matrix effects.

Figure 3.13. Comparison of biotinylation methods

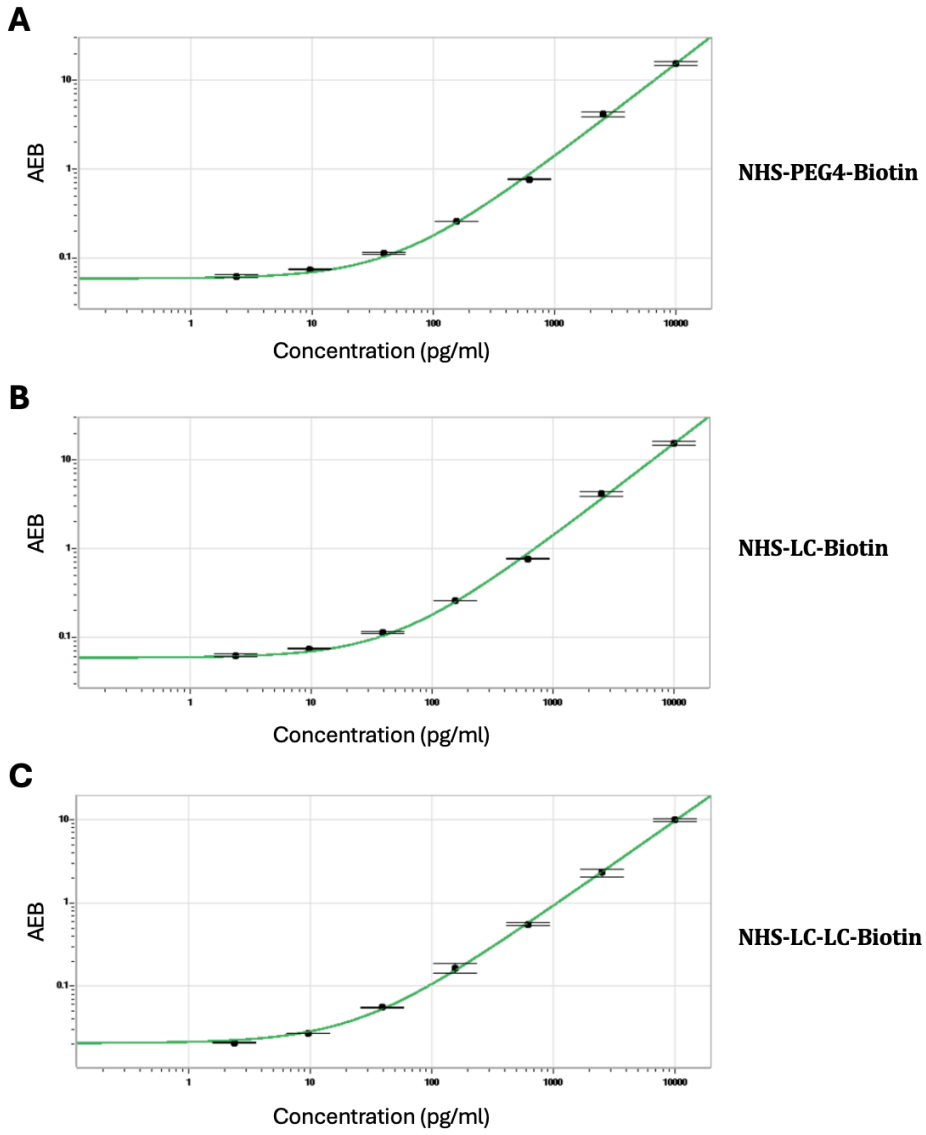

*Standard curves generated using detector antibodies labelled with (**A**) NHS-PEG4-Biotin, (**B**) NHS-LC-Biotin, and (**C**) NHS-LC-LC-Biotin. NHS-LC-LC-Biotin produced the lowest background signal across the dynamic range, while maintaining comparable signal intensity to the other reagents. NHS-LC-LC-Biotin was therefore selected for continued assay development due to its improved signal-to-noise performance.*

Figure 3.14. Standard curve of the final optimised periaxin assay

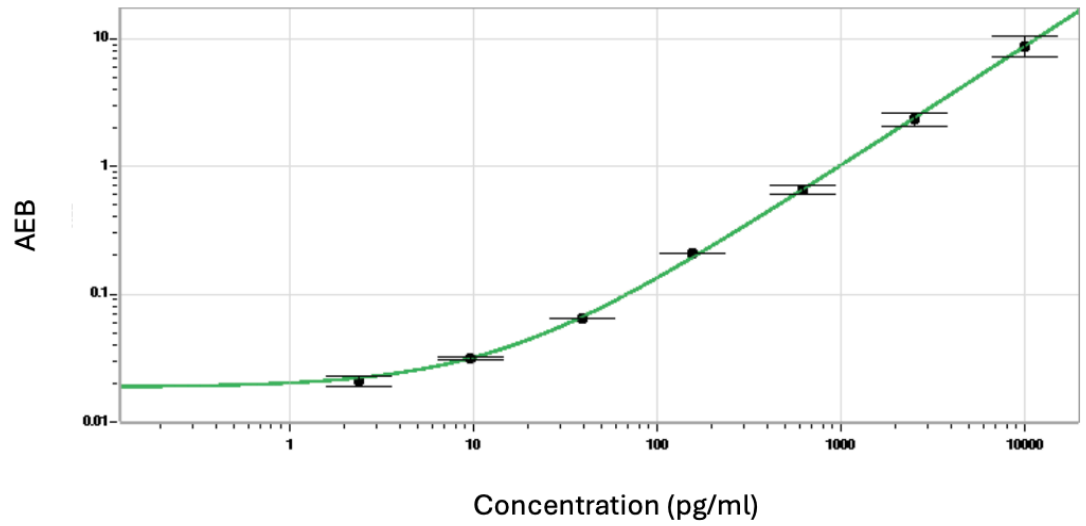

The assay was developed using a 2-step format and incorporates optimised conditions for bead conjugation, detector antibody biotinylation, SBG concentration, and bead composition. The final configuration yielded a strong dose-response with low background and an analytical lower limit of detection of 0.2 pg/ml in buffer, representing a 150-fold increase in sensitivity compared to the ECL-based assay.

3.2.3.2 Choice of sample matrix: serum versus plasma

Both serum and plasma samples from patients with peripheral neuropathy (GBS and CIDP) were available for testing, and periaxin levels were measured in both biofluids. Periaxin was consistently detectable in plasma, whereas serum samples showed undetectable levels in nearly all cases, with only rare exceptions. Fig. 3.15 illustrates matched serum and plasma measurements from 25 individuals, confirming that only plasma yielded measurable periaxin concentrations across the cohort. A direct comparison between EDTA and lithium heparin

(LiH) plasma was also performed, and periaxin was detected exclusively in EDTA plasma. Based on these findings, EDTA plasma was selected as the preferred matrix for all subsequent analyses.

Figure 3.15. Periaxin in plasma vs serum

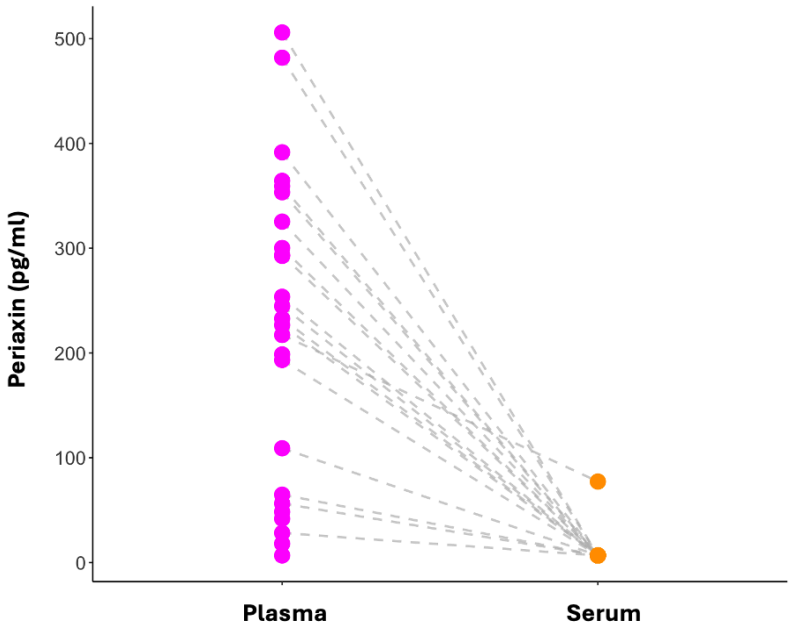

Periaxin was consistently detected in EDTA plasma, while corresponding serum samples showed undetectable levels in nearly all cases. These findings support the use of EDTA plasma as the preferred matrix for periaxin quantification.

3.2.3.3 Dilution linearity and choice of diluent

Method

Dilution linearity was assessed to demonstrate that a plasma sample with a periaxin concentration exceeding the upper limit of the assay range (i.e. above the highest calibration point) can be accurately quantified after dilution into the assay's working range. This analysis evaluates whether the assay maintains a linear dose–response relationship across serial dilutions, thereby confirming the reliability of measurements at different dilution factors. It also informs the selection of an appropriate diluent to minimise matrix effects and ensure accurate quantification. To perform this assessment, a high concentration of recombinant periaxin (50,000 pg/ml) - exceeding the highest standard by five-fold - was spiked into undiluted EDTA plasma. The spiked sample was then serially diluted using a range of five diluents until the theoretical concentration fell below the assay's LLOQ. Each dilution was analysed, and dilution-adjusted concentrations were calculated. Percent recovery (%RE) was then determined for each dilution by comparing the measured value (adjusted for dilution) to the expected concentration. This analysis enabled evaluation of linearity, matrix interference, and overall suitability of the diluent. %RE was calculated using the following formula:

$$\%RE = (\text{measured value} / \text{expected concentration}) \times 100$$

Results

Dilution linearity analysis revealed that among the five diluents tested, diluents C and E provided the most consistent performance. For these two diluents, %RE remained within the acceptable range of 80–120% across all dilution factors that fell within the assay's

quantifiable range (Fig. 3.16, Table 3.2). This indicated reliable dilution-adjusted quantification and minimal matrix interference. In contrast, other diluents showed greater variability in %RE, particularly at intermediate dilutions. Based on these findings, diluents C and E were selected for further assay development and validation.

The manufacturer (Quanterix) does not disclose the full composition of the proprietary diluents used in this study. However, according to available information, Diluent C contains a phosphate buffer with low concentrations of protein stabilisers (bovine-derived), a heterophilic blocker, a surfactant, and ProClin 300 as a preservative. In contrast, Diluent E is based on a high-pH Tris buffer and contains bovine serum components, a heterophilic blocker, a surfactant, and the same preservative. While the exact formulation is not disclosed, the observed performance differences may reflect the effect of buffer pH and protein content on analyte stability, antibody binding, or signal interference. The presence of serum proteins in Diluent E may better mimic plasma conditions, while the simpler composition of Diluent C may reduce nonspecific interactions, both contributing to acceptable recoveries.

Figure 3.16. Dilution linearity

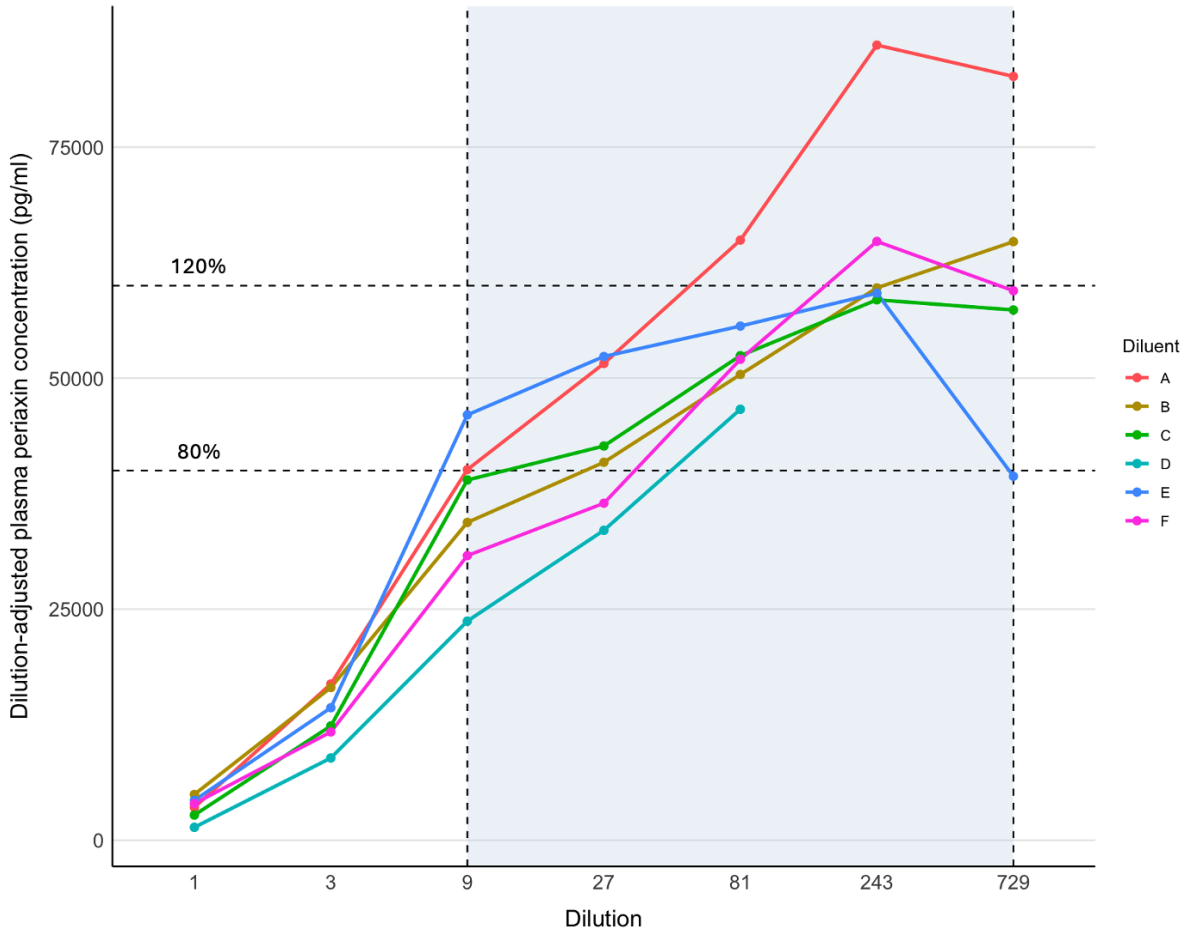

Dilution linearity analysis of recombinant periaxin spiked into EDTA plasma and serially diluted using five different diluents. Dilution-adjusted concentrations were used to calculate %RE relative to expected values. Diluents C and E demonstrated consistent performance, with %RE maintained within the acceptable range of 80–120% across all dilution factors within the assay's working range. These diluents were selected for further assay development.

Table 3.2. Dilution linearity: comparison of diluents

Diluent	Dilution	Measured concentration (pg/ml)	Expected concentration (pg/ml)	%RE
A	1	3546.724925	50000	7.1
	3	16909.47906	50000	33.8
	9	40102.40416	50000	**80.2**
	27	51581.89154	50000	**103.2**
	81	64939.0547	50000	129.9
	243	86040.45391	50000	172.1
	729	82649.7823	50000	165.3
B	1	4955.776057	50000	9.9
	3	16521.37767	50000	33.0
	9	34390.41585	50000	68.8
	27	40892.28418	50000	**81.8**
	81	50395.98612	50000	**100.8**
	243	59767.70687	50000	**119.5**
	729	64766.04384	50000	129.5
C	1	2722.608325	50000	5.4
	3	12369.97589	50000	24.7
	9	38979.07359	50000	**77.9**
	27	42656.92008	50000	**85.3**
	81	52434.43101	50000	**104.9**
	243	58477.32075	50000	**116.9**
	729	57376.89493	50000	**114.7**
D	1	1393.257288	50000	2.8
	3	8900.086488	50000	17.8
	9	23713.60424	50000	47.4
	27	33533.40665	50000	67.1
	81	46633.9768	50000	**93.3**
	243	< LLOD	50000	-
	729	< LLOD	50000	-
E	1	4313.103927	50000	8.6
	3	14335.89996	50000	28.7
	9	46024.49627	50000	**92.0**
	27	52341.1074	50000	**104.7**
	81	55632.70565	50000	**111.3**
	243	59195.36585	50000	**118.4**

3.2.3.4 Parallelism and minimum required dilution

Method

Parallelism and dilution linearity are conceptually similar in that both assess whether measured concentrations remain consistent and proportional following serial dilution. The key difference is the type of sample used. Dilution linearity experiments involve spiking a high concentration of recombinant analyte into matrix, at levels exceeding the assay's upper range, followed by serial dilution. In contrast, parallelism assesses whether the endogenous analyte behaves similarly to the recombinant calibrator, and therefore requires unspiked biological samples with naturally high concentrations of the analyte. These concentrations must fall within the assay's dynamic range.

The purpose of the parallelism experiment here is to determine whether the binding characteristics of endogenous periaxin are equivalent to those of the recombinant calibrator used to generate the standard curve. To assess this, three plasma samples with varying endogenous periaxin levels, evenly distributed across the standard curve, were selected. Each sample was subjected to serial two-fold dilutions until the measured concentration approached or dropped below the assay's detection limit. The measured values at each dilution were adjusted for the dilution factor, and results were compared to identify the point at which dilution-adjusted concentrations began to fall within acceptable limits. The minimum required dilution (MRD) was defined as the lowest dilution at which dilution-adjusted concentrations were consistently within ±20% of the value measured at MRD (i.e., 80–120% agreement). This threshold was chosen to reflect acceptable linearity while accounting for assay precision. Although no universally accepted criteria exist for evaluating parallelism, several recommendations have been proposed. Some suggest that a %CV ≤30%

across dilution series is sufficient,[160] while others advocate for tighter bounds such as ≤20%,[161] or recovery (%RE) within 75–125% compared to the MRD[162,163].

Results

Parallelism was assessed in three plasma samples with endogenous periaxin concentrations spanning the assay's dynamic range. Each sample was serially diluted two-fold, and the measured concentrations were adjusted for the dilution factor to assess consistency across the dilution series. In all three samples, dilution-adjusted concentrations remained within the predefined acceptable recovery range of 80–120% starting from a 1:8 dilution (Fig. 3.17, Table 3.3). Below this threshold (i.e., at lower dilutions such as neat, 1:2, or 1:4), greater variability was observed, likely reflecting matrix effects at higher sample concentrations. Across the valid dilution range, the coefficient of variation of the adjusted values ranged from 70.3% to 104%, confirming that linearity and acceptable parallelism were achieved from 1:8 onward. Based on these results, 1:8 was established as the assay MRD to ensure accurate quantification of endogenous periaxin while minimising matrix interference.

Figure 3.17. Parallelism

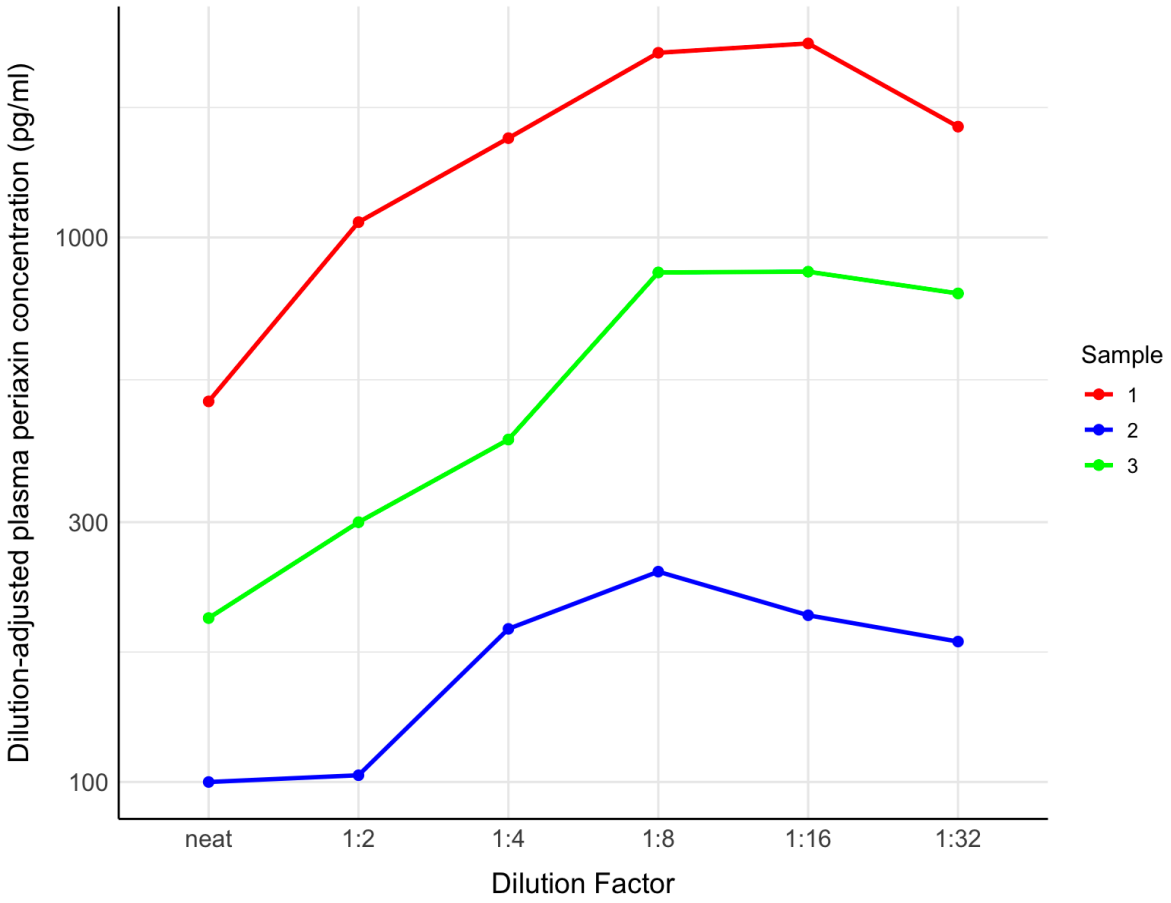

Parallelism analysis of endogenous periaxin in three plasma samples with varying concentrations. Each sample was serially diluted two-fold and measured periaxin concentrations were adjusted for dilution. All three samples demonstrated acceptable linearity from a 1:8 dilution onward, supporting the selection of 1:8 as the assay MRD.

Table 3.3. Parallelism analysis of periaxin in plasma samples

Sample	Dilution	Dilution-adjusted concentration (pg/ml)	%RE
1	Neat	504	-
1	1:2	1067	-
1	1:4	1522.1	-
1	1:8	2184	**100**
1	1:16	2272	**104**
1	1:32	1598	**70.3**
2	Neat	103	-
2	1:2	102.9	-
2	1:4	191.1	-
2	1:8	243.4	**100**
2	1:16	202.4	**83.2**
2	1:32	181.1	**89.5**
3	Neat	201	-
3	1:2	305	-
3	1:4	425.5	-
3	1:8	862.7	**100**
3	1:16	865.4	**100.3**
3	1:32	789.4	**91.2**

3.2.3.5 Spike recovery

A spike recovery experiment was performed to assess whether the concentration–response relationship of the assay is comparable between the calibration curve and biological samples. Poor recovery would suggest that differences between the sample matrix and the calibrator diluent influence the assay signal, indicating the presence of matrix effects. This analysis helps to confirm that the chosen diluent closely mimics the biological environment and

ensures that both recombinant calibrator and endogenous analyte generate comparable responses across the assay's measuring range.

Three EDTA plasma samples with minimal endogenous periaxin were selected and diluted. Each sample was divided into four aliquots. Using the calibrator stock solution, three aliquots were spiked at low, medium, and high concentrations across the linear range of the standard curve. All spikes were added in equal volumes, kept below 10% of the total volume. The fourth aliquot was left unspiked and received an equal volume of measurand-free calibrator diluent to control for dilutional effects. Spike-recovery testing was performed under the following three conditions:

1. Buffer-based standard curve with plasma samples diluted 1:8 (the assay's MRD)

2. Buffer-based standard curve with plasma samples diluted 1:16

3. Matrix-matched standard curve generated in diluted (1:8) plasma with minimal endogenous periaxin

For both buffer-based standard curve conditions, a control sample containing only calibrator diluent (i.e. no plasma) was also included to evaluate the baseline recovery in the absence of matrix. All samples were analysed in the same assay run to eliminate inter-assay variability. The acceptance criterion for recovery was set at 80–120%. Recovery was calculated with the following formula:

$$\text{Recovery} = \left(\frac{\text{concentration in spiked sample} - \text{concentration in unspiked sample}}{\text{expected concentration}} \right) \times 100$$

Results

Spike recovery experiments using a buffer-based calibration curve revealed consistent under-recovery (50-56%) at a 1:8 dilution, indicative of residual matrix effects. Recovery improved to 70–94% at 1:16, suggesting that matrix interference is reduced at this dilution (Table 3.4). However, parallelism analysis had confirmed that from 1:8 onward, endogenous analyte behaved proportionally across dilutions, indicating that 1:8 provides valid quantification despite lower absolute recovery. To preserve assay sensitivity - particularly for low-abundance analytes - and minimise values falling below the LLOD, 1:8 dilution was confirmed as the minimum required dilution. Where necessary, samples may be reassayed at 1:16 to confirm robustness or investigate suspected matrix interference. Notably, when a matrix-matched calibration curve was used (generated in 1:8 diluted plasma with minimal endogenous periaxin), recovery ranged from 72% to 99% (Table 3.5), supporting its use as an alternative approach to mitigate matrix effects without sacrificing sensitivity.

Table 3.4. Buffer-based standard curve with plasma samples diluted 1:8 and 1:16

	Expected concentration (pg/ml)	1:8 dilution			1:16 dilution			
		Observed concentration (pg/ml)			Observed concentration (pg/ml)			
		Plasma 1	Plasma 2	Plasma 3	Plasma 1	Plasma 2	Plasma 3	Diluent only
High	1000	510.9	508.1	500.4	782.9	700.8	705.4	876.8
Medium	500	236.4	274.9	260.6	402.4	428.3	407.5	439.6
Low	250	99.5	140.7	124.8	235.8	195.7	175	248.6
Blank	0	2.9	9.2	4.8	2.8	8.7	5.1	1.1

Table 3.5. Matrix-matched standard curve generated in diluted plasma (1:8)

	Expected concentration (pg/ml)	Observed concentration (pg/ml)		
		Plasma 1	Plasma 2	Plasma 3
High	1000	889.2	783.7	814.4
Medium	500	495.6	411.1	437.2
Low	250	181.4	228.7	205.8
Blank	0	11.4	5.1	<LLOD

To confirm that periaxin concentrations measured at 1:8 and 1:16 dilutions were consistent and not significantly affected by dilution-related matrix effects, five plasma samples were tested at both dilutions within the same assay run. This within-run comparison allowed assessment of dilution-adjusted concentration stability under matched conditions. For each sample, the periaxin concentration measured at 1:16 was compared to that at 1:8, after adjustment for the dilution factor. All five samples showed agreement within the predefined acceptance range of 80–120% (Table 3.6), confirming that quantification remains reliable across these dilutions. These results further support the use of 1:8 as the MRD while allowing for flexibility in re-assaying at 1:16 if needed.

Table 3.6. Direct comparison of dilutions: plasma periaxin measured at 1:8 and 1:16

Sample	1:8	1:16	%CV
1	656	784	119
2	2184	2272	104
3	400	464	116
4	243	202	83
5	53	55	100

3.2.3.6 Lower Limit of Quantification (functional sensitivity)

Method

The Lower Limit of Quantification (LLOQ of functional sensitivity) of an assay represents the lowest analyte concentration that can be measured with acceptable precision, while the lower limit of detection (LLOD) refers to the smallest concentration that can be distinguished from background signal. In practice, the LLOQ is often 5–10 times higher than the LLOD to ensure reliable quantification. To estimate the LLOQ, a standard curve was first generated in assay diluent using serial dilutions of recombinant periaxin spanning a defined concentration range. The LLOQ was initially defined as the lowest calibration point at which intra-assay precision, expressed as the CV [(standard deviation/mean) x 100], was ≤20% across five replicates. To account for potential matrix effects, the LLOQ was subsequently re-evaluated by spiking low concentrations of recombinant periaxin into EDTA plasma samples previously confirmed to contain no detectable endogenous periaxin. This allowed determination of functional sensitivity under realistic sample conditions. The final LLOQ was defined based on assay performance in plasma, which was selected as the preferred matrix for all downstream analyses.

Results

The lowest calibration point with a CV ≤20% was 2.40 pg/ml. To determine the LLOQ in plasma, recombinant periaxin was spiked into a healthy control sample previously confirmed to have undetectable endogenous periaxin levels. Precision was assessed at three low spike concentrations: 1.0, 1.5, and 2.0 pg/ml, each tested in five replicates. At 1.0 pg/ml, the CV was 23.0%, exceeding the acceptable threshold for quantification. At 1.5 pg/ml, the CV was

20.0%, meeting the standard criterion for LLOQ. At 2.0 pg/ml, the assay showed improved precision with a CV of 15.1%. Based on these results, 1.5 pg/ml was defined as the LLOQ in plasma, with 2.0 pg/ml offering more consistent performance. Detailed precision data for each concentration are summarised in Table 3.7.

Table 3.7. Lower Limit of Quantification

Spike (pg/ml)	Measured values (pg/ml)	Mean (pg/ml)	SD (pg/ml)	CV (%)	Interpretation
1.0	0.67, 0.85, 0.90, 1.20, 1.15	0.9	0.2	23	Above CV threshold – not acceptable as LLOQ
1.5	0.86, 1.33, 1.30, 0.92, 1.27	1.1	0.2	20	Borderline – meets CV threshold, acceptable as LLOQ
2.0	1.37, 1.89, 2.10, 1.90, 1.75	1.8	0.3	15	Within CV threshold – acceptable as LLOQ

3.2.3.7 Precision and reproducibility

Method

Intra-assay precision was assessed by calculating the CV for 15 individual plasma samples, each tested in duplicate within a single assay run.[163] Samples were distributed across three independent runs (5 samples per run), and the mean CV across all samples was used to reflect overall within-run variability. To assess *inter-assay precision*, five plasma samples

containing varying levels of endogenous periaxin were measured in duplicate across five independent assay runs.[163] The mean, standard deviation and CV were calculated for each sample to evaluate precision across runs. To assess reproducibility, the *intraclass correlation coefficient* (ICC) was calculated using a two-way random effects model with absolute agreement. The ICC quantifies the proportion of total variance attributable to differences between samples, relative to the total variance (between- and within-sample variability). An ICC value close to 1 indicates excellent reproducibility of measurements across runs.

Results

The mean intra-assay CVs for Runs 1, 2, and 3 were 8.82%, 4.58%, and 4.94%, respectively. The overall mean CV across all 15 samples was 6.11%, reflecting good within-run precision (Table 3.8). Inter-assay precision was evaluated by measuring five plasma samples across five independent assay runs. Mean concentrations ranged from 19.4 pg/mL to 885.0 pg/mL, covering the assay's dynamic range (Table 3.9). The CV for individual samples ranged from 8.8% to 30.8%, with the highest variability observed in the low-concentration sample (Sample 2). Most samples demonstrated CVs below 20%, indicating good reproducibility, particularly at moderate to high concentrations. To assess overall between-run consistency, the ICC was calculated using a two-way random effects model with absolute agreement. The resulting ICC was 0.980, indicating excellent reproducibility of the assay across independent runs.

Table 3.8. Intra-assay precision

Run	Sample	CV (%)	Mean Run CV (%)
1	1	1.3	8.82
	2	30	
	3	1.1	
	4	6.6	
	5	5.1	
2	6	6.9	4.58
	7	7.5	
	8	4.2	
	9	1	
	10	3.3	
3	11	0.8	4.94
	12	11.1	
	13	9.8	
	14	2.1	
	15	0.9	

Table 3.9. Inter-assay precision

Sample	Run 1	Run 2	Run 3	Run 4	Run 5	Mean	SD	CV (%)
1	244	259.2	272	340	204.8	264	49.4	18.7
2	20	24	18	25	10	19.4	5.9	30.8
3	234	267	199	250	235	237	25.1	10.6
4	867	788	912	999	859	885	77.7	8.8
5	419	521	444	506	499	477.8	43.9	9.2

3.2.3.8 Sample stability

Method

Sample stability was evaluated by assessing the effect of delayed processing and multiple freeze–thaw cycles on periaxin concentrations. Three plasma samples with high, intermediate, and low endogenous periaxin levels were used throughout all experiments.

To assess the impact of **delayed centrifugation**, each sample was subjected to five conditions before centrifugation and freezing at −80 °C:

1. processed within 30 minutes of venepuncture;
2. stored for 3 hours at room temperature (RT);
3. stored for 3 hours at 2–8 °C;
4. stored for 24 hours at RT;
5. stored for 24 hours at 2–8 °C.

To evaluate the effect of **delayed freezing**, the same three samples were first centrifuged promptly within 30 minutes of collection, then subjected to the following conditions before freezing:

6. stored for 3 hours at RT;
7. stored for 3 hours at 2–8 °C;
8. stored for 24 hours at RT;
9. stored for 24 hours at 2–8 °C.

For **freeze–thaw stability**, each of the three samples was divided into five aliquotes. Aliquots were subjected to one to four freeze–thaw cycles prior to analysis:

- aliquot 1 underwent one cycle;
- aliquots 2 underwent two freeze-thaw cycles;
- aliquots 3 underwent three freeze-thaw cycles;
- aliquots 4 underwent four freeze-thaw cycles;
- aliquots 5 underwent five freeze-thaw cycles.

Results

Periaxin concentrations were markedly increased when centrifugation was delayed, particularly after prolonged storage of whole blood at room temperature (Table 3.10 and Fig. 3.18). In all three samples, periaxin levels increased between 3 and 24 hours of whole blood storage at RT. For example, in sample 1, concentrations rose from 388 pg/ml to 671 pg/ml, in sample 2 from 120 pg/ml to 188 pg/ml, and in sample 3 from 200 pg/ml to 376 pg/ml. A similar but attenuated increase was observed under refrigerated conditions. This rise is unlikely to reflect true biological release of periaxin, as the protein is Schwann cell–specific and not expressed by circulating blood cells. Instead, the increase may reflect pre-analytical artifacts associated with prolonged sample handling. A plausible explanation for this increase might be the presence of Schwann cell–derived extracellular vesicles or exosomes in the circulation, particularly in individuals with peripheral nerve injury. Periaxin is anchored to the cytoplasmic surface of the Schwann cell plasma membrane, and may be incorporated into the inner membrane of these vesicles. Delayed processing of whole blood, especially at room temperature, may promote vesicle degradation or membrane rupture, leading to the release of periaxin into the plasma prior to centrifugation. In contrast, when centrifugation was

performed promptly, periaxin levels remained relatively stable over time. In sample 1, concentrations were 244 pg/ml after 3 hours at RT and 222 pg/ml after 24 hours at RT - representing minimal decline. Lower periaxin levels were observed when samples were stored at 2–8 °C after centrifugation, with values of 79 pg/ml at 3 hours and 97 pg/ml at 24 hours. This pattern was also seen in samples 2 and 3, indicating a consistent pattern. These lower concentrations at 2–8 °C are unlikely to reflect degradation, which would typically be more pronounced at higher temperatures. Instead, they may be due to cold-induced adsorption of periaxin to the inner surface of collection tubes or to conformational changes that reduce assay detectability, as described for other plasma proteins.[164] In contrast, peripherin and NfL concentrations remained stable across all preanalytical conditions. In all three samples, values fluctuated minimally with changes in processing time or temperature, and no systematic pattern was observed. This supports the robustness of axonal intermediate filaments compared to large coiled-coil proteins such as periaxin, the structural properties of which may contribute to increased vulnerability to adsorption or conformational changes during processing.

Freeze-thaw experiments showed that periaxin levels remained stable through three cycles but declined markedly thereafter, falling to approximately 50% of initial values by the fifth cycle. These results indicate that exceeding three freeze-thaw cycles significantly compromises periaxin stability and should be avoided in biomarker studies.

Table 3.10. Impact of preanalytical conditions on periaxin, peripherin and NfL

Sample	Delay to	Delay time	Temperature	Periaxin (pg/ml)	Peripherin (pg/ml)	NfL (pg/ml)
1	centrifugation	3 h	RT	388.0	15.0	24.0
1	centrifugation	3 h	2–8°C	193.6	14.2	22.0
1	centrifugation	24 h	RT	671.3	15.4	23.0
1	centrifugation	24 h	2–8°C	286.6	14.9	22.7
1	freeze	3 h	RT	243.5	15.6	23.5
1	freeze	3 h	2–8°C	79.4	13.8	21.9
1	freeze	24 h	RT	222.5	14.7	23.2
1	freeze	24 h	2–8°C	97.8	15.1	21.9
2	centrifugation	3 h	RT	120.0	10.0	32.6
2	centrifugation	3 h	2–8°C	7.5	7.1	33.4
2	centrifugation	24 h	RT	188.1	10.6	31.6
2	centrifugation	24 h	2–8°C	21.7	10.1	33.7
2	freeze	3 h	RT	1.0	9.6	29.1
2	freeze	3 h	2–8°C	4.1	8.1	31.2
2	freeze	24 h	RT	0.7	11.1	31.2
2	freeze	24 h	2–8°C	7.2	10.4	32.0
3	centrifugation	3 h	RT	200.0	3.0	10.0
3	centrifugation	3 h	2–8°C	104.0	2.7	11.0
3	centrifugation	24 h	RT	376.0	5.0	10.5
3	centrifugation	24 h	2–8°C	168.0	4.1	9.0
3	freeze	3 h	RT	120.0	3.2	8.5
3	freeze	3 h	2–8°C	52.0	3.8	12.0
3	freeze	24 h	RT	102.4	3.9	11.4
3	freeze	24 h	2–8°C	63.2	4.3	11.7

Figure 3.18. Impact of preanalytical conditions on periaxin, peripherin and NfL

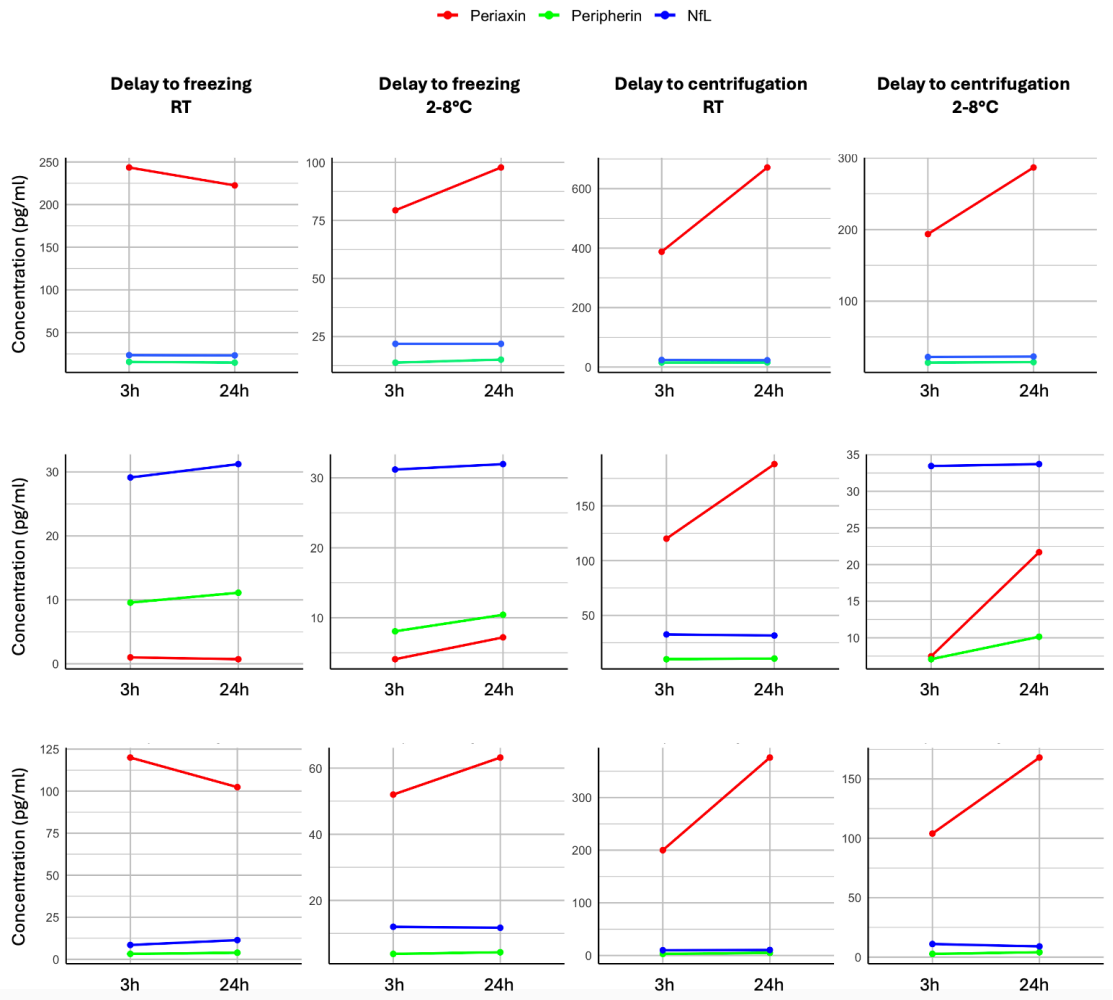

Concentrations of periaxin, peripherin and NfL were measured in three samples (plasma for periaxin and NfL, serum for peripherin) processed under different preanalytical conditions, varying by delay to centrifugation or freezing (3 or 24 hours) and storage temperature (room temperature or 2–8 °C). Periaxin levels were markedly increased when centrifugation was delayed, particularly after 24 hours at RT, possibly suggesting cellular release prior to plasma separation. In contrast, when centrifugation was performed promptly, periaxin concentrations remained relatively stable, although values were consistently lower following storage at 2–8 °C compared to RT. This may be due to temperature-dependent adsorption or conformational changes. Peripherin and NfL levels remained stable across all conditions, indicating greater robustness to preanalytical variation.

Figure 3.19. Effect of freeze-thaw cycles on plasma periaxin levels

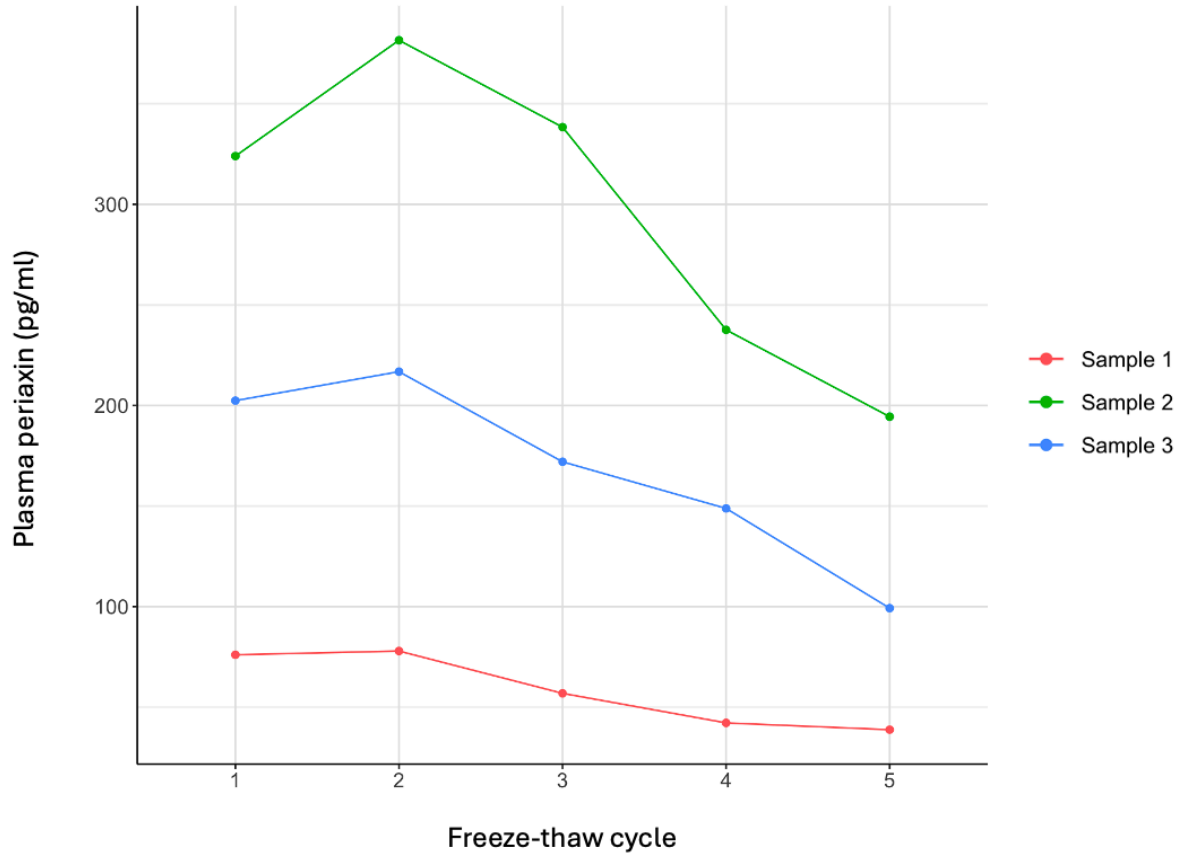

Periaxin concentrations remained stable through three freeze-thaw cycles across all samples, but declined markedly thereafter, falling below 80% of baseline after the third cycle, and reaching approximately 50% of the initial values by the fifth cycle.

3.3 Simoa peripherin assay optimisation

3.3.1 Bead conjugation and detector antibody biotinylation

The Simoa peripherin assay was initially developed using a conventional two-step protocol, with capture antibody conjugation to paramagnetic beads via EDC-only activation in 50 mM MES buffer (pH 6.5), and detector antibody biotinylation using NHS-PEG4-Biotin. This configuration yielded a lower limit of detection of 0.87 pg/mL, equivalent to 6.95 pg/mL after accounting for the 1:8 MRD of serum samples. To enhance assay sensitivity, the following optimisations were implemented:

Bead conjugation refinement:

- S-NHS was added to the bead conjugation step to stabilise intermediate ester formation and enhance coupling efficiency.
- The MES buffer pH was reduced from 6.5 to 5.0 to optimise EDC/S-NHS activation conditions.
- Molarity of the MES buffer was reduced from 50 mM to 25 mM to improve reaction kinetics.

Detector antibody biotinylation:

- NHS-PEG4-Biotin was replaced with NHS-LC-LC-Biotin to improve accessibility of biotin for SBG binding and to reduce background.

These combined changes substantially enhanced assay performance, resulting in a new LLOD of 0.14 pg/mL, corresponding to 1.1 pg/mL post-dilution, an 8-fold improvement in sensitivity.

3.3.2 Optimised Simoa peripherin protocol

Peripherin concentrations in biological samples (serum and culture supernatants) were quantified using the optimised Simoa assay on a Quanterix HD-X Analyzer, following the newly established protocol. For each run, calibrators were freshly prepared by serial dilution of recombinant human peripherin (NM_006262, Origene, purified from transfected HEK293T cells) into assay diluent. Serum samples were diluted 1:8 and loaded at a minimum volume of 230 µL per well. Each 96-well plate included eight calibrator concentrations in duplicate, alongside test samples also run in duplicate. The assay was performed using a two-step protocol. In the first step, paramagnetic beads conjugated to anti-peripherin monoclonal capture antibodies (8G2 clone, P5117, Sigma-Aldrich) were incubated with both the diluted samples and the biotinylated monoclonal detector antibody (A3 clone, sc-377093, Santa Cruz). Following washing to remove unbound components, the second step involved incubation with SBG, followed by a final wash and addition of enzyme substrate (RGP). Sample concentrations were interpolated from the standard curve using a 4PL model. To ensure data reliability, only measurements with intra-assay coefficients of variation below 15% were included in subsequent analyses.

Figure 3.20. Optimisation of the Simoa peripherin assay

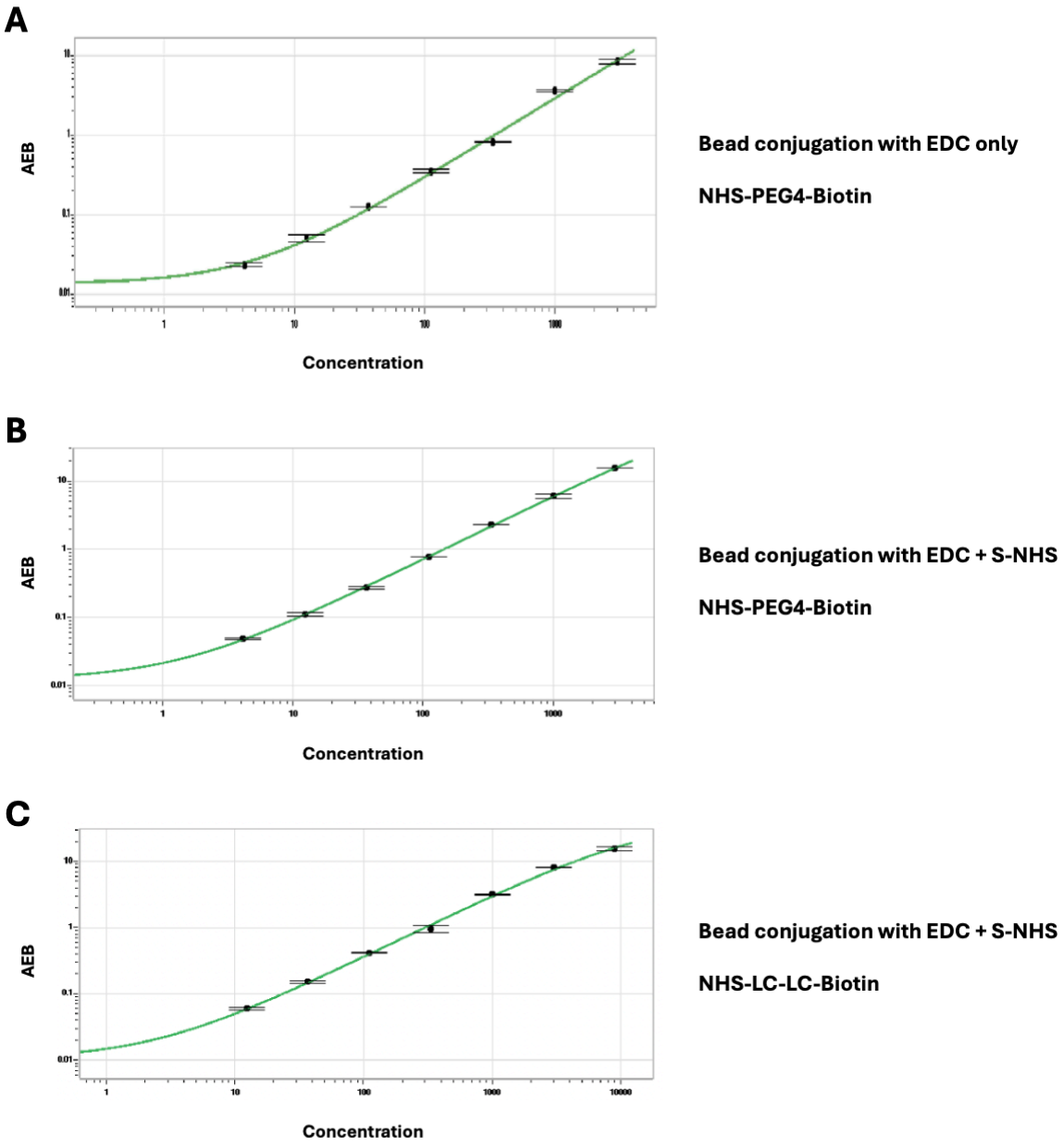

*(**A**) Initial standard curve using EDC-only bead conjugation and NHS-PEG4-Biotin for detector antibody labelling, with a LLOD of 0.87 pg/mL (6.95 pg/mL post-dilution). (**B**) Addition of Sulfo-NHS to the bead conjugation step and buffer optimisation improved coupling efficiency and lowered the LLOD. (**C**) Further replacement of NHS-PEG4-Biotin with NHS-LC-LC-Biotin for detector antibody biotinylation enhanced assay sensitivity, achieving an LLOD of 0.14 pg/mL (1.1 pg/mL post-dilution), representing an 8-fold improvement.*

3.4 Discussion

This chapter describes the development of an ultrasensitive immunoassay for the measurement of periaxin, a protein exclusively expressed by myelinating Schwann cells, in biological samples. Based on the findings presented, several important considerations emerge. First, successful purification of recombinant periaxin from transiently transfected HEK293T cells confirms the suitability of this system for antigen production. HEK293T cells enable high-yield expression of periaxin, with proper structural and antigenic integrity for use in assay calibration.

Simoa technology appears most suitable for periaxin detection given its ultrahigh analytical sensitivity. While ECL-based platforms could be used, their lower sensitivity may not always allow accurate and precise measurements, required for monitoring subclinical disease activity or subtle treatment responses over time. Simoa also offers a fundamental advantage over PEA, which reports relative fold-changes rather than absolute concentrations, making it less appropriate for longitudinal or clinical monitoring where exact quantification is essential. An additional advantage in this study was the ability to quantify periaxin, peripherin and NfL using the same platform, ensuring analytical consistency across biomarkers and streamlining sample processing. The main limitation of Simoa remains its high cost, which may impede widespread clinical adoption, so its use should be weighed against practical considerations such as resource availability and assay throughput.

Matrix studies have shown that periaxin is only reliably measurable in EDTA plasma, with levels undetectable or significantly reduced in serum and lithium heparin plasma. This observation may reflect the susceptibility of periaxin to calcium-dependent proteolysis. EDTA acts as a calcium chelator and rapidly inhibits calcium-dependent proteases at the

point of blood collection, thereby preserving protease-sensitive proteins such as periaxin. In contrast, lithium heparin prevents coagulation through antithrombin-mediated inhibition of thrombin and factor Xa, but does not immediately reduce ionized calcium levels. As a result, residual proteolytic activity may persist during the pre-analytical phase, potentially leading to degradation of periaxin.

Sample handling conditions were also found to substantially affect periaxin stability. Controlled experiments demonstrated that delaying centrifugation, particularly at room temperature, led to a marked increase in periaxin concentrations. This suggests that cellular release of periaxin continues during whole blood storage and is partially mitigated by refrigeration. Once centrifugation was performed, periaxin levels remained relatively stable over time, with minimal changes observed between 3 and 24 hours. Notably, lower periaxin concentrations were consistently observed when samples were stored at 2–8 °C following centrifugation, compared to samples kept at room temperature. As degradation is generally more pronounced at higher temperatures, this reduction is unlikely to reflect proteolysis. Instead, it may be attributed to cold-induced adsorption of periaxin to tube surfaces or conformational changes that reduce antibody accessibility. However, although refrigeration may result in slightly lower measured concentrations, it remains the preferred storage condition following centrifugation, as it preserves overall protein integrity and minimizes enzymatic activity. To ensure reproducibility and comparability across timepoints and cohorts, plasma samples should be centrifuged within a few hours of collection and either frozen immediately or stored refrigerated until freezing. Furthermore, freeze-thaw experiments demonstrated that periaxin levels start to decline beyond the third cycle, highlighting the importance of minimising repeated freeze-thawing to preserve sample integrity and ensure accurate quantification.

The assay currently employs a polyclonal antibody as the detector. While polyclonal antibodies are advantageous in early assay development due to their broad epitope recognition and high sensitivity, they are inherently limited by batch-to-batch variability and potential non-specific binding. These limitations may introduce inconsistency in assay performance with effects on reproducibility over time. To address these limitations, work is underway to develop a monoclonal detector antibody, which is expected to enhance assay specificity and reduce lot-to-lot variation. Despite these considerations, the assay has shown strong precision and reproducibility, with consistent results across samples and runs, supporting its robustness for reliable periaxin quantification in both longitudinal and comparative studies.

Parallelism experiments demonstrated that a minimum dilution of 1:8 is required to achieve linearity, indicating the presence of matrix effects at lower dilutions. Although linearity was improved at this dilution, recovery experiments suggested residual matrix interference. Such effects are common in plasma-based assays and reflect the complex nature of plasma proteins and interfering substances. While a dilution of 1:16 may further minimize matrix effects, it carries the risk of compromising sensitivity, especially in samples with low periaxin concentrations. Thus, 1:8 dilution represents a practical compromise between signal recovery and detection sensitivity.

In summary, the periaxin immunoassay developed using the Simoa platform demonstrates excellent analytical performance, characterized by high sensitivity, precision, reproducibility, and a wide dynamic range. These attributes make it particularly well-suited for detecting low-abundance targets in complex biological matrices and for monitoring longitudinal changes in disease activity or treatment response. While practical considerations such as cost and matrix-specific limitations remain, the assay provides a robust foundation for both experimental and

clinical biomarker studies. The following chapters will describe its application in in vitro models of demyelination and axonal injury, as well as its evaluation in clinical samples from patients with peripheral neuropathies, along with axonal biomarkers and established clinical outcome measures.

4 IN VITRO BIOMARKER VALIDATION

4.1 Introduction

Human induced pluripotent stem cells provide a valuable mechanistic platform for modelling disease in vitro.[165,166] Coculture systems combining IPSC-derived sensory neurons with rodent Schwann cells recapitulate key architectural features of peripheral nerves and allow the study of fundamental biological processes such axoglial interaction, myelination and axonal growth. Myelinating cocultures can also be injured using pathogenic antibodies and complement, reproducing aspects of demyelination and axonal damage observed in the inflammatory neuropathies, and thereby providing a controlled tool for morphological and immunohistochemical analysis of nerve injury. In this context, fluid biomarkers such periaxin, peripherin and NfL can be used as an informative, "tissue-related" tool to assess and understand the biological immunobiology underlying nerve disease. This chapter explores how fluid biomarkers and cell-based models can be integrated to more objectively assess axonal damage and demyelination, evaluate the protective effects of commonly used treatments such as IVIg, study axoglial development, and validate the underlying mechanisms that drive neural injury.

4.2 Periaxin and peripherin expression in cocultures

Method

The expression of periaxin in Schwann cells and peripherin in neurons was confirmed by immunocytochemical staining and confocal microscopy. For periaxin, immunocytochemistry

was performed using the polyclonal anti-periaxin antibody (orb413079, Biorbyt), also used as detector antibody in the Simoa assay. Myelin-specific binding was confirmed by colocalization with myelin basic protein (MBP), which was stained in parallel as a control using a rat anti-MBP antibody (Ab7349, Abcam). Axons were identified using an antibody against the heavy isoform of neurofilament (NF200, chicken anti-NF200, Ab4680, Abcam), followed by streptavidin conjugated to Pacific Blue (511222, Thermo Fisher). Secondary antibodies used for MBP and periaxin detection were a goat anti-rat Alexa Fluor 546 antibody (A11081, Thermo Fisher) and a goat anti-rabbit Alexa Fluor 488 antibody (A11008, Thermo Fisher), respectively. For peripherin, immunocytochemistry was performed using the assay capture antibody [mouse monoclonal anti-peripherin antibody (P5117, Sigma-Aldrich)], alongside the polyclonal anti-periaxin antibody (orb413079, Biorbyt) and the anti-NF200 antibody described above. A goat anti-mouse Alexa Fluor 647 antibody (A21236, Thermo Fisher) was used as the secondary antibody for peripherin detection.

Results

Expression of periaxin and peripherin was confirmed in the myelinating cocultures. Periaxin immunostaining showed clear localisation to myelinated segments and colocalisation with MBP along axons identified by NF200 staining (Fig. 4.1). Peripherin immunostaining demonstrated robust expression within the axonal cytoskeleton of IPSC-derived sensory neurons, with signal observed along NF200-positive fibres (Fig. 4.2).

Figure 4.1. Periaxin expression in myelinating cocultures

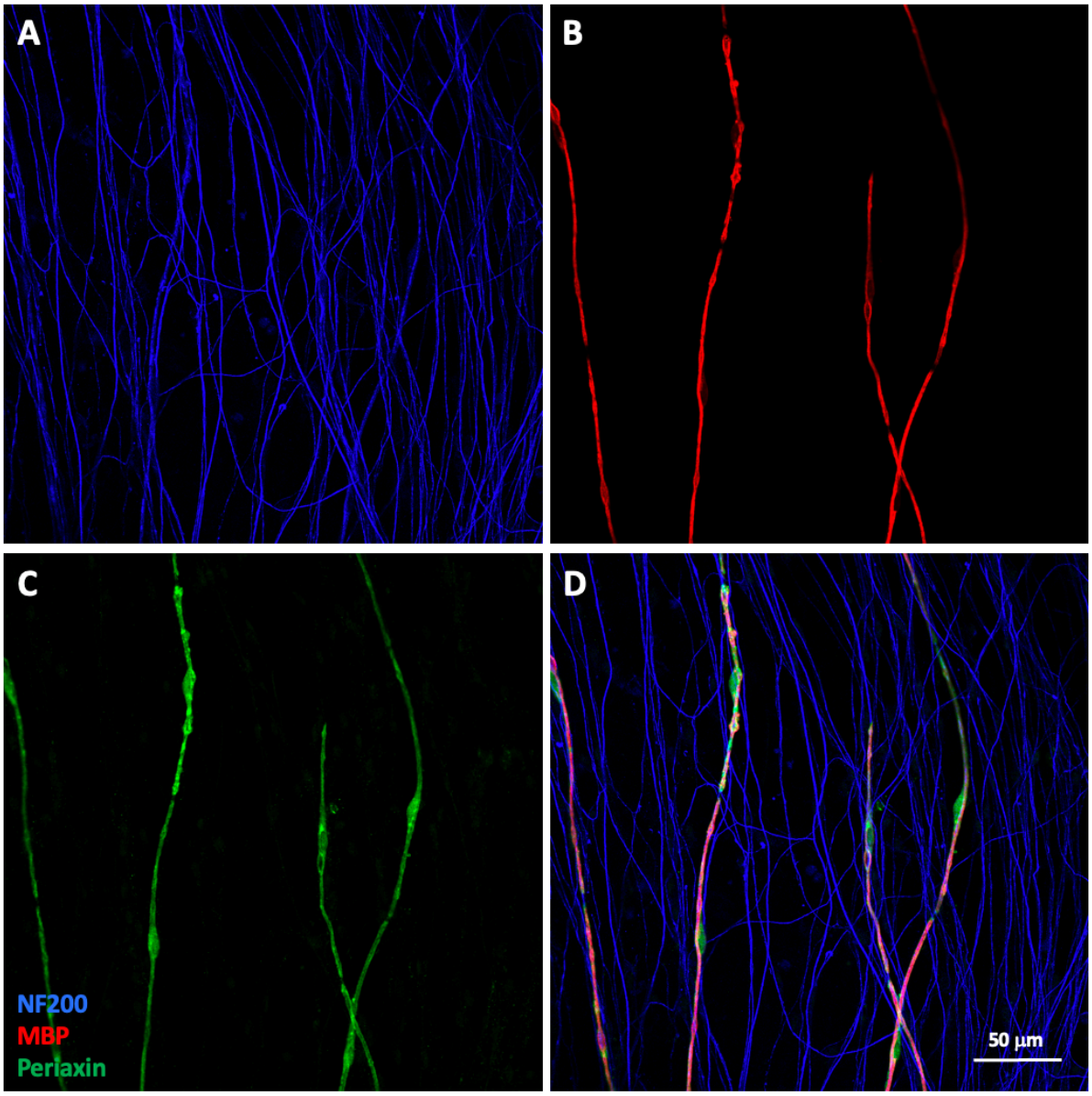

*Immunocytochemical detection of periaxin in myelinating co-cultures. (**A**) Axons stained for neurofilament heavy chain (NF200; blue). (**B**) Myelin basic protein (MBP; red) staining. (**C**) Periaxin (green) staining along myelinated segments. (**D**) Merged image showing colocalization of MBP and periaxin. Scale bar as indicated.*

Figure 4.2. Peripherin expression in myelinating cocultures

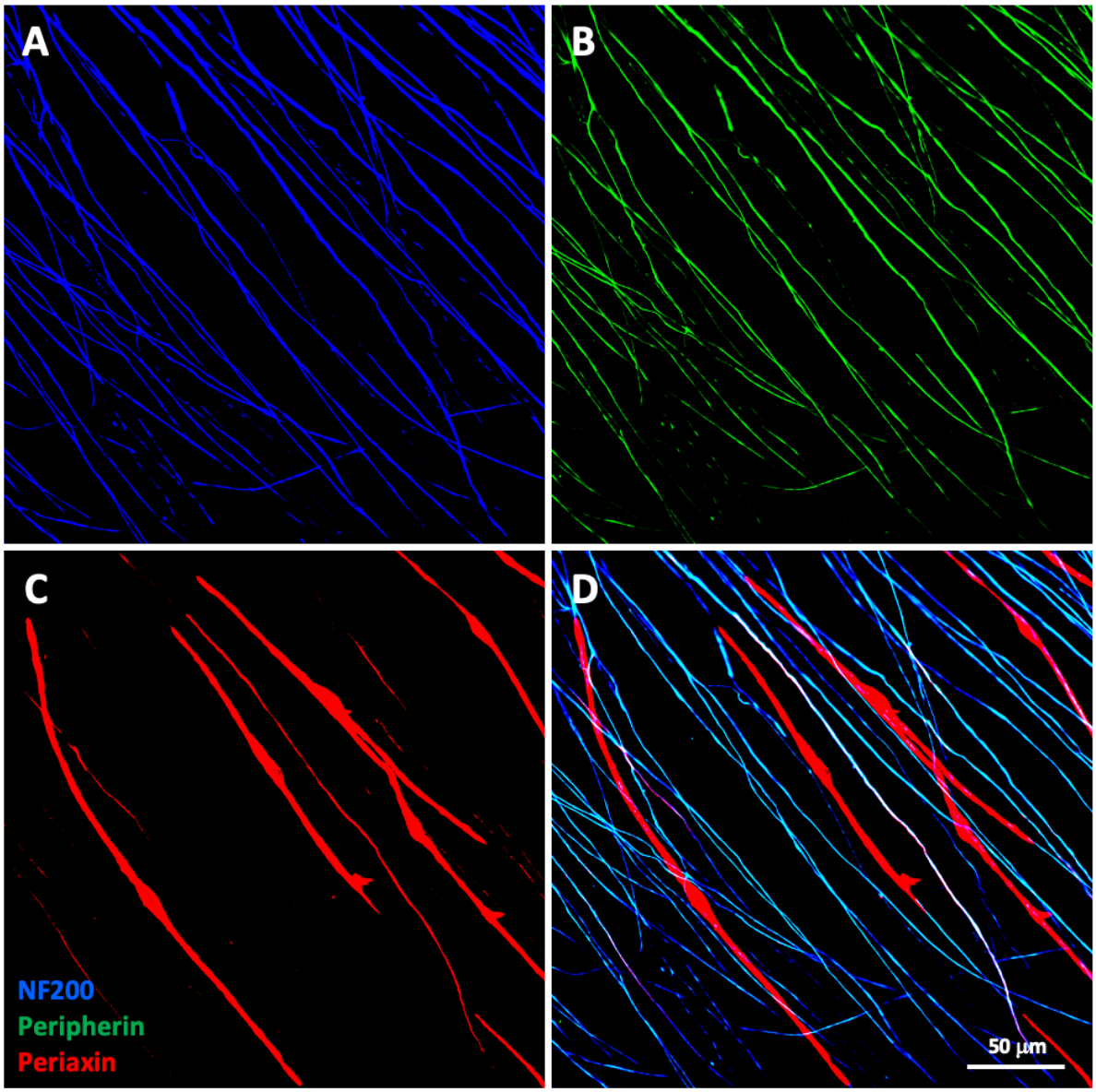

*Immunocytochemical detection of peripherin in iPSC-derived sensory neurons. (**A**) Axons stained for neurofilament heavy chain (NF200; blue). (**B**) Peripherin (green) staining along the axonal cytoskeleton. (**C**) Periaxin (red) staining of Schwann cell myelin. (**D**) Merged image showing colocalization of NF200 and peripherin. Scale bar as indicated.*

4.3 Biomarker release in cocultures with axoglial injury

Method

Detailed methods for inducing antibody-mediated, complement-dependent demyelination and axonal injury are described in Chapter 2. Briefly, demyelination was induced by applying a serum with established IgG myelin reactivity at a 1:50 dilution, whilst for axonal injury a monoclonal anti-GD2 antibody (14G2A) was used at 10 µg/ml, both followed by the addition of 20% normal human serum (NHS 20%) as a source of complement. Culture supernatants were collected from three replicate wells per condition (demyelination, axonal injury, and control) at baseline, 4 hours, 24 hours, and 48 hours post-injury. To assess morphological changes, cultured cells on coverslips were fixed with 4% paraformaldehyde, permeabilized with ice-cold methanol, and stained for NF200 and MBP as markers of axons and myelin, respectively. Immunostaining was performed using a chicken anti-NF200 antibody (Ab4680, Abcam) followed by streptavidin conjugated to Pacific Blue (511222, Thermo Fisher), and a rat anti-MBP antibody (Ab7349, Abcam) detected with a goat anti-rat Alexa Fluor 546 secondary antibody (A11081, Thermo Fisher). Coverslips were mounted with Vectashield mounting medium and fixed cells imaged using an Olympus SpinSR10 spinning disk confocal microscope. Systematic random sampling was used to capture representative fields across the coverslip. Myelin fragmentation was quantified in ImageJ by thresholding the MBP signal and calculating the percentage of fragmented myelin area relative to the total myelin area after subtraction of non-specific particles. Levels of periaxin and peripherin in culture supernatants were quantified at each time point using the newly developed Simoa assays (Fig 4.3). NfL levels were also measured and compared to peripherin at baseline (prior to injury), 4 hours and 24 hours (Fig. 4.4).

Results

Immune-mediated injury resulted in morphological and biochemical evidence of axoglial damage in the myelinating co-cultures and supernatants. Immunocytochemistry and confocal imaging revealed progressive myelin fragmentation following exposure to myelin-reactive serum and complement, with fragmented MBP signal detectable as early as four hours and increasing at 48 hours (Fig. 4.3 A). Quantification confirmed that, after applying pathogenic sera, myelin fragmentation reached approximately 15% at 4 hours and 30% at 48 hours (Fig. 4.3 B). In parallel, periaxin concentrations in the culture supernatant were significantly elevated following demyelination compared to uninjured control and axonal injury conditions. At 48 hours, periaxin levels were 8275.5 ± 155.6 pg/ml (mean ± standard deviation) in cultures with primary demyelination, compared to 3803.0 ± 727.0 pg/ml in axonal injury ($P = 0.003$) and 728.8 ± 161.8 pg/ml in uninjured cultures ($P = 0.0009$) (Fig. 4.3 C-D). The ratio of periaxin to peripherin was consistently higher following demyelination compared to axonal injury or control conditions at all time points (4, 24, and 48 hours), reflecting selective Schwann cell injury (Fig. 4.3 D). Peripherin levels, by contrast, increased progressively over time but were higher after primary axonal injury compared to demyelination (Fig. 4.3 D).

Figure 4.3. Periaxin and peripherin in myelinating culture systems

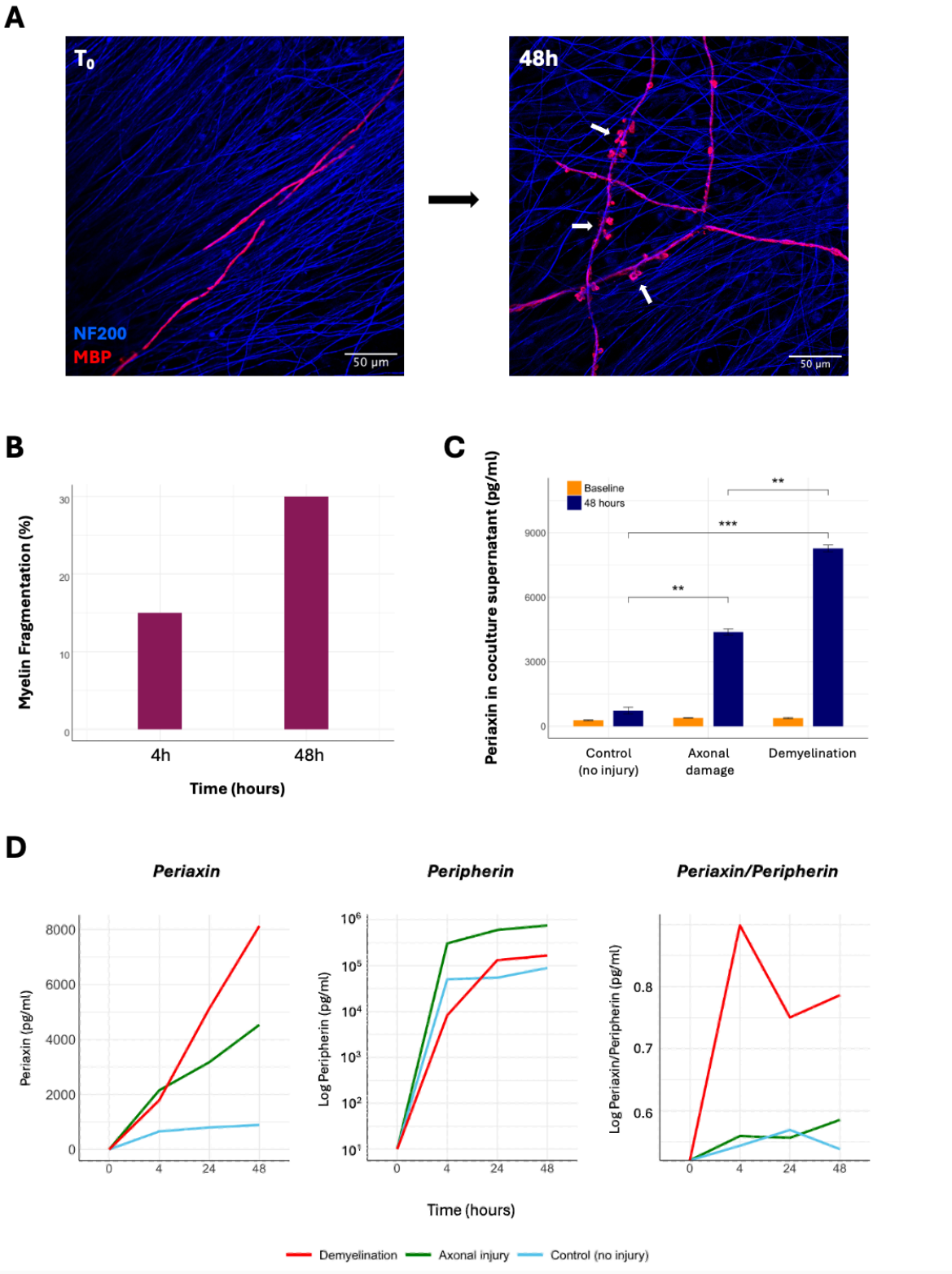

*Immunocytochemistry and confocal imaging of myelinating cocultures with antibody and complement-mediated demyelination imaged at baseline and 48 hours after application of complement. (**B**) Percentage of myelin fragmentation increased from 4 hours to 48 hours. (**C, D**) Periaxin levels in coculture supernatants increased gradually and were higher following demyelination compared to axonal damage (unpaired t-test, P = 0.003) and uninjured control conditions (P = 0.0009) at 48 hours. Similarly, peripherin levels rose rapidly and increased over time, but were higher after primary axonal injury compared to demyelination. The ratio of periaxin to peripherin was consistently higher in cultures with primary demyelination compared to axonal injury and control conditions at 4, 24, and 48 hours (**D**). Culture supernatants were collected from three replicate wells per condition. Each data point in the graphs represents the mean of these three replicates. Error bars are not visible because the replicate values were highly similar, and the small variation between them is not appreciable on the y-axis scale, which ranges from 0 to several thousand.*

Figure 4.4. In vitro comparison between peripherin and NfL

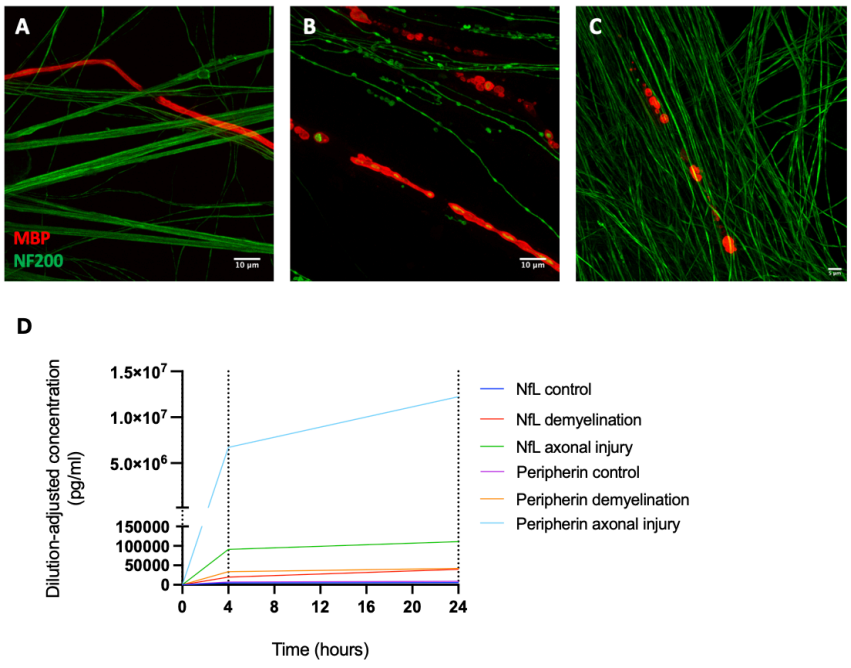

*(**A**) Control culture showing intact axons and myelin in healthy co-culture system. (**B**) Following axon-directed immunological injury, reduction of axonal density, irregular axonal morphology, and blebbing are observed (NF200, green), accompanied by some secondary myelin breakdown (MBP, red). (**C**) Primary demyelination is evident, with preserved axonal structure and prominent myelin blebbing. (**D**) Simoa quantification of NfL and Peripherin in culture supernatants at baseline, 4, and 24 hours. Axonal degeneration results in markedly elevated levels of both biomarkers compared to demyelination and control conditions, with levels rising rapidly and continuing to increase over 24 hours.*[167]

4.4 Periaxin and peripherin during myelination and axonal growth

Method

To establish baseline levels of periaxin and peripherin during physiological differentiation, biomarkers were measured at regular intervals during co-culture development. Periaxin concentrations were assessed weekly following seeding of Schwann cells into cultures of differentiated IPSC-derived sensory neurons to evaluate biomarker release during the process of myelination. In parallel, peripherin concentrations were measured daily during the differentiation of iPSCs into sensory and motor neurons to monitor biomarker release during axonal growth. Supernatants were collected at each time point and biomarker levels were quantified using the Simoa-based assays. To ensure accurate quantification over time, measured concentrations were adjusted to account for the cumulative removal of supernatant at each time point. At each collection, 30 µl was removed from a well containing an initial volume of 300 µl. Because the removed volume was not replaced, this progressive depletion was corrected by applying a dilution factor based on the remaining volume. Specifically, the adjusted concentration $C_{adjusted}$ at time t was calculated as $C_{adjusted} = C_{measured} \times (V_0/V_t)$, where:

- $C_{measured}$ is the biomarker concentration measured at time t
- V_0 is the initial volume (300 µl)
- V_t is the remaining volume in the well at time t after serial removals

Results

Periaxin progressively increased in the weeks following Schwann cell seeding into newly differentiated cultures of iPSC-derived sensory neurons (Fig. 4.5A). Similarly, peripherin rose gradually during the differentiation of both sensory and motor neurons from iPSCs (Fig. 4.5B). During physiological myelination, periaxin concentrations in supernatant were measurable but were

approximately 1000 times lower than levels measured after immune-mediated demyelination. Similarly, during axonal formation and growth, peripherin concentrations were approximately 15,000 times lower than those detected following antibody- and complement-mediated axonal injury (Fig. 4.5C-D).

Figure 4.5. Periaxin and peripherin during myelination and axonal growth

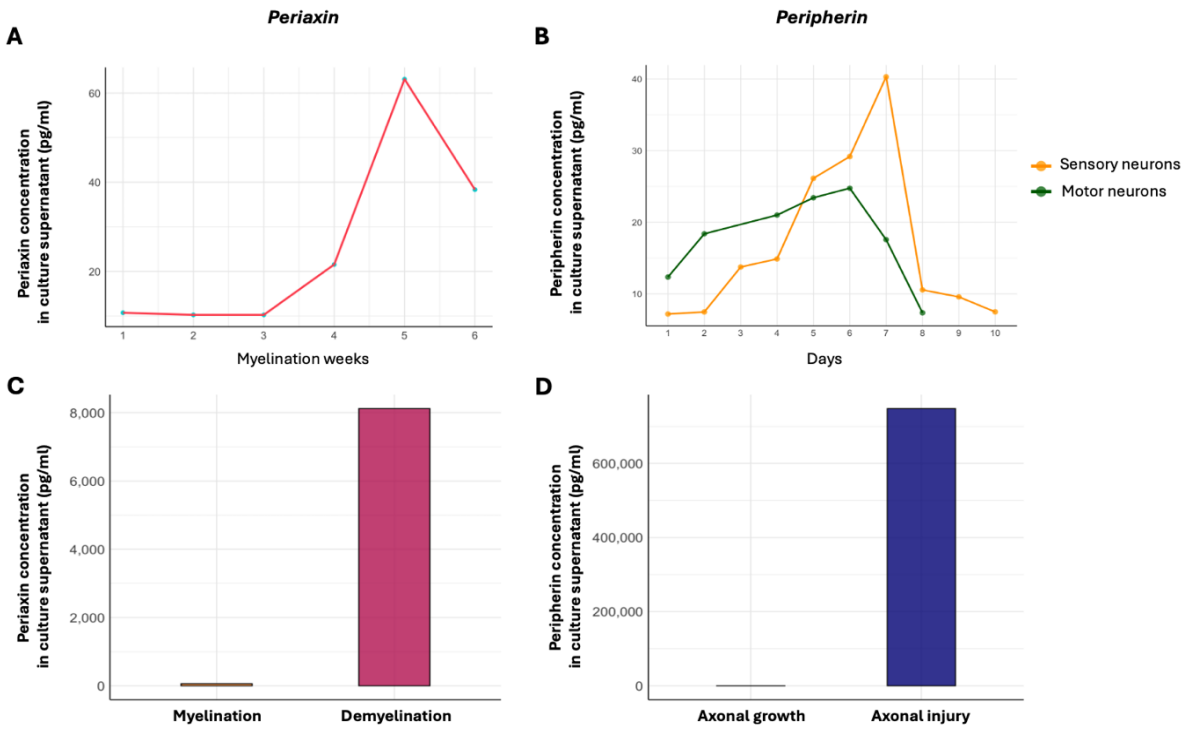

(A) *In cocultures of IPSC-derived sensory neurons and rodent Schwann cells, low levels of periaxin are released during myelination (after seeding of the Schwann cells into the neuronal cultures).* ***(B)*** *Similarly, levels of peripherin rise and fluctuate during axonal growth as stem cells differentiate into sensory or motor neurons.* ***(C-D)*** *Levels of periaxin and peripherin released in the supernatants of cocultures are substantially lower compared to injury levels.*

4.5 Validation of injury mechanisms: morphology and biomarker analysis

Aims and objectives

Experiments were performed to verify that demyelination and axonal injury in vitro are specifically mediated by the combined action of antibodies and complement, and to validate that biomarker levels dynamically reflect the extent and nature of the underlying structural injury. The experiments were designed to distinguish the effects of antibody binding alone, complement activation alone, and the requirement for both processes to induce damage, measured morphologically and biochemically.

Method

The myelinating co-cultures were exposed to the following conditions:

1. complete neurobasal medium + NGF only ("medium only");
2. myelin-reactive serum alone;
3. myelin-reactive serum + active complement (NHS 20%);
4. heat-inactivated myelin-reactive serum + NHS 20%;
5. myelin-reactive serum + heat-inactivated NHS 20%;
6. NHS 20% alone
7. GD2 monoclonal antibody (14G2A) alone at 10 μg/ml;
8. GD2 monoclonal antibody + active complement.

Heat inactivation of serum (myelin-reactive serum and NHS) was performed by incubation at 56°C for 30 minutes. Cultures were incubated with the respective treatments for one hour, followed by the addition of 20% NHS or heat-inactivated NHS where appropriate. Supernatants were collected at baseline (prior to treatment), 4, 12, 24, and 48 hours, and cultures were then fixed for immunocytochemical analysis. Axonal and myelin integrity were assessed by NF200 and MBP staining, as previously described in this chapter. Levels of periaxin and peripherin in the culture supernatants were measured using the Simoa-based assays. These experiments enabled the evaluation of whether changes in biomarker release corresponded to the degree of axonal and myelin injury across different experimental conditions.

Results

Both morphological analyses and biomarker measurements confirmed that demyelination and axonal damage occurred only when antibody and complement were applied together (Fig. 4.6 and Fig. 4.7). In the absence of either component, or when either the antibody or the complement was heat-inactivated, no significant structural injury was observed. This was reflected by preserved axoglial architecture on confocal microscopy and immunocytochemistry, as well as by markedly lower levels of periaxin and peripherin in the culture supernatants. These findings demonstrate that both antibody binding and complement activation are required to induce axoglial injury in this in vitro model, and further support the utility of periaxin and peripherin as biomarkers of demyelination and axonal damage, respectively.

Figure 4.6. Morphological comparison across culture conditions

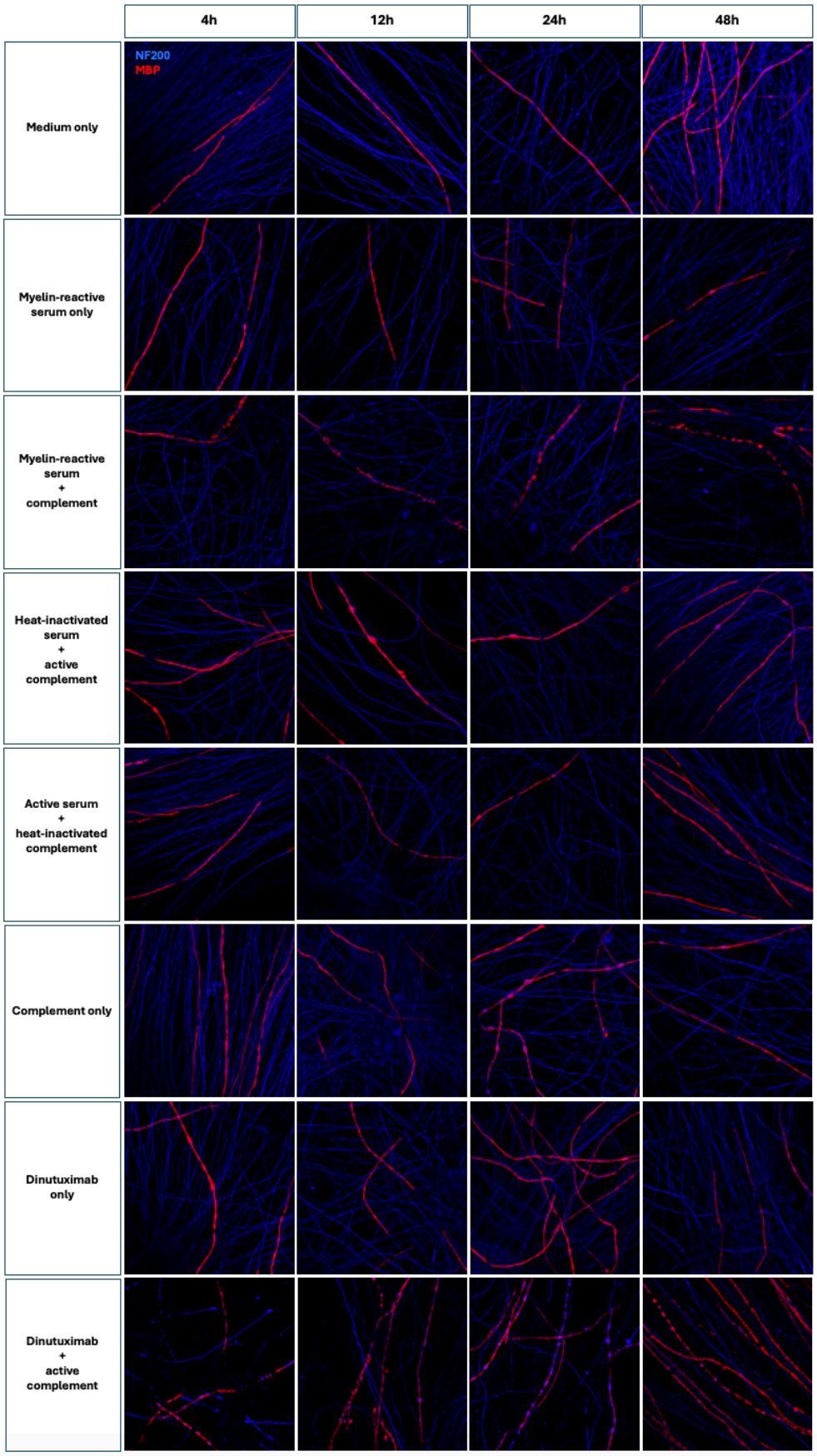

Morphological assessment of myelinating co-cultures under different experimental conditions revealed no significant axonal or myelin damage in cultures treated with medium alone, myelin-reactive serum alone, complement alone, heat-inactivated myelin-reactive serum with active complement, or myelin-reactive serum with heat-inactivated complement. Significant axoglial injury was observed only when both antibody and active complement were present: myelin-reactive serum combined with active complement induced primary demyelination with secondary axonal damage, whereas GD2 monoclonal antibody combined with active complement induced primary axonal injury, characterized by axonal blebbing and secondary myelin fragmentation. The extent of injury increased progressively over time.

Figure 4.7. Comparison of fluid biomarker levels across culture conditions

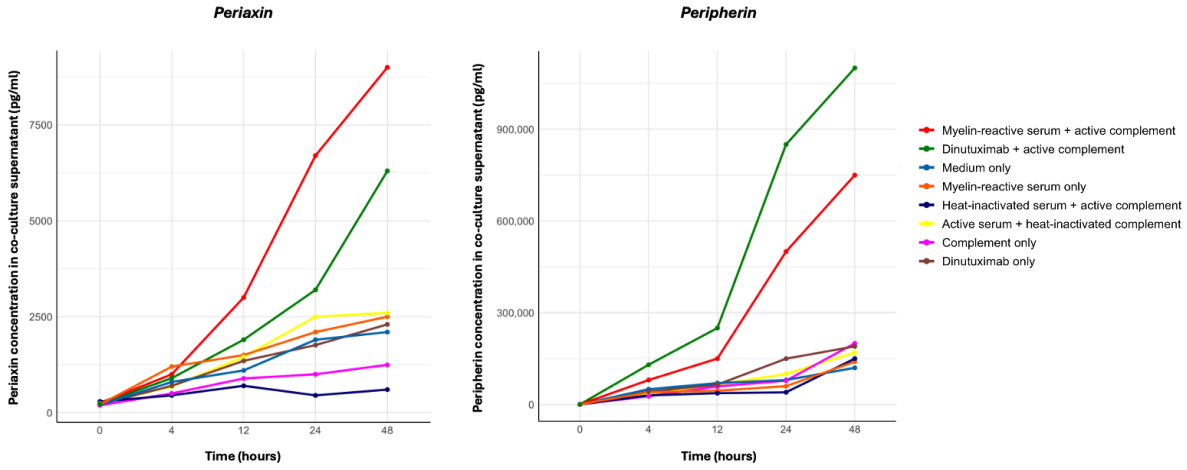

Significant release of both periaxin (left panel) and peripherin (right panel) occurred when both antibody and active complement were present, corresponding to conditions that induced structural axoglial injury. In the absence of either component, or when heat-inactivated antibody or complement was used, biomarker concentrations rose only modestly, likely reflecting spontaneous breakdown rather than immune-mediated injury. Each value (dot in the graph) represents a concentration measured in one well.

4.6 In vitro evaluation of biomarker response to IVIg treatment

Introduction

To assess whether periaxin and peripherin levels in coculture supernatants could reflect the protective effects of IVIg against axoglial injury in vitro, a pharmacologically relevant IVIg spiking experiment was performed. This approach aimed to replicate biomarker changes observed in vivo following IVIg treatment in patients with immune-mediated neuropathies. Based on published pharmacokinetic studies of IVIg in Guillain-Barré syndrome,[168] three concentrations of IVIg were selected to reflect the range of serum IgG increases ("delta IgG") typically achieved approximately two weeks after a standard 2 g/kg infusion.

Method

IVIg was spiked into culture medium at final concentrations of 4 g/L (low), 7.3 g/L (intermediate), and 11 g/L (high). Each IVIg concentration was added to cultures under three different conditions: demyelination medium, axonal injury medium, and normal (control) medium. Supernatants were collected at 12, 24, and 48 hours after IVIg addition for biomarker quantification. At the experimental endpoint, cultures were fixed, immunostained, and imaged using confocal microscopy as previously described in this manuscript.

Results

Levels of periaxin and peripherin varied between IVIg concentrations and injury conditions.

- *Periaxin*. In cocultures treated with demyelinating medium, only intermediate concentrations of IVIg appeared to mitigate damage, as reflected by lower periaxin levels. Comparable periaxin levels were observed in cultures treated with high, low, or no IVIg (Fig. 4.8). In cocultures exposed to axon-damaging medium, periaxin levels were lower in the presence of high or intermediate IVIg, possibly suggesting partial protection. In control cultures (without myelin-reactive serum, anti-GD2 antibody, or complement), periaxin levels remained low across all IVIg concentrations.

- *Peripherin*. Levels under axonal injury conditions were broadly similar across IVIg concentrations until the 48-hour time point, when an increase was observed in cultures treated with low IVIg. In cultures exposed to demyelinating medium, peripherin levels were slightly higher in the absence of IVIg and modestly reduced when low, intermediate, or high IVIg was applied. In control conditions, peripherin remained low across all IVIg concentrations, with a slight increase at 48 hours, likely reflecting physiological stress or baseline axonal damage.

In cocultures exposed to medium inducing axonal damage, morphological assessment by IHC and confocal microscopy showed preservation of axonal integrity at high IVIg doses, whereas early signs of axonal damage, including axonal blebbing and irregular axonal staining, were seen in cultures treated with intermediate, low, or no IVIg (Fig. 4.9). In contrast, in cultures treated with demyelinating medium, some myelin fragmentation – albeit mild - was observed in the absence of IVIg and at intermediate IVIg concentrations. Cultures treated with either high or low IVIg did not show clear evidence of myelin damage.

Figure 4.8. Co-culture levels of periaxin and peripherin in response to IVIg treatment

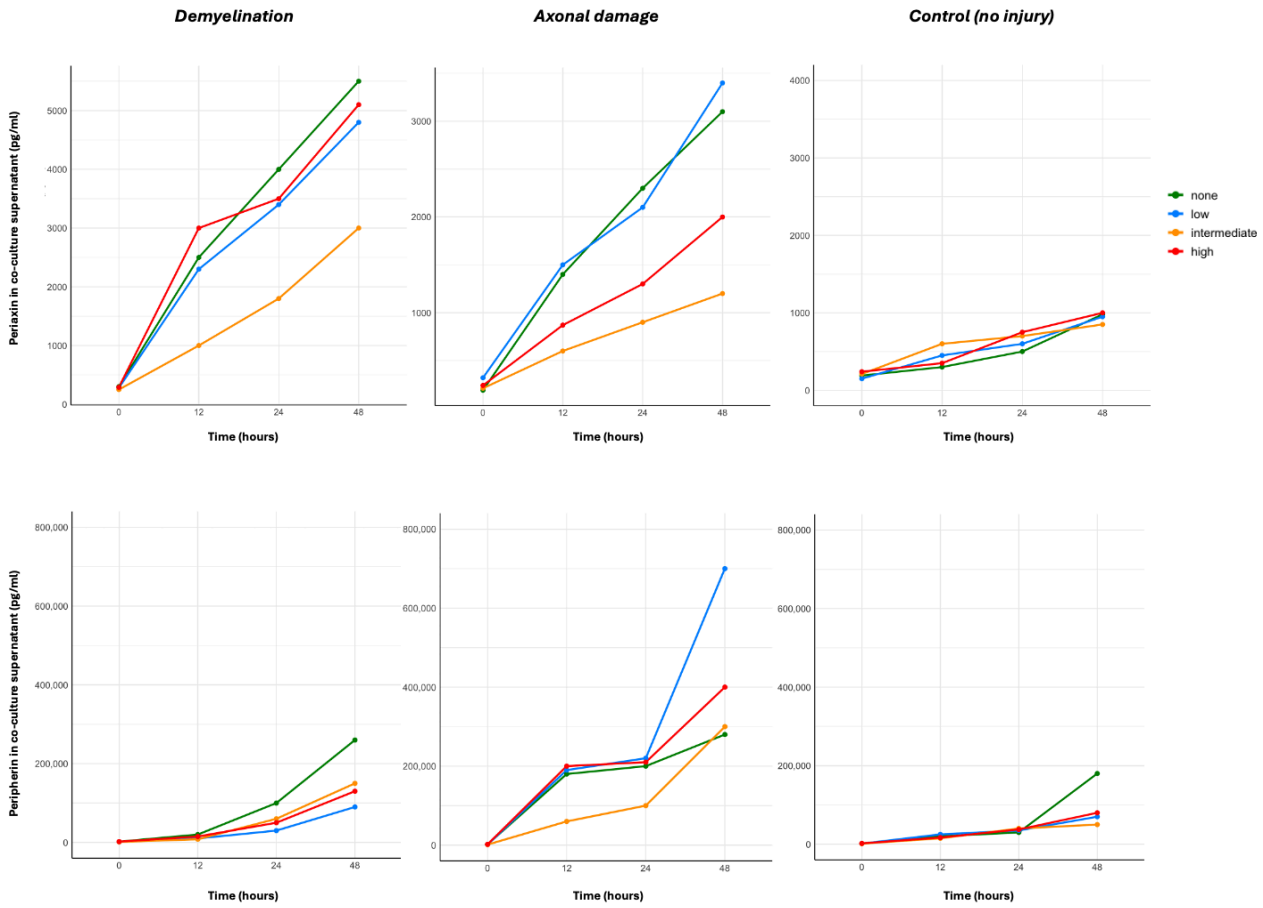

In cultures treated with medium to induce demyelination (left panels), intermediate IVIg concentrations led to lower periaxin levels compared to high, low, or no IVIg. In axon-damaging conditions, periaxin was reduced with high and intermediate IVIg, possibly suggesting partial protection of damage to axons by IVIg. Control cultures showed low periaxin levels across all IVIg concentrations. For peripherin, levels of biomarker release to the supernatant were higher in cultures with low IVIg under axonal damage conditions, whilst cultures treated with high, intermediate, or no IVIg showed similar values. In demyelinating conditions, peripherin was slightly elevated in the absence of IVIg and modestly reduced with increasing IVIg. In control cultures, peripherin remained low exposed to any IVIg conditions with a slight increase by 48 hours. Each value represents the mean of three wells (technical replicates of the same condition).

Figure 4.9. Immunohistochemistry of cocultures treated with axonal or demyelinating injury media and varying IVIg concentrations

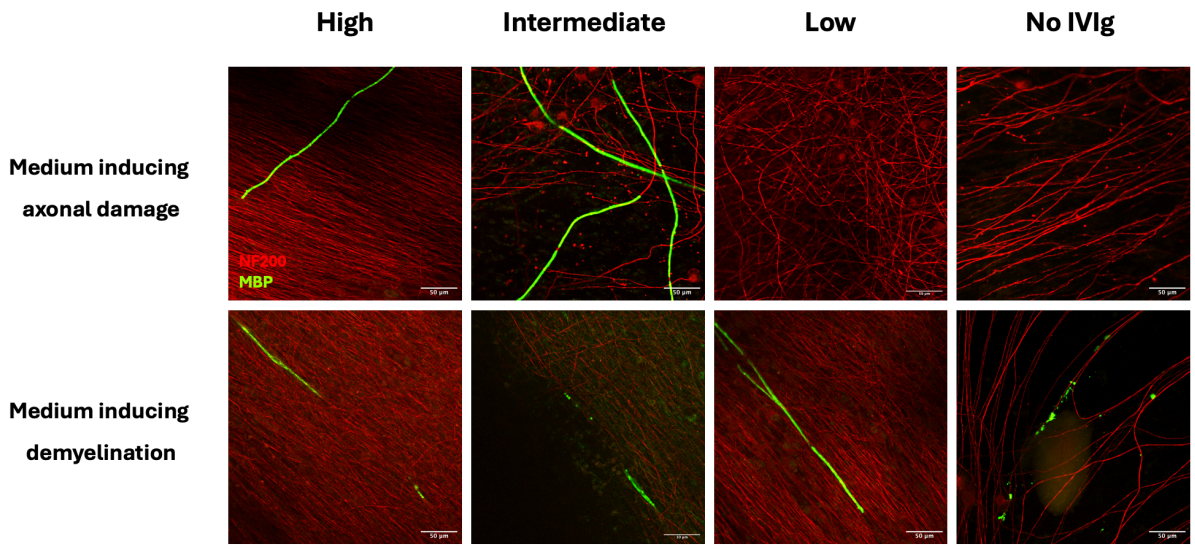

High IVIg concentrations preserved axonal morphology under axonal damage conditions, whereas early injury signs such as axolemmal blebbing and disrupted staining were observed with intermediate, low, or no IVIg. In demyelinating conditions, myelin loss was seen without IVIg, partially mitigated at intermediate IVIg concentrations. No clear demyelination was observed in cultures treated with high or low IVIg concentrations.

4.7 Discussion

Periaxin and peripherin are robustly expressed in cocultures of IPSC-derived sensory neurons and rat Schwann cells. Their direct release into the culture supernatant following injury, combined with the absence of a blood-nerve barrier, leads to high measurable levels compared to those seen in blood, reinforcing the value of these cell-based systems for biomarker validation and disease modelling. Levels of release are consistent with the type of injury anticipated from the conditions. Furthermore, measuring fluid biomarkers

complements morphological assessment with immunohistochemistry, confocal microscopy, and quantification of myelin fragmentation, offering a multiparametric approach to confirming nerve injury.

Supernatant levels of periaxin were higher following demyelination compared to axonal injury, whereas peripherin levels were higher after axonal damage than in primary demyelination. Both biomarkers showed a gradual increase over time. These findings are consistent with the expectation that the biomarker associated with the cell type primarily affected by injury would show the earliest and most pronounced elevation in the culture system. Indeed, the ratio of periaxin to peripherin most effectively distinguishes between demyelination and axonal injury as one would predict. These findings provide a rationale for utilising the peripherin/periaxin ratio in clinical blood samples from patients with inflammatory neuropathies as giving an indication of the predominant tissue target, and results are discussed in Chapter 5, where the clinical relevance of distinguishing between primary demyelination and axonal damage is discussed in depth.

Under physiological conditions, low levels of periaxin are transiently released during early myelination and peripherin during axonal outgrowth. A speculative interpretation is that periaxin may also be released during myelin repair; however, the concentrations observed in this context are substantially lower than those seen with pathological demyelination. This possibility warrants further investigation. Accordingly, elevated levels of periaxin and peripherin in patients with acute or chronic neuropathy are unlikely to reflect physiological repair processes and more likely represent active disease. Distinguishing between active and quiescent disease, and between repair and ongoing pathology, is a major challenge in patients with chronic inflammatory neuropathies - a context in which fluid biomarkers could offer valuable insight and improve disease monitoring.

Cellular damage in GBS and other inflammatory neuropathies is a complement dependent process. Combined morphological and fluid biomarker assessment demonstrated that axoglial injury in culture is also complement dependent, only occurring to any substantial level when antibody and complement are applied together (Fig. 4.6 and Fig. 4.7). In conditions lacking either component, or when the antibody or complement was heat-inactivated, no significant structural damage was observed, as indicated by markedly lower levels of periaxin and peripherin in the culture supernatants alongside overall preserved axoglial architecture. The demonstration that both antibody binding and complement activation are required to induce axoglial injury in vitro highlights the value of this model for testing targeted therapeutic strategies, including complement inhibitors and novel monoclonal antibodies aimed at preventing or reducing nerve damage. The inclusion of periaxin and peripherin as fluid biomarkers further strengthens the model's translational relevance by offering objective and quantifiable measures of demyelination and axonal injury.

IVIG has been demonstrated to hasten recovery from GBS[103] and be effective in the treatment of CIDP[42]. Preliminary findings from these experiments suggest that fluid biomarkers can also be used to assess the effects of IVIg on axonal and myelin integrity in vitro, using this co-culture system. Intermediate IVIg concentrations may protect against immune-mediated axonal damage and demyelination (primary or secondary) in vitro. The absence of a clear protective effect at high IVIg concentrations may reflect potential cellular toxicity at these doses. No firm conclusions can yet be drawn from these findings and, whilst early results are promising, additional studies are needed to determine whether IVIg exerts direct protective effects by blocking antibody binding, modulating complement activation, or through other as-yet-unknown mechanisms. Should IVIg prove ineffective in this context, the model still

provides a flexible platform in which injury severity can be titrated by adjusting the concentration of autoantibodies, complement source, or duration of exposure.

5 FLUID BIOMARKERS IN CIDP AND GBS

5.1 Introduction

No blood or CSF biomarkers specific to GBS or CIDP, or to their underlying cellular damage, have been identified for clinical use. Their diagnosis remains clinical and confirmed - and subsequently monitored - through neurological examination, basic CSF analysis (total protein and cell count), electrophysiological studies, and clinical scoring scales. Peripheral nerve imaging plays a more limited role. These tests are indirect measures of nerve damage, removed in various ways from the cellular pathology. Clinical examination remains pivotal for recording longitudinal disease progression but correlates imprecisely with the underlying pathology and ongoing disease activity. The lack of valid, specific, direct biomarkers of peripheral nerve demyelination potentially limits clinical management as it is not possible to determine if the disease process is still active. This uncertainty can lead to overtreatment-related side effects or excess disability as a result of undertreatment. Furthermore, as demand, consumption and cost of immunomodulation in the inflammatory neuropathies continue to increase, objective and responsive biomarkers are urgently needed to specifically measure peripheral nerve demyelination, individually tailor therapies and improve their cost-effectiveness.

NfL is an important but generic biomarker of axonal damage in the central and peripheral nervous systems.[126,127] In CIDP, plasma NfL is marginally higher before treatment with IVIg compared to healthy controls and in patients with active versus stable disease.[128] Although NfL may decrease in some after treatment, it does not increase again with relapse after treatment withdrawal.[128–130] In GBS, serum NfL levels correlate with disease severity and

axonal neurophysiology, and high baseline levels early in the disease course are associated with poorer functional outcomes and an increased likelihood of requiring ventilatory support.[131,132,169] As such, NfL could contribute to improved clinical measures and prognostic models in CIDP and GBS. However, due to the ubiquitous expression of NfL throughout the nervous system, it is not specific to any one disease, and high levels of NfL can be found in over 80 peripheral and CNS conditions, as well as some non-neurological disorders.[133] The difference between plasma NfL in active or untreated disease compared to controls is marginal in absolute terms and often not definitive in indicating disease activity or progression in individual patients. Previous work from our group demonstrated that peripherin, a type III intermediate filament protein, rises selectively in GBS and not in inflammatory or degenerative CNS disorders, and can differentiate acute axonal injury from slowly progressive demyelination.[167] Although NfL and peripherin have shown potential in identifying nerve injury and correlating with disease activity, both are axonal cytoskeletal proteins and neither can identify primary demyelination in the PNS. As such, there remains an unmet need for a biomarker that is both specific to peripheral nerve and capable of distinguishing demyelinating from axonal neuropathy

5.2 Methods

5.2.1 Participants and sample collection

Two cohorts of plasma samples were collected from patients with CIDP: a discovery cohort (n = 15) and an independent validation cohort (n = 30). In the discovery cohort, eight patients (53%) had multiple longitudinal samples collected, totalling 36 samples. In the validation cohort, nine of the 30 patients (30%) were sampled at more than one time point, resulting in

41 samples. CIDP patients had samples taken at variable intervals, up to 28 weeks apart. In total, 77 CIDP plasma samples were analysed across both cohorts. For the CIDP discovery cohort, samples were collected from patients presenting to the Manchester Centre for Clinical Neurosciences at Salford Royal Hospital (in collaboration with Dr Ryan Keh), through an observational study and biobank established at the John Radcliffe Hospital in Oxford, or from the Department of Neurology at the University of KwaZulu-Natal in Durban, South Africa (in collaboration with Dr Kaminie Moodley). The CIDP validation cohort was distinct and comprised samples from patients presenting to the National Hospital for Neurology and Neurosurgery in London. Samples were also collected from 30 patients with GBS, all presenting to Salford Royal Hospital in Manchester. Of these, 18 (60%) had multiple samples collected longitudinally (66 GBS samples in total). In the majority of GBS patients with multiple samples, these were collected at week 1, 2, 3, 4, and in some cases weeks 5, 6, 7, or 8. All patients had been evaluated by neurologists and electrophysiologists, and the diagnosis of CIDP or GBS had been confirmed by standard published clinical and neurophysiological criteria.[170,171] Single blood samples were also collected from 30 CNS controls with multiple sclerosis (MS) and 30 healthy controls (HC).

Blood samples were centrifuged at 3000g for 5 minutes and frozen at −80°C within five hours of collection. Both serum and plasma samples [collected in ethylenediaminetetraacetic acid (EDTA) tubes] were available for patients in the GBS and CIDP discovery cohorts, and both biofluids were tested in all cases. Periaxin was consistently measured in plasma but, with very few exceptions, was not detected in the serum samples. A direct comparison between lithium heparin (LiH) and EDTA plasma samples was performed, and periaxin was only measured in EDTA plasma. Consequently, EDTA plasma was selected for assays in subsequent analyses. Samples were tested for periaxin, peripherin (as previously described)[167]

and NfL using the Quanterix NF-light® Advantage Kit. Demographic information (age, sex) was available for all CIDP, GBS, MS patients, and healthy controls. Electrophysiology was available for 44/45 (98%) CIDP patients in the discovery and validation cohorts, and 23/30 (77%) GBS patients. Inflammatory-Rasch-built Overall Disability Scale (I-RODS) and Overall Neuropathy Limitations Scale (ONLS) were available for 18/30 (60%) GBS patients, whereas I-RODS and Medical Research Council Sum Score (MRC-SS) were linked to 41/45 (91%) CIDP patients. Treatment details were obtained for all CIDP patients and 26/30 (87%) GBS patients.

CIDP was classified as clinically *active* in 17/45 patients (38%) who demonstrated objective evidence of end-of-dose fluctuations between pre- and post-treatment with IVIg or during interval assessments between consecutive clinical reviews. A minimal clinically important difference (MCID) was defined as a change of at least four centile I-RODS points or two ONLS points. Patients who did not meet these criteria, as well as those in remission for at least six months, were classified as having *inactive* CIDP (16/45, 36%). Patients with discordant clinical outcome measures that prevented clear classification were categorised as indeterminate and were not assigned to either the active or inactive CIDP groups (12/45, 26%). All patients with active CIDP were receiving treatment: 15 were on IVIg, one on corticosteroids, and one on a combination of corticosteroids and cyclophosphamide. Among the 16 patients with inactive disease, two had achieved remission and were off treatment, while the remaining 14 had stable disease and were either on no treatment, or on maintenance IVIg or subcutaneous immunoglobulin (SCIg).

5.2.2 Statistical analysis

Statistical analysis was performed using R (R Core Team, version 4.3.3, 2024). Mann-Whitney U and Kruskal-Wallis tests were used to compare demographic and clinical data between the different groups. Spearman's correlation coefficient was used to assess the reciprocal correlations of periaxin, peripherin, NfL, and their correlation with age, as well as the correlation between biomarker levels (and their ratios) and clinical scales. Additionally, levels of periaxin, peripherin, NfL, their ratios, and disability scales were categorized into low, intermediate, and high groups by identifying the minimum and maximum values and dividing each range into quartiles, with the lower and upper cut-offs defined by the 25th and 75th percentiles, respectively. The relationships between each categorical variable and the respective disability scores, as well as between peak values and nadir disability scores, were analysed for associations using Fisher's exact test. This approach ensured a balanced distribution, enhanced the detection of non-linear relationships between biomarkers and clinical scales, and reduced the impact of outliers, thereby minimizing the risk of type II errors. To evaluate the relationship between periaxin and clinical scale changes in GBS and CIDP, summary statistics were used rather than correlation analyses due to the limited sample sizes. A linear mixed-effects model was fitted to assess the association between plasma periaxin levels, CIDP classification (active vs inactive), and time since the most recent treatment. The model included CIDP classification and days since treatment as fixed effects, with patient ID included as a random intercept to account for repeated measures.

For biomarker comparisons between GBS electrophysiological subtypes, plasma concentrations were log-transformed to normalize their distribution and stabilize variance. Medians of the log-transformed values were calculated for each group within each comparison. Pairwise comparisons between axonal and demyelinating groups were

performed using the two-sample t-test. Empirical receiver operating characteristic (ROC) curves were used to assess the diagnostic utility of plasma periaxin, peripherin, NfL, and reciprocal ratios to discriminate between electrophysiological subtypes, and only the three with the highest area under the curve (AUC) were shown, including 95% Confidence Interval and cut-off optimising Youden Index.

To minimise the risk of false associations (type I error) when comparing levels across different groups, any samples with concentrations below the LLOD were assigned values of 1.6 pg/ml (periaxin), 1.1 pg/ml (peripherin), or 0.34 pg/ml (NfL), corresponding to the assays' respective detection limits. To investigate whether periaxin is associated with age, sex, or body mass index (BMI), two separate linear regression analyses were performed. In the first model, restricted to healthy controls, age and sex were included as covariates. In the second model, combining data from CIDP and healthy controls, age, sex, BMI, and disability (measured through clinical outcome measures) were included as covariates. Model fit and variability explained were assessed using the coefficient of determination (R2) and adjusted R2 values. A significance value of $P < 0.05$ was used throughout, with Bonferroni correction for multiple comparisons.

5.3 Results

5.3.1 Fluid biomarkers in CIDP

In CIDP samples, median peak plasma periaxin levels were 256.0 pg/ml (IQR: <LLOD - 1286 pg/ml) in the discovery cohort and 261.2 pg/ml (IQR: 14.1–920 pg/ml) in the validation cohort. In contrast, periaxin levels were substantially lower in patients with MS (median 19 pg/ml, IQR: <LLOD–174 pg/ml) and healthy controls (21.9 pg/ml, IQR: <LLOD–126.9

pg/ml). Periaxin concentrations were significantly higher in CIDP compared to both MS and healthy controls (Wilcoxon rank-sum test, P < 0.0001 for both comparisons). Peak peripherin levels in CIDP (median 5.18 pg/ml) were significantly higher than in MS (<LLOD, P = 0.0057) and healthy controls ((<LLOD, P < 0.001). For NfL, CIDP patients had significantly higher levels compared to healthy controls (15.2 vs 5.51 pg/ml, P < 0.0001), but not significantly different from MS (21.5 pg/ml). Group comparisons are shown in Fig. 5.1.

Patients with active CIDP had substantially higher plasma periaxin compared to those with inactive CIDP (median 522.4 vs 57.9 pg/ml, *P* < 0.0001, Wilcoxon rank-sum test; Fig. 5.2A). This difference remained significant in a linear mixed-effects model that accounted for repeated measures and included CIDP classification and time since the most recent treatment as fixed effects (P = 0.0012), with a mean reduction of 311.55 pg/ml in the inactive group. There was no significant association between plasma periaxin levels and time since the most recent treatment (β = -3.90, 95% CI [-10.0, 2.2], *P* = 0.196). No significant differences were seen for peripherin or NfL in active versus stable disease.

Figure 5.1. Periaxin, peripherin and NfL in CIDP and GBS compared to CNS disease and healthy controls

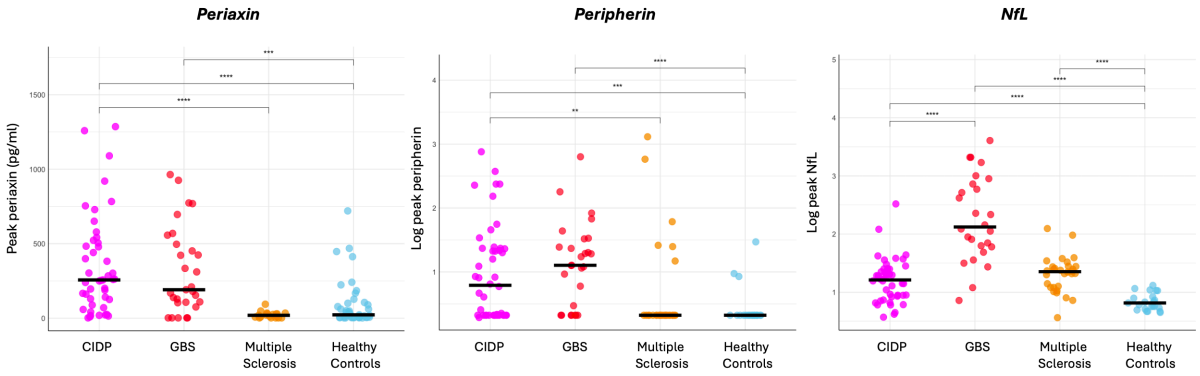

Periaxin concentrations were significantly higher in CIDP compared to both MS and healthy controls ($P < 0.0001$). GBS patients also showed elevated levels overall; however, the group includes individuals with both AIDP and AMAN subtypes, resulting in lower median values. Horizontal bars indicate median values for each group.

Only periaxin levels decreased following treatment with IVIg, with a median time to decline of four weeks (Fig. 5.2B). Notably, two patients experienced an increase in periaxin levels after treatment, both of whom had a clinical relapse weeks or months later.

Figure 5.2. Plasma periaxin discriminates active from inactive CIDP and levels decrease after treatment with immunoglobulin.

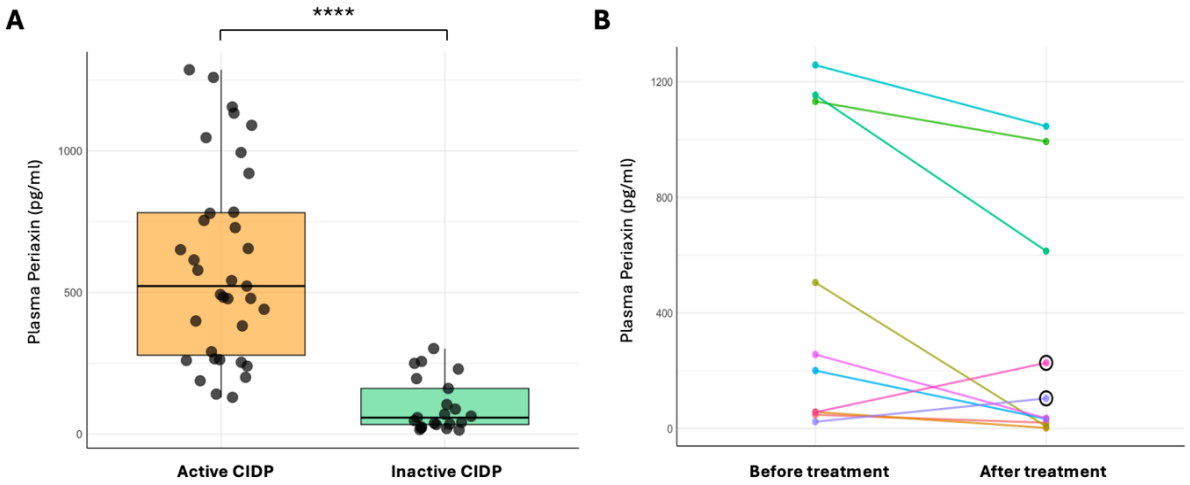

*(**A**) Patients with active CIDP had substantially higher periaxin compared to those with inactive CIDP (median 522.4 vs 57.9 pg/ml, **** $P < 0.0001$, Wilcoxon rank-sum test). Boxes represent the interquartile range (25th to 75th percentile). The horizontal line inside the box denotes the median. The whiskers extend to the most extreme data points within 1.5 × IQR from the quartiles. (**B**) Plasma levels of periaxin decrease following treatment with IVIg. The two circled patients with higher periaxin post-treatment had a subsequent clinical relapse.*

To evaluate whether immunoglobulin could interfere with the technical measurement of periaxin in plasma, 11 mg/ml of 10% IVIg were spiked directly into samples with previously measured low, intermediate, and high periaxin levels. This approach aimed to replicate the increase in IgG following IVIg treatment (delta IgG)[168] at an equivalent concentration of 2 g/kg. Periaxin levels remained stable, within 80–120% of their pre-spike values, with no significant changes observed (Fig. 5.3).

Figure 5.3. Assessment of immunoglobulin interference with assay measurement of plasma periaxin

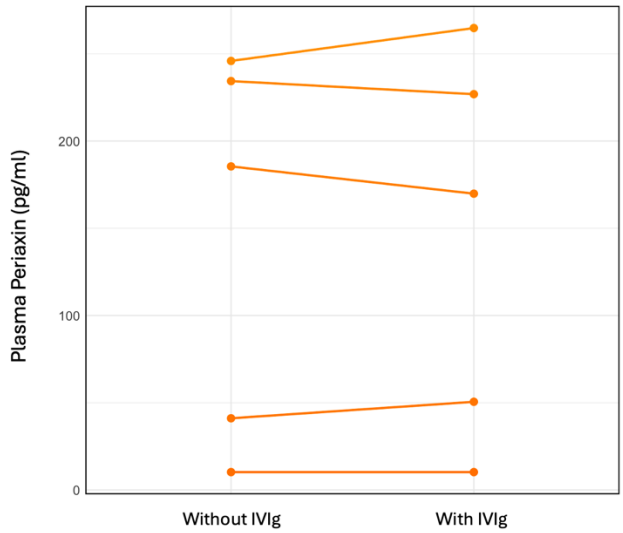

Plasma periaxin levels remained unchanged (80-120% of the previously measured concentrations) after spiking immunoglobulin, suggesting that IgG technical interference with assay measurement is unlikely.

Plasma periaxin demonstrated strong predictive value for identifying patients with CIDP who experienced clinical worsening at one year. ROC curve analysis demonstrated a strong discriminatory ability, with an area under the curve (AUC) of 0.81 (95% CI: 0.67–1), as shown in Fig. 5.4. The optimal periaxin cutoff value was 262.63, which achieved 100% sensitivity and 72.2% specificity, corresponding to a Youden index of 0.722. This cutoff correctly identified all patients who experienced worsening at one year, while 72.2% of those with stable or improved outcomes were appropriately classified. In comparison, peripherin

and NfL showed weaker discriminatory ability, with AUC values of 0.63 (95% CI: 0.26-0.93) and 0.59 (95% CI: 0.32-0.82), respectively.

Figure 5.4. High levels of periaxin predict clinical worsening at 1 year in CIDP.

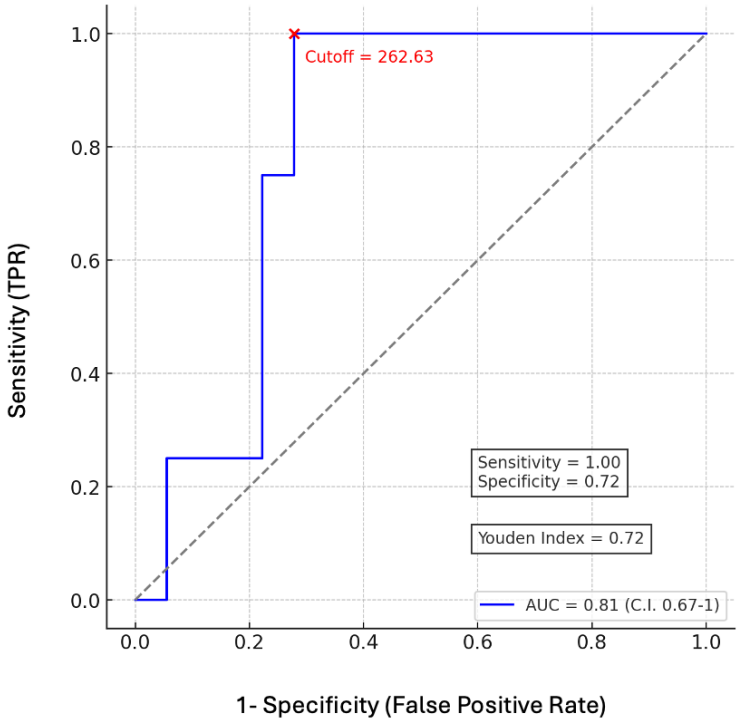

ROC curve for periaxin predicting clinical worsening in CIDP patients (defined as a four-point change in the centile I-RODS or two in the ONLS). The ROC curve is shown in blue, with the diagonal reference line shown in grey. The optimal periaxin cut-off was 262.63 pg/ml, achieving 100% sensitivity and 72.2% specificity, corresponding to a Youden index of 0.722, indicating good discriminative performance. The AUC was 0.81 (95% CI: 0.67-1).

Periaxin and NfL exhibited significant negative correlations with I-RODS (Spearman's rho = -0.400, $P = 0.047$, and rho = -0.577, $P = 0.0025$, respectively). Conversely, no significant

correlation was observed between peripherin and I-RODS. Neither periaxin, peripherin, nor NfL showed a significant correlation with MRC-SS.

5.3.2 Fluid biomarkers in GBS

Median peak periaxin levels in GBS (190.5 pg/ml, IQR = <LLOD to 964 pg/ml) were higher compared to both MS and healthy controls (GBS vs HC, $P < 0.01$, GBS vs MS, $P < 0.01$). Peak periaxin was higher in acute inflammatory demyelinating polyradiculoneuropathy (AIDP) compared to acute motor axonal neuropathy (AMAN): 451 vs 109 pg/ml ($P = 0.008$). Empirical ROC curve analysis demonstrated that periaxin effectively discriminated between the two electrophysiological subtypes (AUC = 0.88, 95% CI 0.72–1) with a Youden cut-off of 179.6 pg/ml, achieving 82% sensitivity and 86% specificity. Discriminatory performance was also good for the ratio of peak periaxin to peak peripherin (AUC = 0.84, 95% CI 0.64–1; cut-off = 11.38, sensitivity 100%, specificity 71%) and best for the ratio of peak periaxin to peak NfL (AUC = 0.94, 95% CI 0.81–1; cut-off = 0.46, sensitivity 100%, specificity 86%), as shown in Fig. 5.5. Median peak peripherin concentrations were 31.9 pg/ml in AMAN and 9.37 pg/ml in AIDP, with a trend toward significance (P = 0.069). Median peak NfL levels were substantially elevated in AMAN (1004 pg/ml) compared to AIDP (127 pg/ml), though this difference did not reach statistical significance (P = 0.315).

Longitudinal measurements showed that plasma periaxin peaked two to three weeks after symptom onset, followed by a gradual decline over the following weeks (Fig. 5.6A). In contrast, peripherin peaked earlier, within the first week of disease onset, then decreased before rising again around weeks six and seven; this secondary rise was more pronounced in patients with AMAN, consistent with our previous findings (Fig. 5.6B). NfL levels remained elevated for several weeks (Fig. 5.6C). A minor secondary peak in periaxin levels was

observed, resembling the pattern seen in peripherin, albeit with a slight delay (Fig. 5.6D). Periaxin, peripherin, and NfL levels were consistently higher from disease onset in patients with axonal GBS compared to those with AIDP (Fig. 5.6D-F), but periaxin reached higher peaks compared to both axonal biomarkers in AIDP (Fig. 5.6D).

Figure 5.5. Peak periaxin, combined with axonal biomarkers, discriminates demyelinating from axonal GBS.

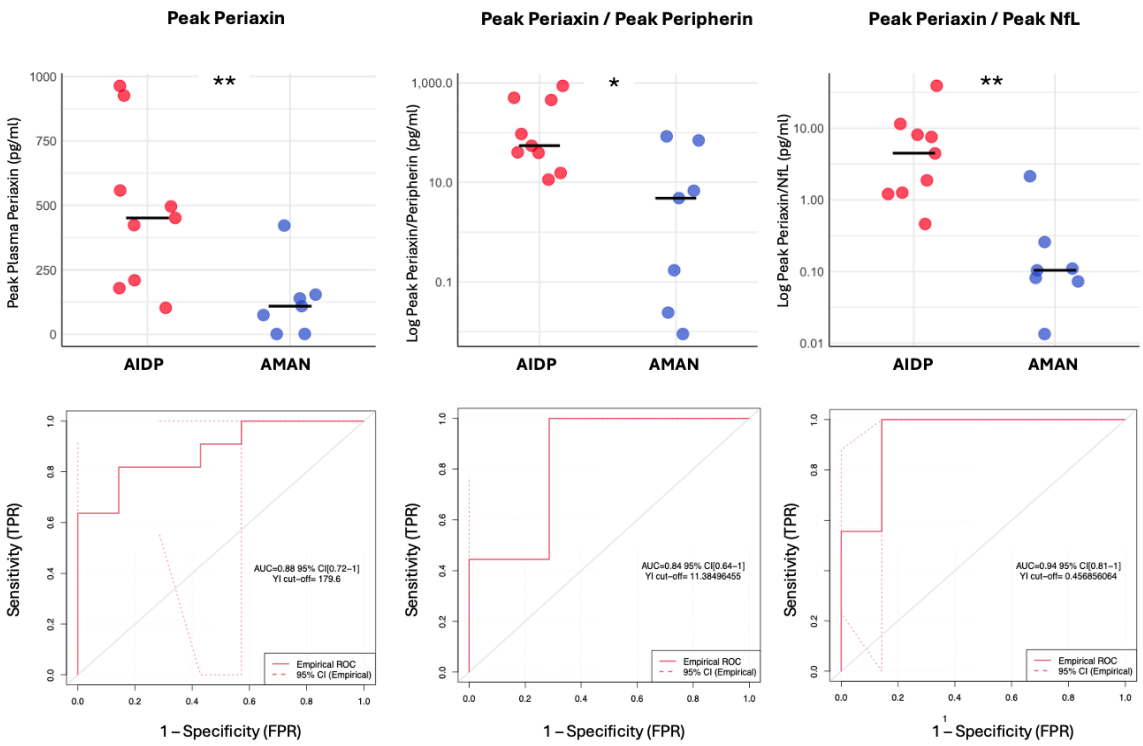

Peak periaxin was higher in AIDP compared to AMAN: 451 vs 109 pg/ml (P = 0.008). Empirical ROC curve analysis shows that periaxin discriminates between the two electrophysiological subtypes (AUC = 0.88, 95% CI 0.72–1) with a Youden cut-off of 179.6 pg/ml, sensitivity 82% and specificity 86%. Discriminatory performance improved with the ratio of peak periaxin to peak peripherin and was highest for peak periaxin/peak NfL (AUC = 0.94, 95% CI: 0.81–1; cut-off = 0.46, sensitivity 100%, specificity 86%).

Figure 5.6. Periaxin and axonal fluid biomarkers over time in GBS

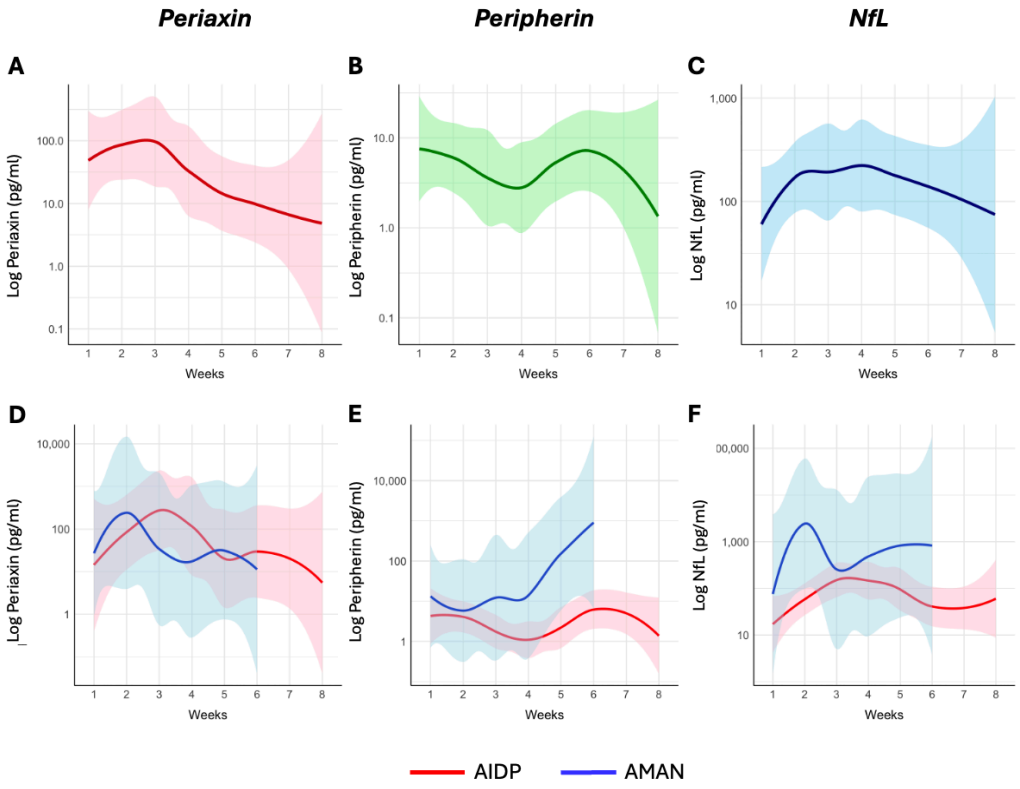

*Trends in plasma levels of periaxin (**A, D**), peripherin (**B, E**), and NfL (**C, F**) over time in patients with GBS. Plots **A-C** show trends of the biomarkers for all patients combined, whereas plots **D-F** illustrate trends separately for patients with demyelinating versus axonal disease, as classified by nerve conduction studies. In all plots, solid lines represent smoothed trends over time (LOESS smoothing), with the shaded areas indicating 95% confidence intervals (based on the standard error of the LOESS fit).*

No significant Spearman's correlation was observed between periaxin and either I-RODS or ONLS across all time points or between peak levels and nadir disability scores. When fluid biomarkers and clinical scales were categorically classified (Supplementary Table 1), NfL showed significant associations with I-RODS and peak NfL with nadir ONLS (Fisher's exact test, $P < 0.001$). Peak levels of all three biomarkers showed strong and consistent associations with nadir disability scores of both scales (Table 5.1).

Table 5.1. Correlations between fluid biomarkers and clinical scales in GBS

Biomarker	Clinical scale	P value	Significance
Periaxin	I-RODS	0.67919	
Periaxin	ONLS	0.46446	
Peripherin	I-RODS	0.15033	
Peripherin	ONLS	0.1346	
NfL	I-RODS	< 0.001	Significant
NfL	ONLS	< 0.001	Significant
Periaxin / Peripherin	I-RODS	0.88389	
Periaxin / Peripherin	ONLS	0.85479	
Peripherin / Periaxin	I-RODS	0.90226	
Peripherin / Periaxin	ONLS	0.89204	
Periaxin / NfL	I-RODS	0.10465	
Periaxin / NfL	ONLS	0.16765	
NfL / Periaxin	I-RODS	0.12484	
NfL / Periaxin	ONLS	0.06094	
Peak Periaxin	Nadir I-RODS	< 0.001	Significant
Peak Periaxin	Nadir ONLS	< 0.001	Significant
Peak Peripherin	Nadir I-RODS	< 0.001	Significant
Peak Peripherin	Nadir ONLS	< 0.001	Significant
Peak NfL	Nadir I-RODS	< 0.001	Significant
Peak NfL	Nadir ONLS	< 0.001	Significant
Peak Periaxin / Peak Peripherin	Nadir I-RODS	< 0.001	Significant
Peak Periaxin / Peak Peripherin	Nadir ONLS	< 0.001	Significant
Peak Peripherin / Peak Periaxin	Nadir I-RODS	< 0.001	Significant
Peak Peripherin / Peak Periaxin	Nadir ONLS	< 0.001	Significant
Peak Periaxin / Peak NfL	Nadir I-RODS	< 0.001	Significant
Peak Periaxin / Peak NfL	Nadir ONLS	< 0.001	Significant
Peak NfL / Peak Periaxin	Nadir I-RODS	< 0.001	Significant
Peak NfL / Peak Periaxin	Nadir ONLS	< 0.001	Significant

Amongst the GBS patients with longitudinal samples, 10 had periaxin levels measured on admission (week 1). Of these, seven remained clinically stable after one week, with six of

them (86%) showing low or moderately elevated periaxin levels at baseline. Two patients who improved had high baseline periaxin levels. The one patient whose condition worsened after one week had intermediate periaxin levels. No clear associations or predictive patterns were identified for changes at one month.

Finally, periaxin was measured in the CSF of 10 patients with AIDP, and all samples were below the limit of detection. These samples had been collected from a separate group of patients and were not matched with any of the plasma samples included in the GBS cohort.

5.3.3 Fluid biomarkers in healthy individuals

Among healthy controls, 29 out of 30 individuals (97%) had measurable but low periaxin levels (median 14.5 pg/ml, IQR = 38.2). Associations between periaxin concentrations and demographic or clinical variables were assessed using two separate linear regression models. The first model, restricted to healthy controls, included age and sex as covariates and was not statistically significant ($F = 1.04$, $P = 0.376$), accounting for only 11.5% of the variance in periaxin levels ($R^2 = 0.115$; adjusted $R^2 = 0.004$). Neither age ($P = 0.173$) nor sex ($P = 0.739$) emerged as significant predictors. In a second model that included both healthy controls and disease groups, age, BMI, sex, and disability were entered as covariates. This model was also not statistically significant ($F = 0.948$, $P = 0.467$), explaining 22.6% of the variance ($R^2 = 0.226$; adjusted $R^2 = –0.012$). None of the covariates - age ($P = 0.482$), BMI ($P = 0.219$), or sex ($P = 0.807$) - were significantly associated with periaxin levels.

5.4 Discussion

These results show that periaxin and peripherin can differentiate peripheral from central nervous system disease, with higher levels in CIDP compared to patients with inflammatory demyelinating CNS pathology or healthy controls. NfL also differentiates PNS disease from healthy individuals but does not distinguish central from peripheral nervous system pathology, in line with its ubiquitous expression throughout the neuroaxis. Periaxin discriminates active from inactive CIDP, and plasma levels decrease following treatment with intravenous immunoglobulin. In CIDP, high levels of periaxin strongly predict clinical worsening at 1 year. In GBS, periaxin and the ratio of periaxin to axonal biomarkers such as NfL and peripherin discriminate most cases of electrophysiologically classified demyelinating from axonal neuropathy.

Two glial proteins, Transmembrane Protease Serine 5 (TMPRSS5) and Glial Fibrillary Acidic Protein (GFAP), as well as a myelin sphingolipid (sphingomyelin), have previously been proposed as biomarkers of peripheral demyelination. Plasma TMPRSS5 is higher in patients with CMT1A compared to healthy controls, but does not correlate with nerve conduction studies and is not significantly elevated in other genetic neuropathies such as CMT1B, CMT1X, CMT2A, or CMT2E when compared with controls.[140,167] No data are currently available on TMPRSS5 in any immune-mediate neuropathies. GFAP, a CNS and PNS intermediate filament protein, has been shown to be higher in the serum of patients with some forms of chronic axonal neuropathy (diabetic, vasculitic, toxic-alcoholic, and idiopathic) compared to CIDP, multifocal motor neuropathy (MMN) and healthy controls, and in MMN versus controls.[141] Higher levels of GFAP correlate with lower sensory nerve action potential amplitudes and disease severity. However, in the peripheral nervous system, GFAP is expressed by non-myelinating Schwann cells and satellite glial cells, and not by

myelinating Schwann cells.[172] For this reason, and in light of the limitations of the currently published data, GFAP would seem to have limited utility in directly measuring PNS demyelination. Sphingomyelin is higher in the CSF of patients with CIDP and demyelinating GBS compared to non-demyelinating CNS disease and healthy controls, whereas levels do not differ across groups when measured in the serum.[142] Together with its lack of PNS specificity, the clinical use of sphingomyelin is limited by the fact that it can only be measured in CSF. Ideal neuropathy biomarkers would be specific to peripheral nerve, detectable in plasma or serum, able to distinguish primary demyelinating versus axonal pathology, and have a wide dynamic range with lower levels in other diseases and healthy controls.

The ability to detect a significant rise in plasma periaxin in patients with demyelinating peripheral neuropathy as opposed to CNS demyelinating disease or healthy individuals has important clinical implications. Immunohistochemistry of human brain, cranial nerves, and spinal cord sections shows that periaxin is absent in the central nervous system and only expressed peripherally by myelinating Schwann cells. This is in contrast to NfL, which is abundantly expressed throughout the CNS, and peripherin, which is also found in the cell bodies of motor neurons in the anterior horns of the spinal cord.[167] Thus, periaxin might have a key role in the ability to distinguish GBS from acute spinal cord disease, and may suggest a diagnosis of GBS in patients with rare initial hyperreflexia or sphincter disturbance.[48] Periaxin may also be used to quantitate the relative proportion of peripheral demyelination in conditions affecting both CNS and PNS such as combined central and peripheral demyelination (CCPD).

Over half of CIDP patients require ongoing immunotherapy to maintain disease stability.[47] This typically involves treatment with immunoglobulin, corticosteroids, alternative

immunosuppressive agents, or plasma exchange. However, monitoring disease activity remains challenging, as clinicians rely on clinical assessments and neurophysiology, that are unable to identify ongoing damage. As a result, there is a risk of misjudging disease activity, potentially leading to unnecessary treatment escalation or insufficient therapeutic intervention. Meanwhile, the financial burden of immunotherapies continues to grow, with IVIg alone costing the National Health Service over £300 million annually. As such, a biomarker of disease activity, particularly demyelination, is urgently needed. Periaxin is the first PNS-specific biomarker to effectively discriminate clinically active from quiescent CIDP. Current outcome measures are limited to assessing clinical disease – that which is outwardly visible - whereas periaxin, a structural Schwann cell protein, provides a window into the underlying immunopathological process. Elevated or rising levels of periaxin likely reflect active peripheral nerve demyelination, and subsequent falling levels would suggest decay or removal of circulating periaxin, without further Schwann cell damage. Levels of periaxin are lower after treatment in CIDP patients, and in some cases rise again, likely reflecting the short duration of action of IVIg.

The lack of strong correlation between periaxin and clinical scales, both at individual time points and peak disability, is not unexpected. Clinical scales are static measures of established functional disability, whilst fluid biomarkers are dynamic and inherently more responsive. Their imperfect correlation strengthens the argument for developing fluid biomarkers even further. Disability reflects the balance between injury and repair over the lifetime of the disease and, as such, combining clinical scales with fluid biomarkers may offer a more informative assessment of disease progression and treatment response.

Since Feasby et al,[173] GBS has been divided by neurophysiological findings into acute inflammatory demyelinating polyradiculoneuropathy (AIDP) and acute motor (and sensory)

axonal neuropathy (AMAN and AMSAN). However, the 2023 European Academy of Neurology/Peripheral Nerve Society (EAN/PNS) GBS Guidelines no longer endorse this clinical distinction. There is currently no gold standard for selecting among the various published diagnostic criteria for GBS, and no definitive features reliably distinguish demyelinating from axonal subtypes. Nonetheless, significantly different levels of periaxin were observed between patients classified neurophysiologically as AIDP and those with axonal conduction patterns. This difference may reflect a genuine pathological distinction, with primary injury affecting Schwann cells in AIDP and axons in AMAN, though both processes ultimately lead to disruption of the axoglial unit. These findings in patient plasma are consistent with in vitro observations, where periaxin levels in culture supernatants were higher following demyelination than axonal injury, and increased progressively over time.

The biological significance of the delayed peripherin peak remains unclear, similar to the near-concomitant minor peak in periaxin (Fig. 5.6D). The secondary peaks could be due to a lag in axonal injury with secondary demyelination (potentially due to treatment wearing off and a re-emergence of disease activity), or axoglial regeneration: both hypotheses are plausible. As discussed in Chapter 4, results from the in vitro coculture models of myelination and axonal growth - used to assess whether remyelination influences plasma periaxin levels - demonstrated that low levels of periaxin are transiently released during early myelin development, prior to any injury. This pattern mirrors the release of peripherin during axonal outgrowth. It is not inconceivable that some periaxin may also be released during myelin repair following damage. However, the levels associated with myelination were substantially lower than those observed post-injury. Wallerian degeneration, the process of axonal and myelin breakdown distal to the site of nerve injury, may contribute to elevated plasma periaxin levels by releasing myelin-associated proteins into the circulation. Periaxin levels during advanced or chronic phases of nerve degeneration might reflect this process

rather than active primary demyelination or repair. Longitudinal studies investigating the mechanisms of periaxin release, as well as its relationship with Schwann cell pathology and axonal degeneration, will be crucial to better understand its significance and optimise its clinical use as a biomarker.

In GBS, early diagnosis allows prompt treatment, reduces long-term disability and improves prognosis. On a research level, accurately distinguishing between demyelinating and axonal GBS may improve patient classification and recruitment to experimental studies. On a more general level, fluid biomarkers of neuropathy could serve as surrogate outcome measures for primary or secondary end points, improving the efficiency of clinical trials.

Used together, periaxin, NfL and peripherin appear to discriminate between GBS electrophysiological subtypes. The area under the ROC curve for distinguishing demyelinating versus axonal GBS was highest for the ratio peak periaxin / peak NfL, demonstrating the superiority of biomarker panels over individual biomarkers in enhancing accuracy and precision of neuropathy classification. Further work is needed to elucidate whether composite fluid biomarkers can improve current prognostic models.

In the small CSF cohort from GBS patients, all samples were negative for periaxin and this may be due to small tissue volume (short segments of nerve roots releasing tiny amounts of protein), reduced structural stability of periaxin in the CSF matrix compared to plasma, and/or protein distribution in the subarachnoid space. This could be evaluated in future studies. However, venepuncture is safer, more accessible, and better tolerated than lumbar puncture, which is invasive and may result in complications. Blood-based biomarkers appear better suited for longitudinal monitoring of diseases primarily affecting the peripheral nervous system, and are likely to increase patient compliance in both clinical and research settings.

Limitations

One limitation of this study is the relatively small sample size and the restricted range of patient populations included. Both GBS and CIDP are relatively rare diseases, and well-characterised cohorts with longitudinal plasma biosamples are particularly scarce. Furthermore, plasma is collected less routinely than serum in clinical settings, further limiting cohort availability. Expanding cohort sizes and including more diverse populations - while maintaining rigorous sampling and clinical characterisation - will be essential to validate and generalise these findings.

Future collaborative studies should aim to incorporate broader disease groups and clinical contexts to confirm the reproducibility of results and strengthen the evidence base for periaxin, peripherin and NfL as combinatorial biomarkers. Leveraging larger, multicentre datasets will be critical to evaluate their clinical utility and to establish their diagnostic and monitoring role in peripheral neuropathies.

6 FLUID BIOMARKERS IN OTHER NEUROPATHIES

6.1 Other inflammatory neuropathies

6.1.1 Introduction

The limitations of current outcome measures previously discussed for CIDP and GBS also apply to other inflammatory neuropathies, where clinical heterogeneity and slow disease progression can complicate diagnosis, monitoring, and therapeutic decisions. This chapter evaluates the potential clinical utility of periaxin, peripherin and NfL in three additional immune-mediated neuropathies: MMN, anti-MAG neuropathy, and POEMS syndrome. MMN is a chronic, immune-mediated disorder characterized by asymmetric, predominantly upper limb weakness, with electrophysiological evidence of motor conduction block at non-compressible sites. Its variable presentation frequently leads to diagnostic delays or misclassification. Amongst the most common misdiagnoses of MMN is amyotrophic lateral sclerosis (ALS) in cases with predominant lower motor neurone (LMN) presentation. Anti-MAG neuropathy is a demyelinating disorder associated with autoantibodies targeting MAG in Schwann cells; determining which patients may benefit from immunotherapy remains a clinical challenge. POEMS syndrome is a paraneoplastic disorder defined by a monoclonal plasma cell dyscrasia, peripheral neuropathy, and a broad range of systemic manifestations. In all three diseases, fluid biomarkers may support assessment of disease activity and help guide treatment decisions. In the context of clinical trials, fluid biomarkers may serve as more objective and responsive surrogate outcome measures. This chapter evaluates periaxin, peripherin and NfL in MMN, anti-MAG neuropathy and POEMS syndrome, and assesses

their potential contribution to clinical management and trial design in these paraproteinemic neuropathies.

6.1.1 Methods

Plasma or serum samples were obtained from patients with MMN (n = 15), anti-MAG neuropathy (n = 10), and POEMS syndrome (n = 17). Levels of periaxin, peripherin and NfL were measured using the Simoa assays and compared across the three disease groups and against healthy controls. An additional comparison group included patients with amyotrophic lateral sclerosis (ALS, n = 30), obtained through a collaboration with the Oxford Motor Neuron Disease Centre. These included individuals with predominantly lower motor neuron (LMN) or upper motor neuron (UMN) involvement, or mixed presentation. The extent of LMN involvement in ALS was quantified using the LMN burden score, ranging from –10 to +10, with higher positive values indicating a greater burden of LMN features, including absent deep tendon reflexes, muscle atrophy, and fasciculations. Patients with MMN neuropathy were classified as having clinically active disease if they demonstrated objective peri-dose fluctuations between pre- and post-treatment assessments with immunoglobulin. A MCID was defined as a change of at least four points on the centile MMN-RODS or I-RODS, or a change of two points on the MRC-SS. Patients who did not meet these thresholds were considered to have inactive disease. Those with discordant clinical outcome measures or without available clinical scale data were categorised as indeterminate. The same MCID criteria were used to assess whether patients were clinically improved, worsened, or stable one year after the sample collection time point. Patients with POEMS syndrome were classified as having active disease if vascular endothelial growth factor (VEGF) levels were elevated (>1000 pg/ml) at the time of sampling. All MMN patients fulfilled diagnostic

criteria for definite MMN, were receiving regular immunoglobulin therapy at variable intervals (ranging from weekly subcutaneous immunoglobulin to six weekly IVIg), and were evaluated at the NHNN in London or at John Radcliffe hospital in Oxford by consultant neurologists. All anti-MAG neuropathy patients had a definite diagnosis, supported by the presence of characteristic phenotype, IgM kappa paraprotein and significantly elevated anti-MAG antibody titres. All POEMS syndrome patients fulfilled diagnostic criteria, were receiving active treatment, and were also evaluated at NHNN. Electrophysiological assessment was conducted in all patients as part of their clinical work-up. All samples had been collected previously for other studies and were analysed retrospectively.

6.1.2 Results

In patients with MMN, median periaxin levels were 285.1 pg/ml, peripherin 12.6 pg/ml, and NfL 5.5 pg/ml. In MAG, median levels were 206.7 pg/ml for periaxin, 1.1 pg/ml for peripherin, and 16.8 pg/ml for NfL. In POEMS syndrome, periaxin was 225.3 pg/ml, peripherin 1.1, and NfL 64.3 pg/ml. Compared to healthy controls, periaxin levels were significantly elevated in MMN ($p < 0.001$), MAG ($p < 0.05$), and POEMS ($p < 0.001$), as shown in Fig. 6.1.

Among ALS patients, median periaxin levels did not significantly differ between LMN-predominant (340.8 pg/ml), mixed (673.6 pg/ml), and UMN-predominant (348.8 pg/ml) subgroups (Fig. 6.2A). Similarly, peripherin levels were <LLOD, 4.7 pg/ml and 1.5 pg/ml (Fig. 6.2B), and NfL was 164.3 pg/ml, 444.6 pg/ml, and 442.3 pg/ml in the LMN-predominant, mixed, and UMN-predominant groups, respectively (Fig. 6.2C). When comparing active MMN to LMN-predominant ALS, median periaxin levels were similar between groups (404.0 vs 341.0 pg/ml), as were peripherin levels (3.71 vs 1.12). The only

significant difference was for NfL, which was markedly higher in ALS (164.0 vs 5.35 pg/ml; $p < 0.001$), Fig. 6.3.

Figure 6.1. Periaxin, peripherin and NfL in MMN, anti-MAG neuropathy, and POEMS syndrome

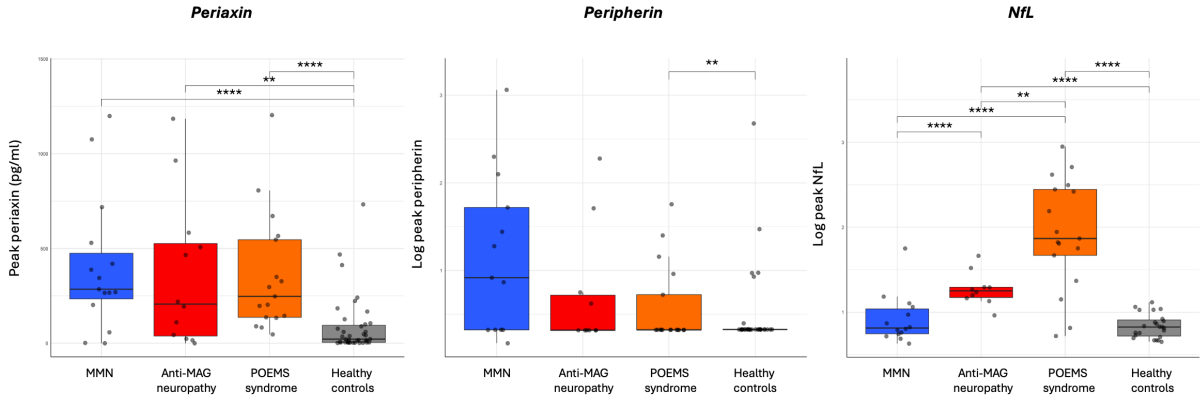

Median periaxin levels were significantly elevated in MMN, MAG and POEMS compared to healthy controls. Median peripherin levels were highest in MMN and low in MAG and POEMS, while NfL was markedly elevated in POEMS, with lower levels in MMN and MAG. Box plots display group medians, interquartile ranges, and statistical comparisons. Asterisks denote significance levels: < 0.05 (*), p < 0.01 (**), p < 0.001 (***), p<0.0001 (****).

Figure 6.2. Fluid biomarker levels across ALS subtypes

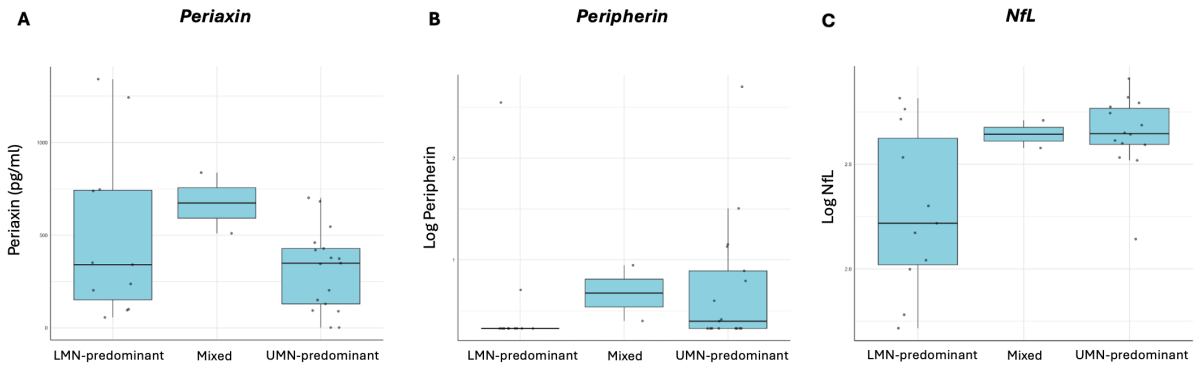

*(**A–C**) Among ALS patients, periaxin, peripherin and NfL levels did not significantly differ between LMN-, mixed, and UMN-predominant subgroups, although NfL showed a trend toward higher levels in the UMN-predominant group.*

Figure 6.3. Fluid biomarkers in active MMN vs LMN-predominant ALS

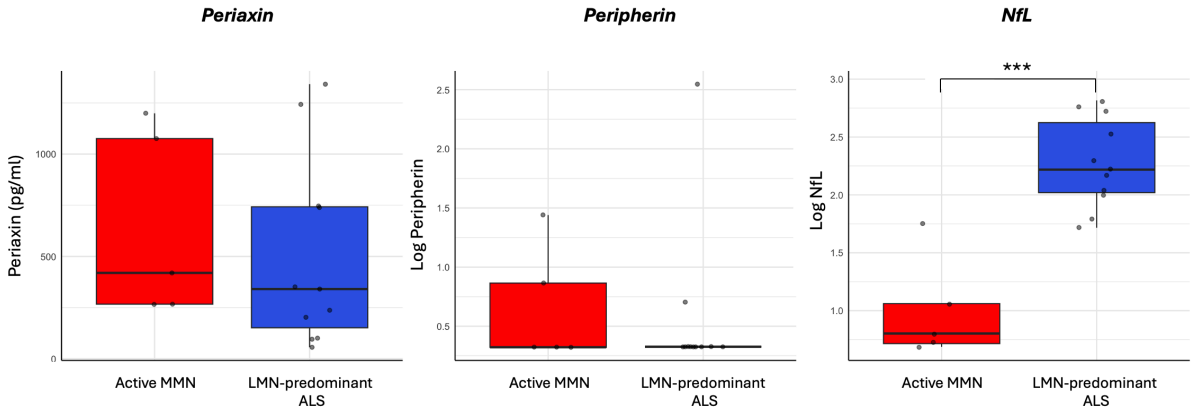

Median periaxin and peripherin levels were similar between groups. NfL was the only biomarker able to discriminate between active MMN and LMN-predominant ALS, with significantly higher levels in the latter ($P < 0.001$).

When MMN, MAG, and POEMS were analysed together, periaxin was significantly higher in active versus stable disease (350.1 vs 112.8 pg/ml, $p = 0.0082$), as shown in Fig. 6.3. NfL levels were also elevated in the active group (50.4 pg/ml) relative to stable disease (12.5 pg/ml), $p = 0.0417$. Peripherin levels did not differ significantly between active and stable disease. In subgroup analyses, periaxin levels were higher in active compared to stable disease in MMN (403.8 vs 269.7 pg/ml), MAG (583.3 vs 19.4 pg/ml), and POEMS (287.3 vs 231.8 pg/ml), though only MAG showed a trend toward significance (p = 0.057). Peripherin was lower in active than stable disease in MMN (3.7 vs 87.8 pg/ml), within normal range in MAG (3.2 vs 1.1 pg/ml), and unchanged in POEMS (<LLOD pg/ml). NfL was significantly higher in active compared to stable disease in POEMS (120.4 vs 13.8 pg/ml; p = 0.035), but similar between activity states in MMN and MAG.

Levels of all three biomarkers were compared between patients with mild versus moderate/severe disability. Median periaxin levels were lower in the moderate/severe group (203.0 pg/ml) compared to the mild group (285.0 pg/ml), but the difference was not statistically significant. Peripherin was similar across both groups (median levels <LLOD in each). NfL was higher in moderate/severe cases (32.1 pg/ml) compared to mild cases (11.7 pg/ml), but this difference also did not reach statistical significance. Comparisons are shown in Fig. 6.5.

In a combined analysis of MMN, MAG and POEMS patients, higher baseline periaxin levels were associated with worse clinical outcomes at 1 year. Patients who later worsened had a median periaxin concentration of 718.0 pg/ml, compared to 220.0 pg/ml in those who remained stable and 52.4 pg/ml in those who improved ($p < 0.01$). In contrast, baseline levels of peripherin and NfL did not significantly differ between outcome groups ($p = 0.327$ and $p = 0.357$, respectively), Fig. 6.6.

Figure 6.4. Periaxin and NfL as biomarkers of disease activity

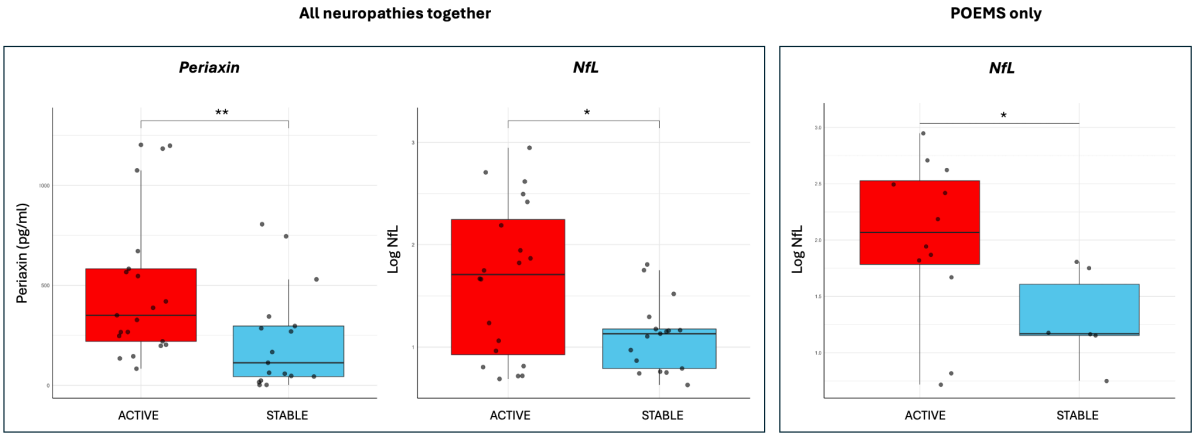

Left: Periaxin and NfL levels were significantly higher in active versus stable disease when MMN, MAG, and POEMS were analyzed together. Right: In POEMS syndrome, NfL levels were significantly elevated in active compared to stable disease.

Figure 6.5. Fluid biomarkers versus disease severity

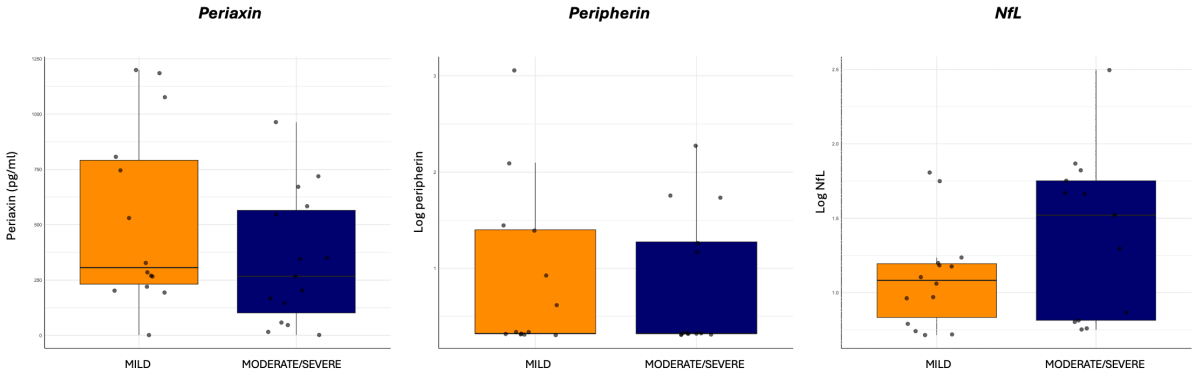

Combined analysis of MMN, MAG and POEMS syndrome. Periaxin, peripherin, and NfL levels were compared between patients with mild versus moderate/severe disability. Median levels differed between groups but did not reach statistical significance.

Figure 6.6. Association between biomarker levels and clinical change at one year

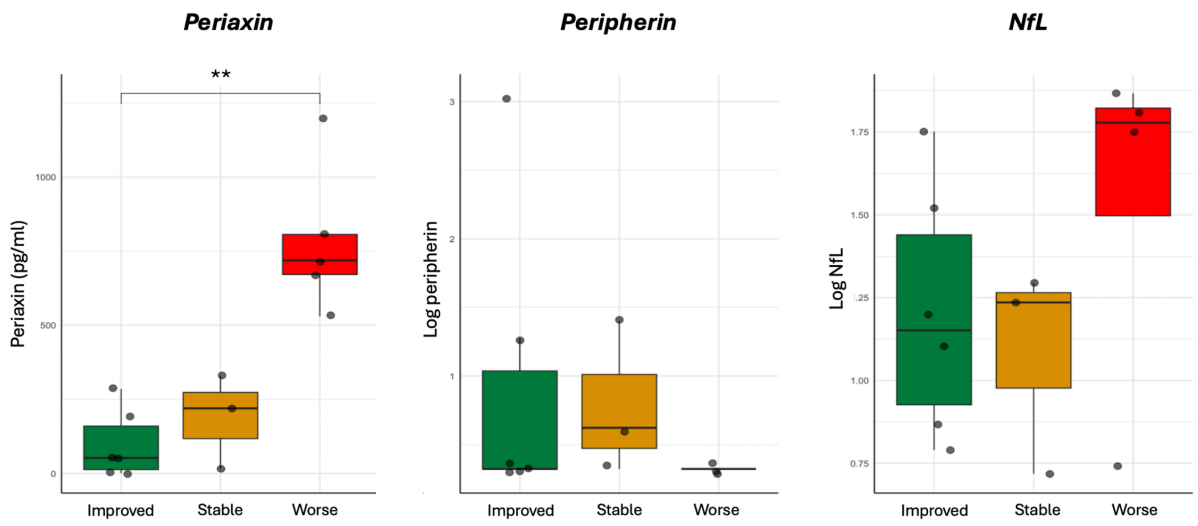

Combined analysis of MMN, MAG and POEMS syndrome. Higher periaxin levels were significantly higher in patients who were clinically worse at 1 year ($p < 0.01$), while peripherin and NfL did not differ significantly between outcome groups.

6.1.3 Discussion

Periaxin, peripherin and NfL exhibit similar but distinct patterns across neuropathies and clinical contexts. Periaxin levels were significantly elevated in MMN, MAG and POEMS compared to healthy controls, supporting an association of periaxin with immune-mediated demyelination. In ALS, periaxin did not differ significantly between LMN- and UMN-predominant patients and were comparable to those observed in active MMN. This finding aligns with in vitro observations, where high periaxin levels can be detected in cocultures with primary axonal damage. Myelinating Schwann cells depend on axonal integrity to survive, and secondary demyelination inevitably ensues if axons are injured, likely explaining

the elevated periaxin levels in ALS, which is not a primarily demyelinating disease. Whilst not statistically significant, periaxin may still hold potential in distinguishing ALS from inflammatory neuropathies, and analysis of larger cohorts will elucidate this. NfL levels, although not reaching statistical significance, were numerically higher in UMN-predominant ALS compared to mixed or LMN forms, consistent with corticospinal tract involvement. This is in line with NfL's non-specific expression throughout the nervous system. Peripherin did not distinguish LMN- from UMN-predominant ALS, likely because most ALS cases exhibit some degree of peripheral axonal involvement, regardless of clinical phenotype. It is also worth noting that peripherin is not exclusively expressed in the PNS: it has been reported in the brainstem, optic tracts, internal capsule, cerebellum, cranial nerves and corpus callosum, primarily in mouse models.[175]

When inflammatory neuropathies were analysed together, both periaxin and NfL were significantly elevated in active versus stable disease, supporting their potential as dynamic markers of disease activity, and confirming previous findings in CIDP. Subgroup analyses reinforced these results, with marked periaxin elevations in active MAG (albeit without significance) and increased NfL in active POEMS.

Neither peripherin nor NfL showed significant associations with disability severity, although NfL levels tended to be higher in patients with moderate to severe impairment. Notably, higher baseline periaxin levels predicted clinical worsening at one year, suggesting a possible prognostic role beyond cross-sectional activity assessment. While somewhat unexpected - given the central role of axonal damage more than demyelination in determining disability - this may reflect the downstream consequences of persistent or severe demyelination leading to secondary axonal loss.

Collectively, these results reinforce the role of periaxin as a sensitive and disease-relevant biomarker in immune-mediated neuropathies, with particular relevance to disease activity and prognosis. NfL retains a complementary role as an undoubtedly robust biomarker of axonal degeneration.

Limitations

This is a preliminary study and should be interpreted in light of several limitations. The sample size was small, which reduced the power to detect more subtle associations, especially in subgroup analyses. Additionally, samples were not collected prospectively, and the retrospective analysis introduces potential variability in sample timing and pre-analytical conditions. The availability of plasma was limited, as serum is more commonly stored in biorepositories. These limitations highlight the need for larger, prospective studies with standardised sampling to confirm and extend these initial findings.

6.2 Inherited neuropathies

6.2.1 Introduction

The inherited neuropathies are a clinically and genetically heterogeneous group of disorders affecting the peripheral nervous system. The most common is Charcot–Marie–Tooth disease (CMT), where over 100 causative genes have been identified to date. In the UK and globally, most individuals with CMT carry a duplication of the PMP22 gene or mutations in MFN2 or GJB1, leading to the subtypes CMT1A, CMT2A, and CMTX1, respectively. CMT is typically classified as either “demyelinating” or “axonal” based on electrophysiological and pathological findings, reflecting whether the primary dysfunction affects myelinating

Schwann cells or axons. According to this classification, CMT1A is demyelinating and CMT2A axonal. CMTX1 is classified as “intermediate” because nerve conduction studies reveal intermediate conduction velocities, typically in the range of 25-40 m/s, often less slow in females.

Hereditary transthyretin (TTR) amyloidosis is a multisystem disorder caused by pathogenic variants of TTR, which affects the peripheral nervous system and causes a disabling, often painful neuropathy, with progressive axonal degeneration in both the somatic and autonomic PNS. The development of highly effective, disease modifying gene-silencing therapies has strengthened the argument to develop objective and sensitive biomarkers able to detect nerve disease, to guide decision making on whether to start or stop treatment.[176]

NfL is elevated in both CMT and TTR amyloid neuropathy, with evidence in the latter showing correlation with disease severity and potential utility in identifying conversion to symptomatic disease.[176,177] Used in combination, periaxin, peripherin and NfL may improve clinical evaluation and disease monitoring in the inherited neuropathies. This section explores the potential diagnostic and prognostic utility of fluid biomarkers in patients with CMT and TTR amyloid neuropathy, along with established clinical outcome measures.

6.2.2 Methods

Plasma concentrations of periaxin, peripherin and NfL were measured using the Simoa-based immunoassays in patients with CMT1A (n=20), CMT2A (n=10), CMTX1 (n=10), and TTR neuropathy (n=16), alongside healthy controls (HC, n=30). Disease severity was evaluated using the CMT Neuropathy Score (CMTNS) or the CMT Examination Score (CMTES). All patient samples were obtained from existing biorepositories for previously conducted studies.

Biomarker analyses were performed retrospectively using available plasma samples and clinical data.

6.2.3 Results

Median levels of periaxin were significantly higher in CMT1A compared to TTR ($p = 0.0056$) and healthy controls ($P < 0.001$), and in CMTX1 ($p < 0.001$), CMT2A ($P < 0.001$), and TTR ($p = 0.0049$) compared to HC (Fig. 6.7A). A trend toward higher periaxin levels in CMT1A (median 300.7 pg/ml) compared to CMT2A (196.5 pg/ml) was observed but did not reach statistical significance. Peripherin levels were elevated in CMT1A compared to HC ($p = 0.0039$, Fig. 6.7B). Median peripherin levels were also higher in CMT2A and CMTX1 compared to healthy controls, but these did not remain significant ($p = 0.27$ and $p = 0.051$, respectively) after correction for multiple comparisons (FDR). NfL distinguished all neuropathy groups from HC, with significantly higher levels observed in CMT1A ($p < 0.001$), CMT2A ($p < 0.001$), CMTX1 ($p < 0.001$), and TTR ($p < 0.001$), Fig. 6.7C.

In a regression analysis adjusted for sex and disease severity (CMTES), only NfL levels demonstrated a significant positive association with age ($p < 0.001$, Fig. 6.7D). The same association was not observed for periaxin or peripherin.

Peripherin was associated with disease severity, with higher concentrations seen in patients with greater CMTES ($p = 0.016$, Fig. 6.8). Among CMT patients with available CMTNS data, plasma periaxin was significantly higher in those with moderate/severe disease compared to those with mild disease ($p = 0.014$), as shown in Fig. 6.9A. There was a trend toward higher periaxin levels in patients who showed clinical worsening at 1 and 2 years,

defined as a ≥2-point increase in CMTES, albeit without reaching statistical significance (Fig. 6.9B-C).

Figure 6.7. Periaxin, peripherin and NfL in CMT and TTR amyloid neuropathy

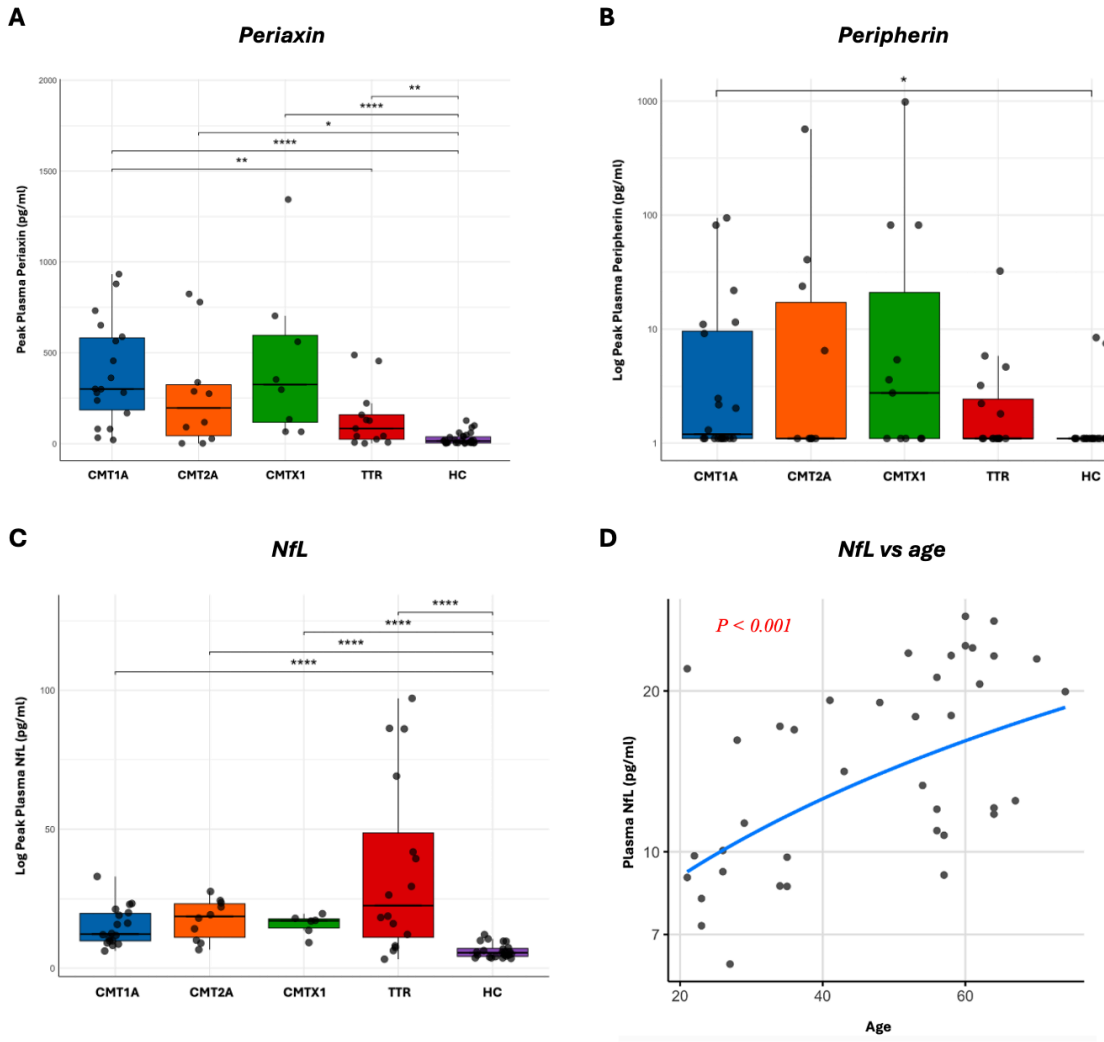

*(**A**) Periaxin levels were significantly higher in CMT1A compared to TTR and HC, and elevated in CMTX1, CMT2A, and TTR compared to HC. (**B**) Peripherin was higher in CMT1A versus HC; trends were seen in CMT2A and CMTX1 but did not remain significant after correction. (**C**) NfL levels were significantly increased in all neuropathy groups compared to HC. (**D**) Only NfL showed a positive association with age after adjustment for sex and disease severity. P values as indicated in the text. Statistical comparisons were performed using the Mann–Whitney test with adjustment for multiple comparisons (Benjamini–Hochberg method).*

Figure 6.8. Peripherin vs CMTES

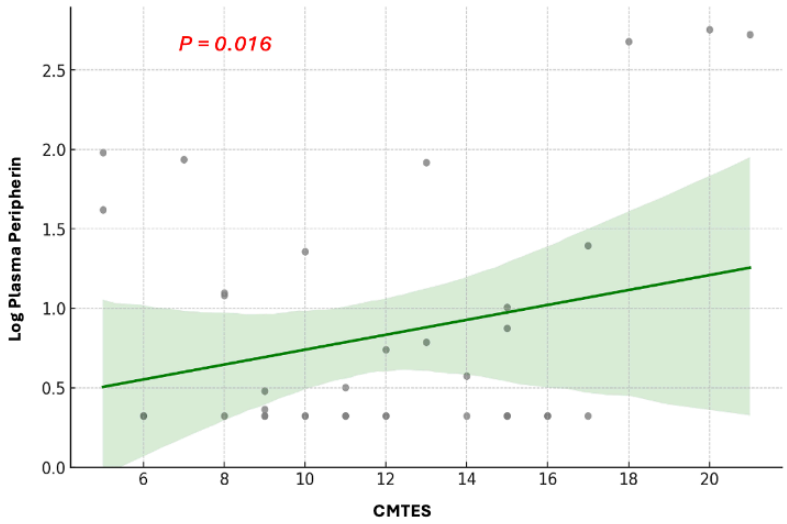

A linear regression analysis (adjusted for age and sex) revealed a significant positive association between CMTES and peripherin (p = 0.016), with higher CMTES linked to higher peripherin concentrations.

Figure 6.9. Periaxin vs CMTNS and CMTES

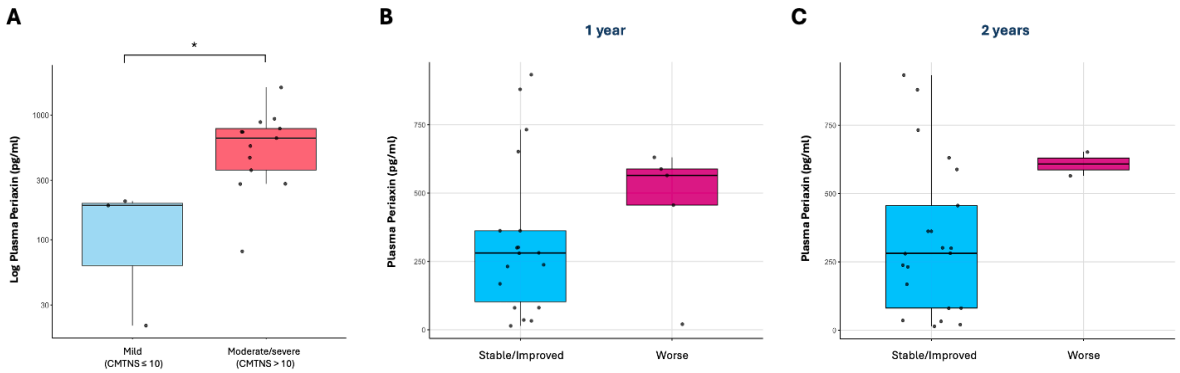

*Plasma periaxin levels in CMT patients. (**A**) Periaxin was significantly higher in patients with moderate/severe disease compared to mild disease, as assessed by the CMTNS (p = 0.014). (**B–C**) A trend toward higher periaxin levels was observed in patients with clinical worsening at 1 and 2 years, as measured by the CMTES, though not statistically significant.*

6.2.4 Discussion

CMT is a chronic, in most cases slowly progressive, peripheral nerve disease, where clinical changes are often minimal during the period of a clinical trial.[178] Pathological axoglial modifications do not always translate into clinical changes, and traditional patient- or clinician-reported outcome measures may not be sensitive enough to detect disease progression. Fluid biomarkers of neuropathy have the potential to fill this gap. This is also particularly relevant in TTR amyloid neuropathy, where gene-silencing therapies are only licensed in patients with evidence of peripheral nerve involvement.

Plasma NfL was significantly increased in all neuropathy groups compared to healthy individuals, and this finding is consistent with the existing literature on neurofilaments in CMT and TTR amyloid neuropathy,[178,179,176,177] with the comparison between the latter and healthy controls being the most significant. The observed correlation between NfL and age is also consistent with previous literature and likely reflects age-related changes in the central nervous system.[127] In contrast, neither periaxin nor peripherin showed a significant association with age, in line with findings from the inflammatory neuropathy cohorts (Chapter 4). The absence of age dependence is a potential advantage: if confirmed in larger studies, it would eliminate the need for age-based adjustment and simplify the interpretation of results.

Axonal damage is the main determinant of clinical disability in peripheral nerve disease.[180] As a biomarker of demyelination, periaxin alone is not expected to objectively reflect functional impairment or predict clinical outcomes. Nevertheless, elevated levels of periaxin and peripherin were associated with greater clinical severity, suggesting an unexpected potential role in quantifying disease burden when used alongside established

outcome measures. Moreover, high plasma periaxin levels may predict future clinical deterioration in CMT, pointing to possible prognostic utility, similar to findings observed in CIDP. However, further detailed analyses are warranted and will be pursued as additional longitudinal samples become available. Consistent with the inflammatory neuropathy findings, the combinatorial use of periaxin, NfL and peripherin is expected to discriminate active from quiescent disease, and measure disease progression in chronic diseases where traditional outcome measures fail to do so.

Ongoing work aims to refine the discriminatory capacity of periaxin, peripherin and NfL between CMT1 and CMT2 subtypes, and to assess their true potential as biomarkers of disease activity and progression. Larger cohorts are currently under investigation to clarify the individual and combined contributions of all three biomarkers - alongside established clinical scales - to the comprehensive evaluation of genetic neuropathies.

Limitations

This preliminary study shares several limitations with the immune-mediated cohort. The sample size was modest, limiting statistical power, particularly for subgroup comparisons. Additionally, the retrospective nature of the analysis means that samples and clinical data were not collected at standardised time points, potentially introducing variability in relation to disease stage, treatment status, and sample handling. Such variability can make it more difficult to interpret biomarker levels consistently across patients. Plasma availability was also limited, as discussed for the inflammatory neuropathies. To better understand the longitudinal dynamics of periaxin, NfL and peripherin in the inherited neuropathies, larger prospective studies with standardised sample collection are needed. Such studies - designed to track biomarker changes over several years - are currently ongoing and will be essential to establish their prognostic and monitoring utility.

7 DISCUSSION

This thesis has described the development and optimisation of ultrasensitive immunoassays for the measurement of periaxin and peripherin as fluid biomarkers of demyelination and axonal injury in the peripheral nervous system. Whilst individual chapters have addressed methodological development, analytical validation, and application in specific disease contexts, this concluding discussion integrates the main findings, considers their broader implications, outlines limitations, and proposes future directions for research and clinical application.

There remains an important need for objective biomarkers reflecting a number of disease contexts in peripheral neuropathies. Conventional outcome measures, such as neurological examination, clinical scales and electrophysiology, are limited by their semi-quantitative nature, insufficient sensitivity to subtle pathological changes, and poor suitability for longitudinal monitoring. The work presented here addresses this unmet need by establishing a biologically grounded panel of ultrasensitive biomarkers that can enhance diagnostic precision and disease tracking.

Periaxin and peripherin are exclusively and predominantly expressed in the PNS, respectively, with limited expression of the latter in the central nervous system. Combined with NfL, a well-established biomarker of axonal injury, periaxin and peripherin provide a comprehensive panel to dissect pathophysiological mechanisms and improve disease classification in peripheral neuropathy. Both Simoa assays have a broad dynamic range, comparable to the already widely adopted NfL assays, supporting their potential integration into research and clinical workflows. The utility of periaxin and peripherin is further

reinforced by their capacity to discriminate between disease states. Results so far demonstrate that periaxin distinguishes active from inactive CIDP, declines following treatment with IVIg, and predicts clinical deterioration at one year. In GBS, periaxin, particularly when used alongside peripherin and NfL, differentiates demyelinating from axonal subtypes based on electrophysiological criteria. These findings are supported by in vitro models of immune-mediated injury, where periaxin levels increase more following primary demyelination compared to axonal injury. Peripherin, in turn, differentiates acute axonal damage in GBS from chronic, slowly progressive demyelination in CIDP. In contrast, NfL does not reliably differentiate between CNS and PNS pathology - except in select comparisons such as active MMN versus motor neuron disease. This highlights the added value of PNS-specific biomarkers.

An exploratory aim of this work was to assess whether peripherin could differentiate between LMN- and UMN-predominant forms of amyotrophic lateral sclerosis. This may be useful in clinical trials to improve patient classification and study recruitment. As discussed in Chapter 6, a preliminary evaluation of 30 ALS patients revealed no significant difference in peripherin levels between these clinical subtypes. Several factors may underlie this finding. First, the half-life of peripherin in circulation remains unknown; if clearance is rapid (as it appears to be from GBS findings, where levels rise and fall within three weeks of disease onset), this could limit its ability to reflect slowly progressive pathology. Second, although peripherin is primarily expressed in the PNS, it is not entirely PNS-specific, and some CNS release may occur. Third, even UMN-predominant patients may have subclinical PNS involvement, further blurring the distinction. In contrast, NfL levels tended to be higher - albeit without reaching statistical significance - in UMN-predominant ALS, consistent with its established association with corticospinal tract degeneration. Future studies with larger

sample sizes and longitudinal sampling, alongside efforts to characterise the half-life and clearance kinetics of peripherin, will be essential to determine the true potential of axonal fluid biomarkers in distinguishing ALS phenotypes and monitoring disease progression.

In vitro models of neuropathy provide a valuable platform to deepen mechanistic insight into peripheral nerve injury, particularly when integrated with high-resolution morphological techniques such as immunohistochemistry and confocal microscopy. Periaxin and peripherin are robustly expressed in cocultures of iPSC-derived sensory neurons and rat Schwann cells, and their direct release into the culture supernatant following immune-mediated injury results in high, quantifiable levels. This reinforces the utility of these cell-based systems for biomarker validation and disease modelling.

7.1 Study limitations

Several limitations should be acknowledged. First, cohort sizes were modest, largely due to the reliance on EDTA plasma for periaxin measurement - a matrix not routinely stored in biorepositories designed for broader clinical research. Secondly, periaxin appears less stable than peripherin or NfL, necessitating strict adherence to standard operating procedures for sample handling. Not all samples were handled identically pre-analytically and, as demonstrated in Chapter 3, periaxin tends to degrade - or possibly aggregate - after the third freeze–thaw cycle. Additionally, delay in centrifugation can impact on sample stability and periaxin quantification. This introduces potential variability, and caution is required when interpreting results and comparing samples that may have been handled differently prior to testing. Nevertheless, all samples included in the present study were centrifuged within five hours of collection and promptly stored at –80°C, avoiding prolonged storage at room temperature. Thirdly, some in vitro experiments were performed with only a single replicate

per condition. This limits the generalisability and robustness of the findings, as individual wells can differ significantly due to intrinsic variability in cell culture - such as differences in cell density, maturation state, or local microenvironment. Results should therefore be interpreted with caution. Nonetheless, the observed findings were consistent with expected biological patterns, further supporting the utility of cell-based models of axoglial injury in studying biomarker dynamics. Finally, the biological half-lives of periaxin and peripherin remain undefined, representing an important avenue for future investigation and interpretation of longitudinal changes in biomarker levels.

7.2 Future directions

Looking ahead, efforts should focus on the recruitment of larger, deeply phenotyped patient cohorts across both inflammatory and inherited neuropathies. Standardisation of sample collection protocols will be crucial to maximise cross-study comparability. Collaborative studies, both national and international, will accelerate validation and facilitate broader implementation.

Further in vitro studies using myelinating culture systems will be essential to validate and refine biomarker applications. Larger-scale experiments are needed to substantiate the preliminary findings described in this thesis and will form a key component of future work aimed at advancing biomarker development.

Assay development may also benefit from further technological innovation. For periaxin, sensitivity and reproducibility could be enhanced by the development of a monoclonal detector antibody, although lowering the limit of detection is not strictly necessary, as the current Simoa-based assay already allows reliable detection in most plasma samples. In

contrast, peripherin is frequently below the detection threshold, which may reflect either genuinely low or absent levels - possibly due to short half-life and rapid degradation - or insufficient assay sensitivity. In this context, the use of novel platforms such as NULISA (nuclease-linked immuno-sandwich assay), which employs DNA-based detection to achieve greater signal amplification, may substantially improve the sensitivity and specificity of peripherin measurement and enable more accurate assessment of axonal injury, along with NfL.

Finally, the integration of PNS-specific biomarkers into clinical trial design holds promise. In addition to enhancing diagnostic accuracy and facilitating patient stratification, the combined use of periaxin and peripherin is expected to provide objective measures, improving the robustness and interpretability of study outcomes. Ultimately, the goal is to translate these advances into clinical practice to enhance diagnostic precision, guide treatment decisions, and improve outcomes for individuals affected by peripheral neuropathies.

8 CONCLUSION

This work establishes periaxin and peripherin as promising fluid biomarkers of demyelination and axonal injury in the peripheral nervous system, offering complementary value to current outcome measures and existing biomarkers such as NfL. Through the development of ultrasensitive assays and their application in clinical and experimental settings, the combined use of periaxin, peripherin and NfL demonstrates potential to improve disease classification, monitoring, and prognostication. Bench-to-bedside translation of these findings stands to advance both clinical care and research in peripheral neuropathies. While further validation and assay refinement are required, the tools and knowledge developed in this thesis lay the foundation for a more objective, mechanistically informed approach to peripheral neuropathy, with the ultimate aim of improving patient outcomes and driving forward the field of peripheral nerve research.

9 BIBLIOGRAPHY

1. Broers MC, Bunschoten C, Nieboer D, Lingsma HF, Jacobs BC. Incidence and Prevalence of Chronic Inflammatory Demyelinating Polyradiculoneuropathy: A Systematic Review and Meta-Analysis. *Neuroepidemiology*. 2019;52(3-4):161-172. doi:10.1159/000494291

2. Łukawska M, Potulska-Chromik A, Lipowska M, et al. Pediatric CIDP: Diagnosis and Management. A Single-Center Experience. *Front Neurol*. 2021;12:667378. doi:10.3389/fneur.2021.667378

3. Dyck PJ, Lais AC, Ohta M, Bastron JA, Okazaki H, Groover RV. Chronic inflammatory polyradiculoneuropathy. *Mayo Clin Proc*. 1975;50(11):621-637.

4. Vallat JM, Sommer C, Magy L. Chronic inflammatory demyelinating polyradiculoneuropathy: diagnostic and therapeutic challenges for a treatable condition. *Lancet Neurol*. 2010;9(4):402-412. doi:10.1016/S1474-4422(10)70041-7

5. Said G, Krarup C. Chronic inflammatory demyelinative polyneuropathy. *Handb Clin Neurol*. 2013;115:403-413. doi:10.1016/B978-0-444-52902-2.00022-9

6. Koike H, Nishi R, Ikeda S, et al. Ultrastructural mechanisms of macrophage-induced demyelination in CIDP. *Neurology*. 2018;91(23):1051-1060. doi:10.1212/WNL.0000000000006625

7. Prineas JW, McLeod JG. Chronic relapsing polyneuritis. *J Neurol Sci*. 1976;27(4):427-458. doi:10.1016/0022-510x(76)90213-6

8. Griffin JW, Stoll G, Li CY, Tyor W, Cornblath DR. Macrophage responses in inflammatory demyelinating neuropathies. *Ann Neurol*. 1990;27 Suppl:S64-68. doi:10.1002/ana.410270717

9. Vital C, Vital A, Lagueny A, et al. Chronic inflammatory demyelinating polyneuropathy: immunopathological and ultrastructural study of peripheral nerve biopsy in 42 cases. *Ultrastruct Pathol*. 2000;24(6):363-369. doi:10.1080/019131200750060023

10. Mathey EK, Park SB, Hughes RAC, et al. Chronic inflammatory demyelinating polyradiculoneuropathy: from pathology to phenotype. *J Neurol Neurosurg Psychiatry*. 2015;86(9):973-985. doi:10.1136/jnnp-2014-309697

11. Sommer C, Koch S, Lammens M, Gabreels-Festen A, Stoll G, Toyka KV. Macrophage clustering as a diagnostic marker in sural nerve biopsies of patients with CIDP. *Neurology*. 2005;65(12):1924-1929. doi:10.1212/01.wnl.0000188879.19900.b7

12. Shimizu F, Sawai S, Sano Y, et al. Severity and Patterns of Blood-Nerve Barrier Breakdown in Patients with Chronic Inflammatory Demyelinating

Polyradiculoneuropathy: Correlations with Clinical Subtypes. *PLOS ONE*. 2014;9(8):e104205. doi:10.1371/journal.pone.0104205

13. Krendel DA, Parks HP, Anthony DC, St Clair MB, Graham DG. Sural nerve biopsy in chronic inflammatory demyelinating polyradiculoneuropathy. *Muscle Nerve*. 1989;12(4):257-264. doi:10.1002/mus.880120402

14. Schneider-Hohendorf T, Schwab N, Uçeyler N, Göbel K, Sommer C, Wiendl H. CD8+ T-cell immunity in chronic inflammatory demyelinating polyradiculoneuropathy. *Neurology*. 2012;78(6):402-408. doi:10.1212/WNL.0b013e318245d250

15. Mausberg AK, Dorok M, Stettner M, et al. Recovery of the T-cell repertoire in CIDP by IV immunoglobulins. *Neurology*. 2013;80(3):296-303. doi:10.1212/WNL.0b013e31827debad

16. Uncini A, Susuki K, Yuki N. Nodo-paranodopathy: Beyond the demyelinating and axonal classification in anti-ganglioside antibody-mediated neuropathies. *Clin Neurophysiol*. 2013;124(10):1928-1934. doi:10.1016/j.clinph.2013.03.025

17. Querol LA, Hartung HP, Lewis RA, et al. The Role of the Complement System in Chronic Inflammatory Demyelinating Polyneuropathy: Implications for Complement-Targeted Therapies. *Neurotherapeutics*. 2022;19(3):864-873. doi:10.1007/s13311-022-01221-y

18. Liberatore G, De Lorenzo A, Giannotta C, et al. Frequency and clinical correlates of anti-nerve antibodies in a large population of CIDP patients included in the Italian database. *Neurol Sci Off J Ital Neurol Soc Ital Soc Clin Neurophysiol*. 2022;43(6):3939-3947. doi:10.1007/s10072-021-05811-0

19. Yamamoto M. B cell targeted therapy for immunoglobulin G4-related disease. *Immunol Med*. 2021;44(4):216-222. doi:10.1080/25785826.2021.1886630

20. Perugino CA, Stone JH. IgG4-related disease: an update on pathophysiology and implications for clinical care. *Nat Rev Rheumatol*. 2020;16(12):702-714. doi:10.1038/s41584-020-0500-7

21. Dunkelberger JR, Song WC. Complement and its role in innate and adaptive immune responses. *Cell Res*. 2010;20(1):34-50. doi:10.1038/cr.2009.139

22. Mair D, Madi H, Eftimov F, Lunn MP, Keddie S. Novel therapies in CIDP. *J Neurol Neurosurg Psychiatry*. 2025;96(1):38-46. doi:10.1136/jnnp-2024-334165

23. Van den Bergh PYK, van Doorn PA, Hadden RDM, et al. European Academy of Neurology/Peripheral Nerve Society guideline on diagnosis and treatment of chronic inflammatory demyelinating polyradiculoneuropathy: Report of a joint Task Force-Second revision. *Eur J Neurol*. 2021;28(11):3556-3583. doi:10.1111/ene.14959

24. Kyle RA, Therneau TM, Rajkumar SV, et al. Prevalence of monoclonal gammopathy of undetermined significance. *N Engl J Med*. 2006;354(13):1362-1369. doi:10.1056/NEJMoa054494

25. Kelly JJ, Kyle RA, O'Brien PC, Dyck PJ. Prevalence of monoclonal protein in peripheral neuropathy. *Neurology*. 1981;31(11):1480-1483. doi:10.1212/wnl.31.11.1480

26. Carroll AS, Lunn MPT. Paraproteinaemic neuropathy: MGUS and beyond. *Pract Neurol*. 2021;21(6):492-503. doi:10.1136/practneurol-2020-002837

27. Ramchandren S, Lewis RA. An update on monoclonal gammopathy and neuropathy. *Curr Neurol Neurosci Rep*. 2012;12(1):102-110. doi:10.1007/s11910-011-0237-4

28. Yeung KB, Thomas PK, King RH, et al. The clinical spectrum of peripheral neuropathies associated with benign monoclonal IgM, IgG and IgA paraproteinaemia. Comparative clinical, immunological and nerve biopsy findings. *J Neurol*. 1991;238(7):383-391. doi:10.1007/BF00319857

29. Nobile-Orazio E, Cocito D, Manganelli F, et al. Rituximab versus placebo for chronic inflammatory demyelinating polyradiculoneuropathy: a randomized trial. *Brain J Neurol*. Published online December 10, 2024:awae400. doi:10.1093/brain/awae400

30. Roux T, Debs R, Maisonobe T, et al. Rituximab in chronic inflammatory demyelinating polyradiculoneuropathy with associated diseases. *J Peripher Nerv Syst*. 2018;23(4):235-240. doi:10.1111/jns.12287

31. Benedetti L, Briani C, Franciotta D, et al. Rituximab in patients with chronic inflammatory demyelinating polyradiculoneuropathy: a report of 13 cases and review of the literature. *J Neurol Neurosurg Psychiatry*. 2011;82(3):306-308. doi:10.1136/jnnp.2009.188912

32. King R. Microscopic anatomy: normal structure. *Handb Clin Neurol*. 2013;115:7-27. doi:10.1016/B978-0-444-52902-2.00002-3

33. Nobile-Orazio E. Multifocal motor neuropathy. *J Neuroimmunol*. 2001;115(1-2):4-18. doi:10.1016/s0165-5728(01)00266-1

34. Neurology: A Queen Square Textbook, 3rd Edition | Wiley. Wiley.com. Accessed March 12, 2025. https://www.wiley.com/en-kr/Neurology%3A+A+Queen+Square+Textbook%2C+3rd+Edition-p-9781119715696

35. Yeh WZ, Dyck PJ, Van Den Berg LH, Kiernan MC, Taylor BV. Multifocal motor neuropathy: controversies and priorities. *J Neurol Neurosurg Psychiatry*. 2020;91(2):140-148. doi:10.1136/jnnp-2019-321532

36. Herraets IJT, Goedee HS, Telleman JA, et al. Nerve ultrasound for diagnosing chronic inflammatory neuropathy: A multicenter validation study. *Neurology*. 2020;95(12):e1745-e1753. doi:10.1212/WNL.0000000000010369

37. Goedee HS, Jongbloed BA, van Asseldonk JTH, et al. A comparative study of brachial plexus sonography and magnetic resonance imaging in chronic inflammatory demyelinating neuropathy and multifocal motor neuropathy. *Eur J Neurol*. 2017;24(10):1307-1313. doi:10.1111/ene.13380

38. Burnor E, Yang L, Zhou H, et al. Neurofascin antibodies in autoimmune, genetic, and idiopathic neuropathies. *Neurology*. 2018;90(1):e31-e38. doi:10.1212/WNL.0000000000004773

39. Querol L, Rojas-García R, Diaz-Manera J, et al. Rituximab in treatment-resistant CIDP with antibodies against paranodal proteins. *Neurol - Neuroimmunol Neuroinflammation*. 2015;2(5):e149. doi:10.1212/NXI.0000000000000149

40. Hauw F, Fargeot G, Adams D, et al. Charcot-Marie-Tooth disease misdiagnosed as chronic inflammatory demyelinating polyradiculoneuropathy: An international multicentric retrospective study. *Eur J Neurol*. 2021;28(9):2846-2854. doi:10.1111/ene.14950

41. Eftimov F, Winer JB, Vermeulen M, de Haan R, van Schaik IN. Intravenous immunoglobulin for chronic inflammatory demyelinating polyradiculoneuropathy. *Cochrane Database Syst Rev*. 2013;(12):CD001797. doi:10.1002/14651858.CD001797.pub3

42. Hughes R, Bensa S, Willison H, et al. Randomized controlled trial of intravenous immunoglobulin versus oral prednisolone in chronic inflammatory demyelinating polyradiculoneuropathy. *Ann Neurol*. 2001;50(2):195-201. doi:10.1002/ana.1088

43. Dyck PJ, O'Brien PC, Oviatt KF, et al. Prednisone improves chronic inflammatory demyelinating polyradiculoneuropathy more than no treatment. *Ann Neurol*. 1982;11(2):136-141. doi:10.1002/ana.410110205

44. Nobile-Orazio E, Cocito D, Jann S, et al. Intravenous immunoglobulin versus intravenous methylprednisolone for chronic inflammatory demyelinating polyradiculoneuropathy: a randomised controlled trial. *Lancet Neurol*. 2012;11(6):493-502. doi:10.1016/S1474-4422(12)70093-5

45. Xiang Q, Cao Y, Song Z, et al. Cyclophosphamide for Treatment of Refractory Chronic Inflammatory Demyelinating Polyradiculoneuropathy: A Systematic Review and Meta-analysis. *Clin Ther*. 2022;44(8):1058-1070. doi:10.1016/j.clinthera.2022.06.008

46. Zuercher AW, Spirig R, Baz Morelli A, Rowe T, Käsermann F. Next-generation Fc receptor–targeting biologics for autoimmune diseases. *Autoimmun Rev*. 2019;18(10):102366. doi:10.1016/j.autrev.2019.102366

47. Lunn MP, Manji H, Choudhary PP, Hughes RA, Thomas PK. Chronic inflammatory demyelinating polyradiculoneuropathy: a prevalence study in south east England. *J Neurol Neurosurg Psychiatry*. 1999;66(5):677-680. doi:10.1136/jnnp.66.5.677

48. Bellanti R, Rinaldi S. Guillain-Barré syndrome: a comprehensive review. *Eur J Neurol*. n/a(n/a):e16365. doi:10.1111/ene.16365

49. Sejvar JJ, Baughman AL, Wise M, Morgan OW. Population incidence of Guillain-Barré syndrome: a systematic review and meta-analysis. *Neuroepidemiology*. 2011;36(2):123-133. doi:10.1159/000324710

50. Guillain-Barré syndrome in a local area in Japan, 2006-2015: an epidemiological and clinical study of 108 patients - PubMed. Accessed November 2, 2023. https://pubmed.ncbi.nlm.nih.gov/29337417/

51. Rivera-Lillo G, Torres-Castro R, Burgos PI, et al. Incidence of Guillain-Barré syndrome in Chile: a population-based study. *J Peripher Nerv Syst*. 2016;21(4):339-344. doi:10.1111/jns.12182

52. High Incidence of Guillain-Barré Syndrome in Children, Bangladesh - PMC. Accessed November 2, 2023. https://www.ncbi.nlm.nih.gov/pmc/articles/PMC3381380/

53. Seasonal variation in Guillain-Barré syndrome: a systematic review, meta-analysis and Oxfordshire cohort study - PubMed. Accessed November 2, 2023. https://pubmed.ncbi.nlm.nih.gov/25540247/

54. Jackson BR, Zegarra JA, López-Gatell H, et al. Binational outbreak of Guillain-Barré syndrome associated with Campylobacter jejuni infection, Mexico and USA, 2011. *Epidemiol Infect*. 2014;142(5):1089-1099. doi:10.1017/S0950268813001908

55. Styczynski AR, Malta JMAS, Krow-Lucal ER, et al. Increased rates of Guillain-Barré syndrome associated with Zika virus outbreak in the Salvador metropolitan area, Brazil. *PLoS Negl Trop Dis*. 2017;11(8):e0005869. doi:10.1371/journal.pntd.0005869

56. Shahrizaila N, Lehmann HC, Kuwabara S. Guillain-Barré syndrome. *Lancet Lond Engl*. 2021;397(10280):1214-1228. doi:10.1016/S0140-6736(21)00517-1

57. Willison HJ, Jacobs BC, Van Doorn PA. Guillain-Barré syndrome. *The Lancet*. 2016;388(10045):717-727. doi:10.1016/S0140-6736(16)00339-1

58. Doets AY, Verboon C, van den Berg B, et al. Regional variation of Guillain-Barré syndrome. *Brain*. 2018;141(10):2866-2877. doi:10.1093/brain/awy232

59. Langmuir AD, Bregman DJ, Kurland LT, Nathanson N, Victor M. An epidemiologic and clinical evaluation of Guillain-Barré syndrome reported in association with the administration of swine influenza vaccines. *Am J Epidemiol*. 1984;119(6):841-879. doi:10.1093/oxfordjournals.aje.a113809

60. Goud R, Lufkin B, Duffy J, et al. Risk of Guillain-Barré Syndrome Following Recombinant Zoster Vaccine in Medicare Beneficiaries. *JAMA Intern Med*. 2021;181(12):1623-1630. doi:10.1001/jamainternmed.2021.6227

61. Abara WE, Gee J, Marquez P, et al. Reports of Guillain-Barré Syndrome After COVID-19 Vaccination in the United States. *JAMA Netw Open*. 2023;6(2):e2253845. doi:10.1001/jamanetworkopen.2022.53845

62. Keh RYS, Scanlon S, Datta-Nemdharry P, et al. COVID-19 vaccination and Guillain-Barré syndrome: analyses using the National Immunoglobulin Database. *Brain J Neurol*. 2023;146(2):739-748. doi:10.1093/brain/awac067

63. Patone M, Handunnetthi L, Saatci D, et al. Neurological complications after first dose of COVID-19 vaccines and SARS-CoV-2 infection. *Nat Med*. 2021;27(12):2144-2153. doi:10.1038/s41591-021-01556-7

64. Gensicke H, Datta AN, Dill P, Schindler C, Fischer D. Increased incidence of Guillain-Barré syndrome after surgery. *Eur J Neurol*. 2012;19(9):1239-1244. doi:10.1111/j.1468-1331.2012.03730.x

65. Rudant J, Dupont A, Mikaeloff Y, Bolgert F, Coste J, Weill A. Surgery and risk of Guillain-Barré syndrome: A French nationwide epidemiologic study. *Neurology*. 2018;91(13):e1220-e1227. doi:10.1212/WNL.0000000000006246

66. Zhang L, Arrington S, Keung YK. Guillain-Barré syndrome after transplantation. *Leuk Lymphoma*. 2008;49(2):291-297. doi:10.1080/10428190701760003

67. Gu Y, Menzies AM, Long GV, Fernando SL, Herkes G. Immune mediated neuropathy following checkpoint immunotherapy. *J Clin Neurosci Off J Neurosurg Soc Australas*. 2017;45:14-17. doi:10.1016/j.jocn.2017.07.014

68. Súkeníková L, Mallone A, Schreiner B, et al. Autoreactive T cells target peripheral nerves in Guillain–Barré syndrome. *Nature*. Published online January 17, 2024:1-9. doi:10.1038/s41586-023-06916-6

69. Griffin JW, Li CY, Macko C, et al. Early nodal changes in the acute motor axonal neuropathy pattern of the Guillain-Barré syndrome. *J Neurocytol*. 1996;25(1):33-51. doi:10.1007/BF02284784

70. Hafer-Macko C, Hsieh ST, Ho TW, et al. Acute motor axonal neuropathy: An antibody-mediated attack on axolemma. *Ann Neurol*. 1996;40(4):635-644. doi:10.1002/ana.410400414

71. McGonigal R, Rowan EG, Greenshields KN, et al. Anti-GD1a antibodies activate complement and calpain to injure distal motor nodes of Ranvier in mice. *Brain*. 2010;133(7):1944-1960. doi:10.1093/brain/awq119

72. Susuki K, Rasband MN, Tohyama K, et al. Anti-GM1 Antibodies Cause Complement-Mediated Disruption of Sodium Channel Clusters in Peripheral Motor Nerve Fibers. *J Neurosci*. 2007;27(15):3956-3967. doi:10.1523/JNEUROSCI.4401-06.2007

73. Halstead SK, Zitman FMP, Humphreys PD, et al. Eculizumab prevents anti-ganglioside antibody-mediated neuropathy in a murine model. *Brain*. 2008;131(5):1197-1208. doi:10.1093/brain/awm316

74. The endogenous calpain inhibitor calpastatin attenuates axon degeneration in murine Guillain-Barré syndrome - McGonigal - 2023 - Journal of the Peripheral Nervous System - Wiley Online Library. Accessed October 23, 2023. https://onlinelibrary.wiley.com/doi/10.1111/jns.12520

75. Halstead SK, O'Hanlon GM, Humphreys PD, et al. Anti-disialoside antibodies kill perisynaptic Schwann cells and damage motor nerve terminals via membrane attack complex in a murine model of neuropathy. *Brain J Neurol*. 2004;127(Pt 9):2109-2123. doi:10.1093/brain/awh231

76. McGonigal R, Campbell CI, Barrie JA, et al. Schwann cell nodal membrane disruption triggers bystander axonal degeneration in a Guillain-Barré syndrome mouse model. *J Clin Invest*. 2022;132(14):e158524. doi:10.1172/JCI158524

77. Wu LY, Zhou Y, Qin C, Hu BL. The effect of TNF-alpha, FcγR and CD1 polymorphisms on Guillain-Barré syndrome risk: evidences from a meta-analysis. *J Neuroimmunol*. 2012;243(1-2):18-24. doi:10.1016/j.jneuroim.2011.12.003

78. Geleijns K, Roos A, Houwing-Duistermaat JJ, et al. Mannose-binding lectin contributes to the severity of Guillain-Barré syndrome. *J Immunol Baltim Md 1950*. 2006;177(6):4211-4217. doi:10.4049/jimmunol.177.6.4211

79. Leonhard SE, Mandarakas MR, Gondim FAA, et al. Diagnosis and management of Guillain-Barré syndrome in ten steps. *Nat Rev Neurol*. 2019;15(11):671-683. doi:10.1038/s41582-019-0250-9

80. Fokke C, van den Berg B, Drenthen J, Walgaard C, van Doorn PA, Jacobs BC. Diagnosis of Guillain-Barré syndrome and validation of Brighton criteria. *Brain J Neurol*. 2014;137(Pt 1):33-43. doi:10.1093/brain/awt285

81. van Doorn PA, Van den Bergh PYK, Hadden RDM, et al. European Academy of Neurology/Peripheral Nerve Society Guideline on diagnosis and treatment of Guillain–Barré syndrome. *Eur J Neurol*. n/a(n/a). doi:10.1111/ene.16073

82. Bellanti R, Keddie S, Lunn MP, Rinaldi S. Ultrasensitive assay technology and fluid biomarkers for the evaluation of peripheral nerve disease. *J Neurol Neurosurg Psychiatry*. Published online October 11, 2023:jnnp-2023-332031. doi:10.1136/jnnp-2023-332031

83. Thomma RCM, Fokke C, Walgaard C, et al. High and Persistent Anti-GM1 Antibody Titers Are Associated With Poor Clinical Recovery in Guillain-Barré Syndrome. *Neurol Neuroimmunol Neuroinflammation*. 2023;10(4):e200107. doi:10.1212/NXI.0000000000200107

84. A Simplified, Graded, Electrodiagnostic Criterion for Guillain-Barré Syndrome That Incorporates Sensory Nerve Conduction Studies | Scientific Reports. Accessed April 24, 2024. https://www.nature.com/articles/s41598-019-44090-w

85. Derksen A, Ritter C, Athar P, et al. Sural sparing pattern discriminates Guillain-Barré syndrome from its mimics. *Muscle Nerve*. 2014;50(5):780-784. doi:10.1002/mus.24226

86. Pestronk A, Choksi R, Yee WC, Kornberg AJ, Lopate G, Trotter J. Serum antibodies to heparan sulfate glycosaminoglycans in Guillain-Barré syndrome and other demyelinating polyneuropathies. *J Neuroimmunol*. 1998;91(1-2):204-209. doi:10.1016/s0165-5728(98)00182-9

87. Vucic S, Cairns KD, Black KR, Chong PST, Cros D. Neurophysiologic findings in early acute inflammatory demyelinating polyradiculoneuropathy. *Clin Neurophysiol Off J Int Fed Clin Neurophysiol*. 2004;115(10):2329-2335. doi:10.1016/j.clinph.2004.05.009

88. Scarpino M, Lolli F, Carrai R, et al. Diagnostic accuracy of neurophysiological criteria for early diagnosis of AIDP: A prospective study. *Neurophysiol Clin Clin Neurophysiol*. 2016;46(1):35-42. doi:10.1016/j.neucli.2015.12.008

89. Chanson JB, Echaniz-Laguna A. Early electrodiagnostic abnormalities in acute inflammatory demyelinating polyneuropathy: a retrospective study of 58 patients. *Clin*

Neurophysiol Off J Int Fed Clin Neurophysiol. 2014;125(9):1900-1905. doi:10.1016/j.clinph.2014.01.007

90. Fehmi J, Davies AJ, Antonelou M, et al. Contactin-1 Antibodies Link Autoimmune Neuropathies to Nephrotic Syndrome. Published online December 16, 2020. doi:10.2139/ssrn.3739819

91. Ruts L, van Koningsveld R, Jacobs BC, van Doorn PA. Determination of pain and response to methylprednisolone in Guillain-Barré syndrome. *J Neurol*. 2007;254(10):1318-1322. doi:10.1007/s00415-006-0515-2

92. Howard RS. Poliomyelitis and the postpolio syndrome. *BMJ*. 2005;330(7503):1314-1318.

93. Wakerley BR, Yuki N. Mimics and chameleons in Guillain–Barré and Miller Fisher syndromes. *Pract Neurol*. 2015;15(2):90-99. doi:10.1136/practneurol-2014-000937

94. Solomon T, Lewthwaite P, Perera D, Cardosa MJ, McMinn P, Ooi MH. Virology, epidemiology, pathogenesis, and control of enterovirus 71. *Lancet Infect Dis*. 2010;10(11):778-790. doi:10.1016/S1473-3099(10)70194-8

95. Kranick SM, Nath A. Neurologic Complications of HIV-1 Infection and Its Treatment in the Era of Antiretroviral Therapy. *Contin Lifelong Learn Neurol*. 2012;18(6 Infectious Disease):1319-1337. doi:10.1212/01.CON.0000423849.24900.ec

96. https://fyra.io. Porphyric Neuropathy. Practical Neurology. Accessed January 30, 2024. https://practicalneurology.com/articles/2020-july-aug/porphyric-neuropathy

97. Tri SL, Vinh KN, Dang TQ, Umapathi T. Myoedema: a forgotten sign in acute colchicine myopathy. *BMJ Case Rep CP*. 2023;16(10):e257076. doi:10.1136/bcr-2023-257076

98. Corticosteroids for Guillain-Barré syndrome - PubMed. Accessed October 31, 2023. https://pubmed.ncbi.nlm.nih.gov/27775812/

99. Group GBSST. Double-blind trial of intravenous methylprednisolone in Guillain-Barré syndrome. *The Lancet*. 1993;341(8845):586-590. doi:10.1016/0140-6736(93)90351-G

100. Hughes RA, Newsom-Davis JM, Perkin GD, Pierce JM. Controlled trial prednisolone in acute polyneuropathy. *Lancet Lond Engl*. 1978;2(8093):750-753. doi:10.1016/s0140-6736(78)92644-2

101. Hughes RA, Brassington R, Gunn AA, van Doorn PA. Corticosteroids for Guillain-Barré syndrome. *Cochrane Database Syst Rev*. 2016;10(10):CD001446. doi:10.1002/14651858.CD001446.pub5

102. Effect of methylprednisolone when added to standard treatment with intravenous immunoglobulin for Guillain-Barré syndrome: randomised trial - PubMed. Accessed October 31, 2023. https://pubmed.ncbi.nlm.nih.gov/14738791/

103. Hughes RAC, Swan AV, van Doorn PA. Intravenous immunoglobulin for Guillain-Barré syndrome. *Cochrane Database Syst Rev*. 2014;2014(9):CD002063. doi:10.1002/14651858.CD002063.pub6

104. Kapoor M, Hunt I, Spillane J, et al. IVIg-exposure and thromboembolic event risk: findings from the UK Biobank. *J Neurol Neurosurg Psychiatry*. 2022;93(8):876-885. doi:10.1136/jnnp-2022-328881

105. Fehmi J, Bellanti R, Misbah SA, Bhattacharjee A, Rinaldi S. Treatment of CIDP. *Pract Neurol*. Published online September 15, 2022:pn-2021-002991. doi:10.1136/pn-2021-002991

106. Misawa S, Kuwabara S, Sato Y, et al. Safety and efficacy of eculizumab in Guillain-Barré syndrome: a multicentre, double-blind, randomised phase 2 trial. *Lancet Neurol*. 2018;17(6):519-529. doi:10.1016/S1474-4422(18)30114-5

107. Annexon Biosciences Reports Top-line Phase 1b Results for Novel C1q Inhibitor ANX005 in Guillain-Barré Syndrome - Annexon Biosciences. Accessed January 11, 2024. https://annexonbio.com/news/annexon-biosciences-reports-top-line-phase-1b-results-for-novel-c1q-inhibitor-anx005-in-guillain-barre-syndrome/

108. Takahashi R, Yuki N. Streptococcal IdeS: therapeutic potential for Guillain–Barré syndrome. *Sci Rep*. 2015;5:10809. doi:10.1038/srep10809

109. Wang Y, Shi Q, Lv H, et al. IgG-degrading enzyme of Streptococcus pyogenes (IdeS) prevents disease progression and facilitates improvement in a rabbit model of Guillain-Barré syndrome. *Exp Neurol*. 2017;291:134-140. doi:10.1016/j.expneurol.2017.02.010

110. Rajabally YA, Uncini A. Outcome and its predictors in Guillain-Barre syndrome. *J Neurol Neurosurg Psychiatry*. 2012;83(7):711-718. doi:10.1136/jnnp-2011-301882

111. Chiò A, Cocito D, Leone M, et al. Guillain-Barré syndrome: a prospective, population-based incidence and outcome survey. *Neurology*. 2003;60(7):1146-1150. doi:10.1212/01.wnl.0000055091.96905.d0

112. van den Berg B, Bunschoten C, van Doorn PA, Jacobs BC. Mortality in Guillain-Barre syndrome. *Neurology*. 2013;80(18):1650-1654. doi:10.1212/WNL.0b013e3182904fcc

113. Lawn ND, Wijdicks EF. Fatal Guillain-Barré syndrome. *Neurology*. 1999;52(3):635-638. doi:10.1212/wnl.52.3.635

114. Turan Z, Topaloglu M, Ozyemisci Taskiran O. Medical Research Council-sumscore: a tool for evaluating muscle weakness in patients with post-intensive care syndrome. *Crit Care*. 2020;24(1):562. doi:10.1186/s13054-020-03282-x

115. Kleyweg RP, Van Der Meché FGA, Schmitz PIM. Interobserver agreement in the assessment of muscle strength and functional abilities in Guillain-Barré syndrome. *Muscle Nerve*. 1991;14(11):1103-1109. doi:10.1002/mus.880141111

116. van Nes SI, Vanhoutte EK, van Doorn PA, et al. Rasch-built Overall Disability Scale (R-ODS) for immune-mediated peripheral neuropathies. *Neurology*. 2011;76(4):337-345. doi:10.1212/WNL.0b013e318208824b

117. Randomized controlled trial of intravenous immunoglobulin versus oral prednisolone in chronic inflammatory demyelinating polyradiculoneuropathy - PubMed. Accessed March 22, 2024. https://pubmed.ncbi.nlm.nih.gov/11506402/

118. Vanhoutte EK, Faber CG, Merkies ISJ, PeriNomS study group. 196th ENMC international workshop: Outcome measures in inflammatory peripheral neuropathies 8-10 February 2013, Naarden, The Netherlands. *Neuromuscul Disord NMD*. 2013;23(11):924-933. doi:10.1016/j.nmd.2013.06.006

119. Incat disability score: A critical analysis of its measurement properties - Breiner - 2014 - Muscle & Nerve - Wiley Online Library. Accessed October 28, 2023. https://onlinelibrary.wiley.com/doi/10.1002/mus.24207

120. Graham RC, Hughes RAC. A modified peripheral neuropathy scale: the Overall Neuropathy Limitations Scale. *J Neurol Neurosurg Psychiatry*. 2006;77(8):973-976. doi:10.1136/jnnp.2005.081547

121. International Validation of the Erasmus Guillain-Barré Syndrome Respiratory Insufficiency Score - PubMed. Accessed October 28, 2023. https://pubmed.ncbi.nlm.nih.gov/35106830/

122. Walgaard C, Lingsma HF, Ruts L, et al. Prediction of respiratory insufficiency in Guillain-Barré syndrome. *Ann Neurol*. Published online 2010:NA-NA. doi:10.1002/ana.21976

123. Luijten LWG, Doets AY, Arends S, et al. Modified Erasmus GBS Respiratory Insufficiency Score: a simplified clinical tool to predict the risk of mechanical ventilation in Guillain-Barré syndrome. *J Neurol Neurosurg Psychiatry*. 2023;94(4):300-308. doi:10.1136/jnnp-2022-329937

124. Walgaard C, Lingsma HF, Ruts L, van Doorn PA, Steyerberg EW, Jacobs BC. Early recognition of poor prognosis in Guillain-Barre syndrome. *Neurology*. 2011;76(11):968-975. doi:10.1212/WNL.0b013e3182104407

125. Cornblath DR, Mellits ED, Griffin JW, et al. Motor conduction studies in Guillain-Barré syndrome: description and prognostic value. *Ann Neurol*. 1988;23(4):354-359. doi:10.1002/ana.410230407

126. Khalil M, Teunissen CE, Otto M, et al. Neurofilaments as biomarkers in neurological disorders. *Nat Rev Neurol*. 2018;14(10):577-589. doi:10.1038/s41582-018-0058-z

127. Khalil M, Teunissen CE, Lehmann S, et al. Neurofilaments as biomarkers in neurological disorders — towards clinical application. *Nat Rev Neurol*. 2024;20(5):269-287. doi:10.1038/s41582-024-00955-x

128. Lieverloo GGA, Wieske L, Verhamme C, et al. Serum neurofilament light chain in chronic inflammatory demyelinating polyneuropathy. *J Peripher Nerv Syst*. 2019;24(2):187-194. doi:10.1111/jns.12319

129. Kapoor M, Carr A, Foiani M, et al. Association of plasma neurofilament light chain with disease activity in chronic inflammatory demyelinating polyradiculoneuropathy. *Eur J Neurol*. 2022;29(11):3347-3357. doi:10.1111/ene.15496

130. Wieske L, Michael MR, In 't Veld SGJG, et al. Proximity extension assay-based discovery of biomarkers for disease activity in chronic inflammatory demyelinating polyneuropathy. *J Neurol Neurosurg Psychiatry*. 2024;95(7):595-604. doi:10.1136/jnnp-2023-332398

131. van Tilburg SJ, Teunissen CE, Maas CCHM, et al. Dynamics and prognostic value of serum neurofilament light chain in Guillain-Barré syndrome. *eBioMedicine*. 2024;102:105072. doi:10.1016/j.ebiom.2024.105072

132. Martín-Aguilar L, Camps-Renom P, Lleixà C, et al. Serum neurofilament light chain predicts long-term prognosis in Guillain-Barré syndrome patients. *J Neurol Neurosurg Psychiatry*. 2021;92(1):70-77. doi:10.1136/jnnp-2020-323899

133. Petzold A. The 2022 Lady Estelle Wolfson lectureship on neurofilaments. *J Neurochem*. 2022;163(3):179-219. doi:10.1111/jnc.15682

134. Boylan KB, Glass JD, Crook JE, et al. Phosphorylated neurofilament heavy subunit (pNF-H) in peripheral blood and CSF as a potential prognostic biomarker in amyotrophic lateral sclerosis. *J Neurol Neurosurg Psychiatry*. 2013;84(4):467-472. doi:10.1136/jnnp-2012-303768

135. Rossor AM, Lu CH, Petzold A, et al. Plasma neurofilament heavy chain is not a useful biomarker in Charcot-Marie-Tooth disease. *Muscle Nerve*. 2016;53(6):972-975. doi:10.1002/mus.25124

136. Qiao X, Zhang S, Zhao W, et al. Serum Phosphorylated Neurofilament-Heavy Chain, a Potential Biomarker, is Associated With Peripheral Neuropathy in Patients With Type 2 Diabetes. *Medicine (Baltimore)*. 2015;94(44):e1908. doi:10.1097/MD.0000000000001908

137. Lu CH, Petzold A, Topping J, et al. Plasma neurofilament heavy chain levels and disease progression in amyotrophic lateral sclerosis: insights from a longitudinal study. *J Neurol Neurosurg Psychiatry*. 2015;86(5):565-573. doi:10.1136/jnnp-2014-307672

138. Lu CH, Kalmar B, Malaspina A, Greensmith L, Petzold A. A method to solubilise protein aggregates for immunoassay quantification which overcomes the neurofilament "hook" effect. *J Neurosci Methods*. 2011;195(2):143-150. doi:10.1016/j.jneumeth.2010.11.026

139. Gaiottino J, Norgren N, Dobson R, et al. Increased neurofilament light chain blood levels in neurodegenerative neurological diseases. *PloS One*. 2013;8(9):e75091. doi:10.1371/journal.pone.0075091

140. Wang H, Davison M, Wang K, et al. Transmembrane protease serine 5: a novel Schwann cell plasma marker for CMT1A. *Ann Clin Transl Neurol*. 2020;7(1):69-82. doi:10.1002/acn3.50965

141. Notturno F, Capasso M, DeLauretis A, Carpo M, Uncini A. Glial fibrillary acidic protein as a marker of axonal damage in chronic neuropathies. *Muscle Nerve*. 2009;40(1):50-54. doi:10.1002/mus.21323

142. Capodivento G, De Michelis C, Carpo M, et al. CSF sphingomyelin: a new biomarker of demyelination in the diagnosis and management of CIDP and GBS. *J Neurol Neurosurg Psychiatry*. 2021;92(3):303-310. doi:10.1136/jnnp-2020-324445

143. Wong AHY, Fukami Y, Sudo M, Kokubun N, Hamada S, Yuki N. Sialylated IgG-Fc: a novel biomarker of chronic inflammatory demyelinating polyneuropathy. *J Neurol Neurosurg Psychiatry*. 2016;87(3):275-279. doi:10.1136/jnnp-2014-309964

144. Misawa S, Kuwabara S, Mori M, Kawaguchi N, Yoshiyama Y, Hattori T. Serum levels of tumor necrosis factor-alpha in chronic inflammatory demyelinating polyneuropathy. *Neurology*. 2001;56(5):666-669. doi:10.1212/wnl.56.5.666

145. Oka N, Akiguchi I, Kawasaki T, Ohnishi K, Kimura J. Elevated serum levels of endothelial leukocyte adhesion molecules in Guillain-Barré syndrome and chronic inflammatory demyelinating polyneuropathy. *Ann Neurol*. 1994;35(5):621-624. doi:10.1002/ana.410350518

146. Kuhle J, Barro C, Andreasson U, et al. Comparison of three analytical platforms for quantification of the neurofilament light chain in blood samples: ELISA, electrochemiluminescence immunoassay and Simoa. *Clin Chem Lab Med CCLM*. 2016;54(10). doi:10.1515/cclm-2015-1195

147. Kmezic I, Samuelsson K, Finn A, et al. Neurofilament light chain and total tau in the differential diagnosis and prognostic evaluation of acute and chronic inflammatory polyneuropathies. *Eur J Neurol*. 2022;29(9):2810-2822. doi:10.1111/ene.15428

148. Arcaro M, Fenoglio C, Serpente M, et al. A Novel Automated Chemiluminescence Method for Detecting Cerebrospinal Fluid Amyloid-Beta 1-42 and 1-40, Total Tau and Phosphorylated-Tau: Implications for Improving Diagnostic Performance in Alzheimer's Disease. *Biomedicines*. 2022;10(10):2667. doi:10.3390/biomedicines10102667

149. Fredriksson S, Gullberg M, Jarvius J, et al. Protein detection using proximity-dependent DNA ligation assays. *Nat Biotechnol*. 2002;20(5):473-477. doi:10.1038/nbt0502-473

150. Gullberg M, Fredriksson S, Taussig M, Jarvius J, Gustafsdottir S, Landegren U. A sense of closeness: protein detection by proximity ligation. *Curr Opin Biotechnol*. 2003;14(1):82-86. doi:10.1016/s0958-1669(02)00011-3

151. Nong RY, Gu J, Darmanis S, Kamali-Moghaddam M, Landegren U. DNA-assisted protein detection technologies. *Expert Rev Proteomics*. 2012;9(1):21-32. doi:10.1586/epr.11.78

152. Cebulla N, Schirmer D, Runau E, et al. Neurofilament light chain levels indicate acute axonal damage under bortezomib treatment. *J Neurol*. 2023;270(6):2997-3007. doi:10.1007/s00415-023-11624-2

153. Comparative Performances of 4 Serum NfL Assays, pTau181, and GFAP in Patients With Amyotrophic Lateral Sclerosis. Neurology. Accessed March 27, 2025. https://www.neurology.org/doi/10.1212/WNL.0000000000213400

154. Clark AJ, Kaller MS, Galino J, Willison HJ, Rinaldi S, Bennett DLH. Co-cultures with stem cell-derived human sensory neurons reveal regulators of peripheral myelination. *Brain*. 2017;140(4):898-913. doi:10.1093/brain/awx012

155. Davies AJ, Lleixà C, Siles AM, et al. Guillain-Barré Syndrome Following Zika Virus Infection Is Associated With a Diverse Spectrum of Peripheral Nerve Reactive Antibodies. *Neurol Neuroimmunol Neuroinflammation*. 2023;10(1):e200047. doi:10.1212/NXI.0000000000200047

156. Gillespie CS, Sherman DL, Blair GE, Brophy PJ. Periaxin, a novel protein of myelinating schwann cells with a possible role in axonal ensheathment. *Neuron*. 1994;12(3):497-508. doi:10.1016/0896-6273(94)90208-9

157. Scherer SS, Xu YT, Bannerman PG, Sherman DL, Brophy PJ. Periaxin expression in myelinating Schwann cells: modulation by axon-glial interactions and polarized localization during development. *Dev Camb Engl*. 1995;121(12):4265-4273. doi:10.1242/dev.121.12.4265

158. Kijima K, Numakura C, Shirahata E, et al. Periaxin mutation causes early-onset but slow-progressive Charcot-Marie-Tooth disease. *J Hum Genet*. 2004;49(7):376-379. doi:10.1007/s10038-004-0162-3

159. A mutation in periaxin is responsible for CMT4F, an autosomal recessive form of Charcot-Marie-Tooth disease - PubMed. Accessed April 28, 2025. https://pubmed.ncbi.nlm.nih.gov/11157804/

160. DeSilva B, Smith W, Weiner R, et al. Recommendations for the bioanalytical method validation of ligand-binding assays to support pharmacokinetic assessments of macromolecules. *Pharm Res*. 2003;20(11):1885-1900. doi:10.1023/b:pham.0000003390.51761.3d

161. Plikaytis BD, Holder PF, Pais LB, Maslanka SE, Gheesling LL, Carlone GM. Determination of parallelism and nonparallelism in bioassay dilution curves. *J Clin Microbiol*. 1994;32(10):2441-2447. doi:10.1128/jcm.32.10.2441-2447.1994

162. Valentin MA, Ma S, Zhao A, Legay F, Avrameas A. Validation of immunoassay for protein biomarkers: bioanalytical study plan implementation to support pre-clinical and clinical studies. *J Pharm Biomed Anal*. 2011;55(5):869-877. doi:10.1016/j.jpba.2011.03.033

163. Andreasson U, Perret-Liaudet A, van Waalwijk van Doorn LJC, et al. A Practical Guide to Immunoassay Method Validation. *Front Neurol*. 2015;6. doi:10.3389/fneur.2015.00179

164. Rai AJ, Vitzthum F. Effects of preanalytical variables on peptide and protein measurements in human serum and plasma: implications for clinical proteomics. *Expert Rev Proteomics*. 2006;3(4):409-426. doi:10.1586/14789450.3.4.409

165. Sandoe J, Eggan K. Opportunities and challenges of pluripotent stem cell neurodegenerative disease models. *Nat Neurosci*. 2013;16(7):780-789. doi:10.1038/nn.3425

166. Corti S, Faravelli I, Cardano M, Conti L. Human pluripotent stem cells as tools for neurodegenerative and neurodevelopmental disease modeling and drug discovery. *Expert Opin Drug Discov*. 2015;10(6):615-629. doi:10.1517/17460441.2015.1037737

167. Keddie S, Smyth D, Keh RYS, et al. Peripherin is a biomarker of axonal damage in peripheral nervous system disease. *Brain J Neurol*. Published online July 12, 2023:awad234. doi:10.1093/brain/awad234

168. Kuitwaard K, de Gelder J, Tio-Gillen AP, et al. Pharmacokinetics of intravenous immunoglobulin and outcome in Guillain-Barré syndrome. *Ann Neurol*. 2009;66(5):597-603. doi:10.1002/ana.21737

169. Altmann P, De Simoni D, Kaider A, et al. Increased serum neurofilament light chain concentration indicates poor outcome in Guillain-Barré syndrome. *J Neuroinflammation*. 2020;17:86. doi:10.1186/s12974-020-01737-0

170. Van den Bergh PYK, Hadden RDM, Bouche P, et al. European Federation of Neurological Societies/Peripheral Nerve Society guideline on management of chronic inflammatory demyelinating polyradiculoneuropathy: report of a joint task force of the European Federation of Neurological Societies and the Peripheral Nerve Society - first revision. *Eur J Neurol*. 2010;17(3):356-363. doi:10.1111/j.1468-1331.2009.02930.x

171. Sejvar JJ, Kohl KS, Gidudu J, et al. Guillain-Barré syndrome and Fisher syndrome: case definitions and guidelines for collection, analysis, and presentation of immunization safety data. *Vaccine*. 2011;29(3):599-612. doi:10.1016/j.vaccine.2010.06.003

172. Yang Z, Wang KKW. Glial Fibrillary acidic protein: From intermediate filament assembly and gliosis to neurobiomarker. *Trends Neurosci*. 2015;38(6):364. doi:10.1016/j.tins.2015.04.003

173. Feasby TE. Axonal Guillain–Barré syndrome. *Muscle Nerve*. 1994;17(6):678-679. doi:10.1002/mus.880170618

174. van Doorn PA, Van den Bergh PYK, Hadden RDM, et al. European Academy of Neurology/Peripheral Nerve Society Guideline on diagnosis and treatment of Guillain–Barré syndrome. *Eur J Neurol*. n/a(n/a). doi:10.1111/ene.16073

175. Manco C, Righi D, Primiano G, et al. Peripherin, A New Promising Biomarker in Neurological Disorders. *Eur J Neurosci*. 2025;61(4):e70030. doi:10.1111/ejn.70030

176. Kapoor M, Foiani M, Heslegrave A, et al. Plasma neurofilament light chain concentration is increased and correlates with the severity of neuropathy in hereditary transthyretin amyloidosis. *J Peripher Nerv Syst JPNS*. 2019;24(4):314-319. doi:10.1111/jns.12350

177. Carroll AS, Razvi Y, O'Donnell L, et al. Serum neurofilament light chain in hereditary transthyretin amyloidosis: validation in real-life practice. *Amyloid Int J Exp Clin Investig Off J Int Soc Amyloidosis*. 2024;31(2):95-104. doi:10.1080/13506129.2024.2313218

178. Sandelius Å, Zetterberg H, Blennow K, et al. Plasma neurofilament light chain concentration in the inherited peripheral neuropathies. *Neurology*. 2018;90(6):e518-e524. doi:10.1212/WNL.0000000000004932

179. Rossor AM, Kapoor M, Wellington H, et al. A longitudinal and cross-sectional study of plasma neurofilament light chain concentration in Charcot-Marie-Tooth disease. *J Peripher Nerv Syst JPNS*. 2022;27(1):50-57. doi:10.1111/jns.12477

180. Grüter T, Motte J, Bulut Y, et al. Axonal damage determines clinical disability in chronic inflammatory demyelinating polyradiculoneuropathy (CIDP): A prospective cohort study of different CIDP subtypes and disease stages. *Eur J Neurol*. 2022;29(2):583-592. doi:10.1111/ene.15156

APPENDIX

Supplementary Table 1. Cut-off concentrations of plasma periaxin, peripherin and NfL

Biomarker	Category	Concentration (pg/ml)
Periaxin	High	> 450
	Intermediate	160 – 450
	Low	< 160
Peripherin	High	> 14
	Intermediate	1.1 – 14
	Low	< 1.1
NfL	High	> 150
	Intermediate	20 - 150
	Low	< 20

Biomarker levels were categorized as low, intermediate, or high by dividing each range into equal thirds. Fisher's exact test was then applied to analyse the associations between these categories and disability scores, including peak and nadir values. This method aimed to achieve a balanced distribution, improve detection of non-linear associations, and minimise the impact of outliers, reducing the risk of type II errors.